Tampere University

OLLI VALTONEN

Enhanced Use of Sinonasal Patient Imaging for Three-Dimensional Applications

Tampere University Dissertations 459

Tampere University Dissertations 459

OLLI VALTONEN

Enhanced Use of Sinonasal Patient Imaging for Three-Dimensional Applications

ACADEMIC DISSERTATION
To be presented, with the permission of
the Faculty of Medicine and Health Technology
of Tampere University,
for public discussion in the auditorium F115
of the Arvo building, Arvo Ylpön katu 34, Tampere,
on 29 October 2021, at 12 o'clock.

ACADEMIC DISSERTATION
Tampere University, Faculty of Medicine and Health Technology
Finland

Responsible supervisor and Custos	Professor Markus Rautiainen Tampere University Finland	
Supervisor	Docent Ilkka Kivekäs Tampere University Finland	
Pre-examiners	Docent Paula Virkkula University of Helsinki Finland	Docent Matti Pukkila University of Eastern Finland Finland
Opponent	Docent Karin Blomgren University of Helsinki Finland	

Cover design: Roihu Inc.

ISBN 978-952-03-2072-0 (print)
ISBN 978-952-03-2073-7 (pdf)
ISSN 2489-9860 (print)
ISSN 2490-0028 (pdf)
http://urn.fi/URN:ISBN:978-952-03-2073-7

PunaMusta Oy – Yliopistopaino
Tampere 2021

To Ruth, Erik, Emilia & the baby-to-be

ACKNOWLEDGEMENTS

First of all, I would like to express my deepest gratitude to my supervisor Professor Markus Rautiainen, MD, PhD for his supportive and straightforward guidance that he granted me during the years spent compiling my dissertation. It has been an honour to have had you supervise my study project.

Second, I sincerely want to thank my supervisor Docent Ilkka Kivekäs, MD, PhD for the inspiring and immediate supervision he provided me during this project. Additionally, following your work and progress in the field of medical research, you have served as an exemplary model for me.

I am greatly indebted to my pre-examiners Docent Paula Virkkula, MD, PhD and Docent Matti Pukkila, MD, PhD for their comprehensive delving into my dissertation as well as for the valuable and constructive feedback they have granted me. I am highly honoured to have Docent Karin Blomgren, MD, PhD as my opponent.

For my co-researchers Jaakko Ormiskangas, MSc (Tech), Ville Rantanen, D.Sc. (Tech) and their mentors Professor Pentti Saarenrinne, D.Sc. (Tech) and Professor Jukka Lekkala, D.Sc. (Tech), I would like to express my gratitude for the immense work you have done for this project in the field of engineering. This project would not have been the same without your expertise.

I would also like to thank Jorma Järnstedt, DDS for providing this project with his radiological expertise and assistance.

I am deeply grateful to Peter Heath, MA for his language revisions in all the phases of my project and for providing me with clear and instructive revisions.

I want to thank Mika Helminen, MSc for his guidance and assistance in producing the statistical analyses.

My thanks go to both Argyro Bizaki-Vallaskangas, MD, PhD and Teemu Harju, MD, PhD for their meritorious scientific work which enabled the present study. I owe you my deepest respect.

I want to thank Docent Jura Numminen MD, PhD for offering me his expertise in rhinology during the different stages of this project.

I would like to show my gratitude to Professor Dennis Poe, MD, PhD from Harvard University and Mark Dean, MD from Ear & Sinus Institute, Fort Worth,

Texas for their role in shaping the idea for this project and for offering their expertise during this project.

I want to thank and show my respect to all my colleagues in the department of otorhinolaryngology at Tampere University Hospital for being such great and warm-hearted people as well as for tapping my shoulder while I was sitting in front of my computer working on this project. Special thanks go to my colleagues Saara Markkanen, MD PhD, Rami Taulu, MD, PhD and Jussi Virtanen MD, (soon PhD) for the efficient collaboration during the finishing phase of this dissertation.

For my father Juha Valtonen, MD, PhD, I want to show my humble respect. You have been my role model along my professional and scientific path. I also want to thank my father and my mother Aila for providing me with the loving home I grew up in and for supporting me in my life. To my brother Iiro, I want to say thank you for being the best brother I could have ever hoped for. I want to thank my parents-in-law, Pirkko and Bror, for all the support and help you have provided to my family.

Finally, with love, my greatest gratitude goes to my loving and understanding wife Ruth. I would not change a day of all the days I have been privileged to share with you. To our two lovely and exuberant children, Erik and Emilia, and the third baby-to-be, I want to say that you are the most precious treasures in my life.

This study was financially supported by the Finnish ORL-HNS Foundation, the Orion Research Foundation sr, the Väinö and Laina Kivi Foundation as well as the Faculty of Medicine and Health Technology at Tampere University.

Tampere, August 2021

Olli Valtonen

ABSTRACT

Patient imaging plays an essential role in the examination of rhinologic patients along with clinical examination methods. The most common imaging methods, computed tomography (CT) and cone beam computed tomography (CBCT), are readily available and provide a good perception of the bony structures, mucous membrane and air space in the nasal cavity and the paranasal sinuses. However, the scans are primarily used by observing consecutive two-dimensional single scans. Due to the complex anatomy of the nasal cavity and paranasal sinuses, the use of the traditional image method presents challenges in obtaining a realistic perception of the three-dimensional anatomy of the nasal cavity and the paranasal sinuses. Thus far, the few experimental studies on the three-dimensional modelling of the sinonasal structures have been based solely on clinical CT scans.

The aim of this dissertation is to examine the applicability of patient imaging in both the virtual and printed 3D modelling of the nasal cavity and the paranasal sinuses. An additional aim is to study whether imaging-based 3D models can be used for studies modelling the nasal cavity airflow.

The present dissertation is based on four studies in which CBCT scans served as the basis for all measurements and procedures. In study I, 72 patients with CBCT scans prior to and at twelve months after maxillary sinus surgery were included. These patients had undergone uncinectomy or balloon dilation due to chronic rhinosinusitis. In study II, five patients with sinonasal CBCT scans were selected and one patient in study III. These patients had symptoms of chronic nasal congestion and had had no prior sinonasal operation. In study IV, 26 patients with CBCT scans prior to and at twelve months after inferior turbinate surgery due to chronic nasal congestion were included. All the studies in the present dissertation examined the CBCT-based virtual 3D modelling of the nasal cavity and the paranasal sinuses. In addition, the CBCT-based sinonasal modelling in 3D prints was examined in studies II and III, and the 3D prints produced were also CBCT scanned for comparison. The obtained results from the 3D models were compared to the results from patient CBCT scan measurements and scoring methods (Lund-MacKay score, Zinreich's modified Lund-MacKay score), clinical examination methods (acoustic rhinometry, rhinomanometry) and patient symptom tests (SNOT-22, VAS, GHSI).

The results showed that the measurement of the maxillary sinus air space volume using virtual 3D modelling was more precise than the CT-based scoring methods of mucous membrane thickness used today. In addition, volumetric measurements of the nasal cavities and the maxillary sinuses as well as the cross-sectional areas of the nasal cavities had statistical correlation with patient symptoms assessed with SNOT-22, VAS and GHSI questionnaires. The cross-sectional area measurements of the nasal cavities also had correlation with the results gained from acoustic rhinometry. Excess artefacts in the patient scans induced by, for example, dental implants were observed to cause difficulties in producing virtual 3D models from the scans.

CT scans proved to be applicable in producing 3D prints in plastic and silicone with a sufficient accuracy. The challenges of the used CBCT-based 3D printing procedures were observed to be the slight roughness of the virtual 3D model surfaces and difficulty in 3D printing the narrow structures with sufficient accuracy. The produced 3D models were, however, found to be good representatives of the original patient anatomies. Moreover, the printed 3D models were applicable to produce realistic rhinomanometric results. The CBCT-based 3D models were also found to function well as good and close to clinical CT quality bases for particle image velocimetry (PIV) measurement and computational fluid dynamics (CFD) calculation studies modelling the airflow in the nasal cavity.

In the present dissertation, it was concluded that CT scans proved to be applicable for measuring the volume and cross-sectional area of the nasal cavity and paranasal sinus air space as well as the 3D modelling of the sinonasal air space. CBCT scans are also sufficient to produce accurate and comparable 3D flow measurements and models that are close to the previous study models based on clinical CT scans. Thus, sufficient accuracy for 3D models and flow measurements can be achieved with CBCT, which induces a lower radiation burden to patients than clinical CT. According to the findings of the present studies, patient scans can be used for notably more profound data acquisition for rhinologic assessment, although the 3D modelling process and analyses need to be more automated.

TIIVISTELMÄ

Nenän ja sen sivuonteloiden oireista kärsivien potilaiden tutkimisessa käytetään kliinisten tutkimismenetelmien lisäksi radiologista kuvantamista. Näistä tietokonetomografia- (TT) ja kartiokeilatietokonetomografiakuvantaminen (KKTT) ovat yleisimpiä, saatavuudeltaan hyviä ja soveltuvat hyvin nenän ja sen sivuonteloiden luisten rakenteiden, limakalvojen ja ilmatilojen arvioimiseen. Kuvaustuloksia tarkastellaan ensisijaisesti selaamalla peräkkäin yksittäisiä kaksiulotteisia leikekuvia. Nenän ja sen sivuonteloiden monimutkaisen rakenteen vuoksi alueen anatomiasta on nykyisellä tarkastelutavalla haastavaa muodostaa kolmiulotteista käsitystä. Tähän mennessä nenän ja sen sivuonteloiden rakenteita on pyritty mallintamaan kolmiulotteisesti vain TT-kuvien pohjalta.

Tämän väitöskirjan tarkoituksena on selvittää potilaskuvantamisen käyttökelpoisuutta nenä- ja sivuonteloiden virtuaalisessa sekä tulostetussa 3D-mallintamisessa. Lisäksi tarkoituksena on tutkia, voiko potilaskuvauksiin perustuvia 3D-malleja käyttää pohjana nenäonteloiden ilmavirtausmallinnustutkimuksiin.

Väitöskirjan tutkimustyö muodostuu neljästä osatyöstä. Tutkimukseen I valittiin 72 potilasta, joille oli tehty KKTT-kuvaus ennen poskiontelotoimenpidettä ja 12 kuukautta sen jälkeen. Potilaille oli tehty poskionteloaukon laajentaminen joko kirurgisesti tai pallolaajentamalla oireisen pitkäkestoisen tulehdustilan vuoksi. Tutkimukseen II valittiin 5 potilasta ja tutkimukseen III valittiin 1 potilas, joilla KKTT-kuva oli otettu nenän pitkäkestoisen tukkoisuusvaivan vuoksi, ja joiden nenää ei ollut aiemmin operoitu. Tutkimukseen IV valittiin 26 potilasta, joille oli tehty KKTT-kuvaus ennen pitkäkestoisen nenän tukkoisuuden vuoksi tehtyä alakuorikkotoimenpidettä ja 12 kuukautta sen jälkeen. Kaikissa tutkimuksissa selvitettiin nenän ja sen sivuonteloiden KKTT-pohjaista ilmatilan 3D-mallintamista virtuaalisesti. Lisäksi tutkimuksissa II ja III selvitettiin KKTT-pohjaista nenä- ja sivuonteloiden 3D-tulostamista ja tulosteet kontrolloitiin KKTT-kuvauksella. 3D-mallinnuksista saatuja tuloksia verrattiin sekä potilaiden tavanomaisista KKTT-kuvista saatuihin mittauksiin ja luokitteluasteikkoihin (Lund-MacKay-luokittelu, Zinreichin muokattu Lund-MacKay-luokittelu) sekä kliinisten tutkimusmenetelmien (akustinen rinometria, rinomanometria) ja oireistoa kuvaavien testien (SNOT-22, VAS, GHSI) tuloksiin.

Tutkimusten tulosten perusteella pystyttiin osoittamaan poskionteloilmatilavuuksien mittaamisen parempi tarkkuus käyttäen 3D-mallinnusta verrattuna nykyisin käytössä oleviin limakalvon paksuutta TT-kuvissa kuvaaviin luokittelumenetelmiin. Lisäksi nenäkäytävien ja poskionteloiden tilavuusmittauksilla sekä nenäkäytävien poikkipinta-alamittauksilla oli havaittavissa tilastollista yhteyttä potilaan kokemiin oireisiin oireistoa kuvaavissa testeissä (SNOT-22, VAS, GHSI). Nenäkäytävän tilavuusmittauksilla oli myös havaittavissa tilastollista yhteyttä akustisen rinometrian antamien tulosten kanssa. 3D-mallinnusten tuottaminen havaittiin vaikeaksi, mikäli potilaskuvissa esiintyi kuvaushetken aikaista vierasesineen, kuten hammasimplantin, aiheuttamaa kuvaussäteilyn runsasta sirontaa.

TT-kuvausten perusteella saatiin tuotettua varsin tarkat 3D-muovi ja -silikonitulosteet. KKTT-pohjaisessa 3D-mallinnuksessa haasteita aiheutti virtuaalisten 3D-mallinnusten pintakarkeus ja kapeiden rakenteiden 3D-tulostaminen riittävällä tarkkuudella. Tulostetut 3D-mallit vastasivat kuitenkin mittausten perusteella hyvin alkuperäistä potilasanatomiaa ja niillä pystyttiin tuottamaan todenmukaisia rinomanometriatuloksia. KKTT-kuvauksiin perustuvat 3D-mallinnukset toimivat tehdyissä tutkimuksissa myös hyvänä, ja tavanomaisiin TT-kuviin vertautuvana, alustana partikkelivirtauslaskennan mittauksille ja numeerisen virtausmekaniikan laskentamalleille, joilla pystytään mallintamaan ilmavirran kulkua nenäonteloissa.

Väitöskirjan tutkimusten perusteella TT osoittautui käyttökelpoiseksi kuvantamismenetelmäksi tehtäessä nenän ja sen sivuonteloiden ilmatilan tilavuus- ja poikkipinta-alamittauksia sekä 3D-mallintamista. KKTT-kuvat ovat riittäviä tuottamaan tarkkoja ja aikaisempiin tavanomaisiin TT-kuviin perustuviin tutkimuksiin verrattavissa olevia 3D-virtausmittauksia ja -mallinnuksia. Näin ollen riittävä tarkkuus 3D-mallinnuksiin ja -virtausmittauksiin voidaan saavuttaa käyttämällä potilaan kuvantamiseen KKTT:aa, jolloin potilas altistuu pienemmälle määrälle röntgensäteilyä kuin perinteistä TT:aa käytettäessä. Väitöskirjassa esitettyjen tutkimusten perusteella potilaskuvia voidaan hyödyntää nykyistä huomattavasti perusteellisemmin nenä- ja sivuontelo-oireisten potilaiden arvioinnissa, kunhan 3D-mallintamista ja tästä tehtäviä analyyseja saadaan paremmin automatisoitua.

CONTENTS

ABBREVIATIONS

CAD	Computer-aided design
CBCT	Cone beam computed tomography
CFD	Computational fluid dynamics
CRS	Chronic rhinosinusitis
CT	Computed tomography
DICOM	Digital imaging and communications in medicine
FDM	Fused deposition modelling
GHSI	Glasgow health status inventory
HU	Hounsfield unit
LM	Lund-MacKay
MDCT	Multidetector computed tomography
MRI	Magnetic resonance imaging
PIV	Particle image velocimetry
PVA	Polyvinyl alcohol
RFTA	Radiofrequency thermal ablation
SNOT-22	22-item sinonasal outcome test
STL	Standard tessellation language
VAS	Visual analogue scale
2D	Two-dimensional
3D	Three-dimensional

LIST OF ORIGINAL PUBLICATIONS

Publication I Valtonen O, Bizaki A, Kivekäs I, Rautiainen M. 2018. Three-Dimensional Volumetric Evaluation of the Maxillary Sinuses in Chronic Rhinosinusitis Surgery. Annals of Otology, Rhinology & Laryngology. 127(12):931-936, 2018.

Publication II Valtonen O, Ormiskangas J, Kivekäs I, Rantanen V, Dean M, Poe D, Järnstedt J, Lekkala J, Saarenrinne P, Rautiainen M. Three-Dimensional Printing of the Nasal Cavities for Clinical Experiments. Scientific Reports. 10(1):502, 2020.

Publication III Ormiskangas J, Valtonen O, Kivekäs I, Dean M, Poe D, Järnstedt J, Lekkala J, Harju T, Saarenrinne P, Rautiainen M. Assessment of PIV performance in validating CFD models from nasal cavity CBCT scans. Respiratory Physiology and Neurobiology. 282:103508, 2020.

Publication IV Valtonen O, Ormiskangas J, Harju T, Rautiainen M, Kivekäs I. Three-Dimensional Measurements in Assessing the Results of Inferior Turbinate Surgery. Annals of Otology, Rhinology & Laryngology. July 1;34894211028516, 2021 (Online ahead of print)

The original publications are referred to in the text by their Roman numerals. The original publications are reprinted in this dissertation with kind permission from the copyright holders.

AUTHOR'S CONTRIBUTION

Publication I The author has taken part in study design. The author has performed the 3D modelling of all the patient CBCT scans, all the measurements based on the 3D models, all the CBCT based stagings and has also produced all the statistical analyses. The author is the main author in this publication.

Publication II The author has taken part in study design. The author has produced all the virtual 3D models of the patient and 3D print CBCT scans for this comparative study as well as performed the majority of the measurements. The author is the main author in this publication.

Publication III The author has taken part in study design. The author has produced the virtual 3D models of both the patient and 3D print CBCT scans that have been used in the PIV measurements and CFD calculations. The author is the second author in this publication.

Publication IV The author has taken part in study design. The author has, with an equal contribution with a co-researcher, produced the 3D modelling of all the patient CBCT scans, volumetric measurements based on 3D models and measured the cross-section areas from patient CBCT scans as well as performed all the statistical analyses. The author is the main author in this publication with an equal contribution with a co-researcher.

1 INTRODUCTION

The clinical assessment of a rhinologic patient consists of a comprehensive patient history, clinical status and additional discretionary clinical assessment methods, such as outpatient tests and patient imaging. Acoustic rhinometry (Hilberg, Jackson, Swift, & Pedersen, 1989) and rhinomanometry (Eccles, 2011a) are among the most common outpatient tests used today. These methods measure the air space cross-sectional area in different regions of the nasal cavity and airflow resistance through the nasal cavity. These tests are usually performed before and after nasal decongestion with topical adrenaline to measure nasal cavity properties. However, these tests do not give an exact perception of the nasal cavities and do not measure the properties of the paranasal sinuses. Thus, to obtain a proper perception of the nasal cavity and the paranasal sinuses, a visual image should be produced with patient imaging.

The anatomical properties in the nasal cavity and the paranasal sinuses as well as the status of the mucous membrane in these structures was first imaged with the plain-film X-ray method in the early 20th century (Burke, Guertler, & Timmons, 1994). This method provided a simple and rough single-film image of the nasal cavity and paranasal sinuses with all the structures illustrated on top of each other. Further development of the imaging techniques first led to CT (Brenner & Hall, 2007) and later to CBCT (Mozzo, Procacci, Tacconi, Martini, & Andreis, 1998) imaging techniques. Nowadays, these are the most used X-ray-based imaging techniques, producing several consecutive 2D images of the region of interest that can be assessed either individually or as a consecutive pack of images. Magnetic resonance imaging (MRI) has also been used for sinonasal imaging. MRI produces visual images in a similar consecutive 2D image fashion but uses nuclear magnetic resonance (Fatterpekar, Delman, & Som, 2008). Moreover, the technique does not cause a radiation burden to patients and is also well suited for soft tissue pathology imaging. Today, however, clinical CT and CBCT are the most frequently used imaging modalities due to sufficient resolution of bone and soft tissue and more extensive availability.

These modern imaging modalities (clinical CT, CBCT and MRI) are traditionally used in rhinologic patients by assessing the 2D images of the region of interest in three separate planes. Thus, the acquired image information requires abstract anatomical 3D perception from the clinician, which is often demanding. In order to reduce the risk of misperception, the use of virtual 3D modelling has been added to the image presentation. Usually, 3D modelling in the head and neck area is used in the virtual presentation of traumatic injuries to the bony structures of the skull and maxillofacial area. Additionally, 3D techniques have also been recently used in maxillofacial fracture surgery and implant planning as well as in orthognathic surgery (Park, Choi, Koh, & Oh, 2015; Steinbacher, 2015). The use of 3D has also increased in dentistry and many other fields of medicine (Chen, C. et al., 2019; Dawood, Marti Marti, Sauret-Jackson, & Darwood, 2015; Giannopoulos et al., 2016). Due to the very complex anatomy of the nasal cavity and paranasal sinuses, however, the 3D technique has been used significantly less in the field of rhinology.

Although imaging methods and outpatient tests are widely used, there is a lack of strong correlation between traditional visual imaging results, outpatient tests and patients' experience of nasal symptoms, especially nasal congestion (Kim, C. S., Moon, Jung, & Min, 1998). Therefore, a more comprehensive understanding of the conditions in the nasal cavity and the paranasal sinuses is required. The 3D modelling of the nasal cavity and the airflow conditions could provide this missing information and lead to better correlations between objective measurements and the subjective experience of the patient.

In recent years, experimental enhancements of the sinonasal clinical CT scans, and to some extent MRI scans, have been published. These enhancements have included the manufacture of 3D prints of the nasal cavity for PIV measurements (Hopkins, L. M., Kelly, Wexler, & Prasad, 2000; Spence, Buchmann, Jermy, & Moore, 2011) and presentations of nasal airflow models based on CFD calculations (Chen, X. B., Lee, Chong, & Wang de, 2010; Na, Chung, Chung, & Kim, 2012). However, these studies are often based on single experimental models or single phantoms. In addition, the studies have often been performed without any comparison to the existing clinical assessment methods of nasal cavity conditions. Furthermore, previous studies have mainly concentrated on using traditional CT scans rather than using the widely used CBCT imaging which, although producing less accurate image quality than traditional CT, is known to cause a lower radiation burden to patients. To date, the full potential of CT as the basis for 3D measurements and modelling as well as for PIV measurements and CFD calculations has not yet been comprehensively studied.

This dissertation summarizes the current knowledge of imaging rhinologic patients and the enhanced use of the imaging modalities for 3D modelling and printing as well as for further tests and analyses with PIV and CFD. The studies in this dissertation compare these enhanced image utilization methods to current clinical assessment methods of a rhinologic patient.

2 REVIEW OF THE LITERATURE

2.1 Anatomy and physiology of the nose and paranasal sinuses

2.1.1 Anatomy of the nose and paranasal sinuses

The nose forms part of the upper airway structures located in the midline of the head. It serves as the first organ of the respiratory system and, additionally, functions as the olfactory organ. It is composed of the outer part and the inner structures. (Netter, 2018)

The main body of the outer part of the nose is formed by bony and cartilaginous structures. The most anterior parts of the nose are made up of the septal, lateral, major alar and minor alar cartilages accompanied by alar fibro fatty tissue. The most upper part of the nose is formed by the nasal part of the frontal bone. This is followed anteriorly by the nasal bones and at the sides of these the lacrimal bones. These, in turn, are then flanked on both sides by the frontal processes of each maxilla.

The inner structures of the nose are composed of the nasal cavity and the paranasal sinuses. The nasal cavity itself is divided into left and right sides by the nasal septum. In its anterior half, the septum is formed by septal cartilage, after which the septum continues with two osseous structures: the vomer bone below and perpendicular plate of the ethmoid bone at the top. The roof of the nasal cavity is a combination of the horizontally positioned cribriform plate of the ethmoid bone at the front and sloping down at an angle the anterior wall of the sphenoid sinus posteriorly and inferiorly. The floor of the nasal cavity is divided into hard and soft palate. The hard palate is composed of the incisive bone and the horizontal plates of the palatine bones. The soft palate, posterior to the hard palate, is composed of the uvula and four muscles under the mucous membrane: tensor veli palatini, palatoglossus, palatopharyngeus and levator veli palatini.

Within both sides of the nasal cavity, three shell-like bones protrude from the lateral walls of the cavity. These bones are called the inferior, middle and superior nasal turbinates. These structures form three passages: the inferior, middle and

superior meatuses. It is possible to identify a rare variant of the fourth nasal turbinate, the Santorini's turbinate, in the posterosuperior aspect of the lateral wall close to the lateral margin of the sphenoid sinus ostium. (von Arx, Lozanoff, & Bornstein, 2019)

On both sides, the nasal cavity is accompanied by paranasal sinuses that are called the maxillary, ethmoid, frontal and sphenoid sinuses. These air-filled extensions of the nasal cavity are located inside the cranial bones of the same name. All the paranasal sinuses have openings, called sinus ostia, to the nasal cavity. Of these, the maxillary sinus, frontal sinus and anterior ethmoid sinus ostia open and drain to the middle meatus under the middle nasal turbinate and form a structure called the ostiomeatal complex. The posterior ethmoid and sphenoid sinuses open and drain to a space called the sphenoethmoidal recess that is situated posterior and superior to the superior turbinate. In some cases, a few posterior ethmoid sinuses can also have ostia to the sphenoid sinus. Anatomical variants of the ethmoid sinuses include agger nasi, Haller's cell, Onodi cell and ethmomaxillary sinus.

In addition to the paranasal sinuses, an opening of the nasolacrimal duct is bilaterally present in the inferior meatuses under the inferior turbinates. Moreover, on both sides of the posterior region of the nasal cavity and the upper region of the nasopharynx, there are openings to the Eustachian tube, which function as an air canal between the nasopharynx and the middle ear.

2.1.2 Vascular supply and innervation

Vascular supply to the nasal cavity and the paranasal sinuses is covered from both the internal and external carotid artery. A branch of the internal carotid artery, the ophthalmic artery, supplies both the anterior and posterior ethmoidal arteries. Two branches of the external carotid artery, maxillary and facial arteries, provide the main blood supply to the nose and the paranasal sinuses. The maxillary artery mainly provides blood circulation via the sphenopalatine, infraorbital and descending palatine arteries. The facial artery channels blood to the nose via the superior labial and lateral nasal arteries. Venous blood drainage passes through the facial vein, which collects venous blood from the supratrochlear and supraorbital veins. (Netter, 2018)

The sensory innervation of the nasal cavity and the paranasal sinuses is provided by two main branches of the trigeminal nerve: the ophthalmic and maxillary nerves (Netter, 2018). The ophthalmic nerve branch that innervates the nasal cavity and the

paranasal sinuses is called the nasociliary nerve, which forms a further branch called the posterior ethmoidal nerve. The maxillary branches are called the nasopalatine nerve and the posterior nasal branches of the maxillary nerve. The nociceptive sensation in the nasal mucosa is innervated by the rapid, thinly myelinated Aδ fibres, while the delayed-onset but more prolonged pain sensation is innervated by the unmyelinated type C fibres (Tai & Baraniuk, 2002). The nasal cavity also contains olfactory nerve endings in the roof of the nasal cavity.

The sensory nerves of the mucous membrane surface have also been found to contain receptors which possibly have a role in forming the sensation of temperature and the level of patency in the nose. Of these, the transient receptor potential cation channel subfamily melastatin member 8 (TRPM8), also called the cold and menthol receptor, has been shown to be the most abundant in nasal mucosa (Keh et al., 2011). Additionally, TRPM8 can be activated by menthol, and thus causes a sensation of cool and decongestion in the nose, although no objective changes in the structures or function of the nasal cavity can be detected (Eccles & Jones, 1983; Liu, S. C. et al., 2015).

The nasal cavity is also innervated by both parasympathetic and sympathetic postganglionic nerve fibres. In the nasal cavity, the activation of parasympathetic innervation increases the secretion from the mucous glands and, at the same time, causes vasodilation in the arteries, arteriovenous anastomoses and veins. Thus, this activation, in part, leads to a runny nose and nasal congestion. In turn, the activation of the sympathetic innervation causes vasoconstriction in the arteries, arterioles and veins of the nasal cavity, and thus leads to the contraction of the mucous membrane and increased nasal patency. (Beule, 2010; Sarin, Undem, Sanico, & Togias, 2006)

2.1.3 Mucous membrane and soft tissues

The 0.3 mm to 5 mm thick mucous membrane of the nasal cavity and the paranasal sinuses, also called nasal mucosa, is mainly composed of ciliated pseudostratified columnar respiratory epithelium, as it forms part of the respiratory tract's respiratory mucosa. Respiratory epithelium covers up to 70% of the nasal mucosa epithelium. The uppermost part of the nasal cavity in the region of the cribriform plate, however, is composed of olfactory epithelium as it functions as part of the olfactory system. Between 5% and 15% of the nasal mucosa epithelium is composed of goblet cells which, together with submucosal glands, produce secretions of endonasal mucus. Three main types of submucosal glands can be identified: anterior serous glands,

seromucous glands and Bowman's glands. The submucosal glands are found mainly in the anterior part of the nasal cavity, but the Bowman's glands are located in the olfactory epithelium. The nasal mucous membrane lies on its basal membrane. The deep part of the nasal cavity mucous membrane in the inferior turbinates contains venous sinusoids supplied by arteriovenous anastomoses. These arteriovenous anastomoses are regulated by the balance between parasympathetic and sympathetic innervation. (Beule, 2010) Similar deep mucous membrane structures containing venous sinusoids can, to some extent, be also found in the middle turbinates and in the area of the nasal septum called the intumescentia septi nasi anterior (Moss, Faraji, Jafari, & DeConde, 2019; Ng, Ramsey, & Corey, 1999).

2.2 Physiology of the nose and paranasal sinuses

2.2.1 Main functions

The nose has several important functions in the human body in addition to being part of the facial appearance. First, it functions as one of the breathing routes alongside the oral route and also affects upper airway airflow dynamics. Second, inhaled air is warmed and humidified as it passes through the nasal cavity and the paranasal sinuses. Furthermore, during exhalation, the nasal cavity condensates water from the exhaled air, and thus saves the body's water resources (Dahl & Mygind, 1998). The nasal cavity also functions as a defence and filtration mechanism against excess particles and pathogens in the inhaled air. The nose has the ability to sense different chemical substances and temperatures, which can lead to protective sneezing or nasal secretion. (Jones, N., 2001; Naclerio, Pinto, Assanasen, & Baroody, 2007)

Olfaction is made possible by the roof of the nasal cavity containing the olfactory bulb. It has been estimated that human olfaction is theoretically able to identify more than 10 000 structurally distinct odorous ligands, and the odorant receptors have been found to be encoded by a large multigene family (Buck & Axel, 1991). In addition, the paranasal sinuses have been found to function as the producers and reservoirs of nitric oxide (NO) which has been proposed to function as an aerocrine messenger (Jankowski et al., 2016).

2.2.2 Immune system mechanisms

The nose plays a significant role in being one of the first lines of defence against the surrounding environment (Fokkens & Scheeren, 2000; Hariri & Cohen, 2016). The nasal cavity and the paranasal sinuses clean particles from the respiratory air using mucociliary function and the consistency of the respiratory mucus as the first line of defence (Becquemin, Swift, Bouchikhi, Roy, & Teillac, 1991). Particles larger than 4 μm to 15 μm in diameter are absorbed before the posterior nasopharynx by the cilia and the above mucus layer. After this, the cilia, which beat approximately 1000 times per minute, transport the particles along with the mucus layer at a pace of 3 mm to 25 mm per minute towards the posterior nasopharynx, where it is swallowed. (Baraniuk & Merck, 2009; Beule, 2010)

The second layer of defence in the nose comprises innate cellular and humoral defences, which can be further divided into non-specific and specific defence mechanisms (Fokkens & Scheeren, 2000; Hariri & Cohen, 2016). Cellular defence mechanisms include granulocytes and macrophages as a non-specific mechanism and lymphocytes as a specific mechanism. Humoral defence mechanisms are based on proteins and immunoglobulins. More specifically, the humoral non-specific immune mechanism is based on proteins, such as complement, lysozyme, lactoferrine, defensins and cathelicidins. The immunoglobulins IgA and IgG (IgG1-IgG4) function as a specific humoral immune defence mechanism. In addition, reactive oxygen and nitrogen species, for example, nitric oxide (NO) produced in the paranasal sinuses and mainly in the maxillary sinuses, have been suggested to have a role in the inflammatory processes in the nasal cavity and the paranasal sinuses (Maniscalco, Sofia, & Pelaia, 2007; Sahin et al., 2011).

Previous studies have shown that the regulation of the activation of the innate immune defence mechanism in the nose is controlled by toll-like receptors (TLR1-11), which recognise microorganisms (Parker & Prince, 2011). In addition, the extraoral bitter taste receptor family (T2R) and sweet taste receptor family (T1R), also found in the upper airways, have been found to play a role in controlling the immune response (Lee, R. J. & Cohen, 2015). A subtype of the T2R receptors, T2R38, has also been shown to regulate mucociliary clearance (Lee, R. J. et al., 2012).

2.2.3 Vascular and erectile tissue in the nasal cavity

Erectile tissue is mainly present in the inferior nasal turbinate mucous membrane, which encases venous sinusoids deep in the mucosa (Baraniuk & Merck, 2009).

Blood is supplied to these structures by arteriovenous anastomoses. The main arteries carrying blood to these anastomoses are the posterior lateral nasal artery branching from the sphenopalatine artery (Lee, H. Y. et al., 2002; MacArthur & McGarry, 2017) and the descending palatine artery branching from the maxillary artery (Scott, Psaltis, & Wormald, 2020). The venous sinusoids give the inferior turbinate mucosa the ability to swell and contract, causing the variability of the cross-sectional area of the air space in the nasal cavity. This variability affects the airflow passing through the nasal cavity, and thus affects the sensation of nasal patency and congestion. Similar erectile tissue is, to some extent, also present in the middle turbinates and in an area in the nasal septum called the nasal septal turbinate or the intumescentia septi nasi anterior (Moss et al., 2019; Ng et al., 1999).

It has been suggested that potential vasodilators, such as calcitonin gene-related peptide, histamine, bradykinin, leukotrienes and prostaglandins, may increase the blood supply to the venous sinusoids and lead to inferior turbinate swelling. Possible vasoconstrictors that cause the opposite effect in the inferior turbinates are neuropeptide tyrosine, norepinephrine and endothelins. (Baraniuk & Merck, 2009)

2.2.4 The nasal cycle

The mucous membrane in the nose has been observed to carry out a somewhat rhythmic procedure called the nasal cycle. During this cycle, the mucous membrane in one side of the nasal cavity is swollen, while the other side has more air space due to contracted nasal mucosa. The circumstances are then switched vice versa every 2-3 hours. During this phenomenon, the bilateral nasal resistance remains approximately constant (Eccles, 2000; Hasegawa & Kern, 1977). Previous studies have proposed that the hypothalamus functions as the central rhythm provider for the nasal cycle (Eccles, 2000) and the asymmetry and reciprocal changes are controlled by two brainstem half-centre oscillators (Williams & Eccles, 2016).

In a previous study, it has been summarised that the proposed purposes of the nasal cycle are to provide rest and to recharge the nasal mucosa cells and glands, to control the balance of the fluxes of heat and water vapour required to condition the inhaled air and to function as a coping mechanism for the anterior airways against the conflicting states of airway surface liquid hydration (White, Bartley, & Nates, 2015). The effects of the nasal cycle on nasal mucosa are the most noticeable in the inferior turbinates, but the effects can, to some extent, also be seen in the nasal

septum, the middle turbinate and even in the paranasal sinuses (Kennedy, Zinreich, Kumar, Rosenbaum, & Johns, 1988).

2.2.5 Nasal airflow and its regulation

The airflow and the amount of air that moves through the nasal cavity depends on several factors. The anatomy of the nasal cavity and, in addition, the region of the nasal valve form the structural limits for the amount of airflow that can move through the nasal cavity. The airflow change from the surrounding air through the nasal valve region to the wider nasal cavity areas causes almost half of the total airflow resistance to the lungs. Moreover, the changes in nasal mucosa, most often due to the nasal cycle, further regulate the airflow in the nasal cavity. (Baraniuk & Merck, 2009)

In calm breathing, the main breathing route is through the nose, but in more forceful breathing the main route is changed to go via the mouth. During calm breathing, the normal breathing rate is approximately 12 times per minute with a tidal volume of 0.5 l which results in a total breathing volume of close to 12 l/min (Eccles, 2000). In calm breathing, the airflow moving through the nasal cavity is considered to be mostly laminar. However, the pressure-flow relationship in the nasal cavity during breathing phases has been shown to be more curvilinear than linear and, due to this, it has been suggested that the airflow is not purely laminar but actually a mixture of turbulent and orifice flow (Eccles, 2000; Wheatley, Amis, & Engel, 1991). The turbulence of the airflow is more prominent when breathing rates are increased, for example, during physical activity or sniffing. In these circumstances, the airflow is considered to be turbulent.

2.3 Symptoms of a rhinologic patient

Nasal congestion is described as a patient's experience of insufficient airflow through the nose and/or a sense of facial fullness. The mechanisms causing these non-specific symptoms are mucosal inflammation, abnormalities in the nasal cavity structure and/or sensory perception modulation in the nasal mucosa intermediated by the trigeminal nerve branches. Different causes of nasal congestion are, for example, acute and chronic rhinosinusitis, allergic and nonallergic rhinitis, nasal

polyposis, turbinate hypertrophy, septal deviation, concha bullosa, adenoid hypertrophy and neoplasia. (Naclerio, Bachert, & Baraniuk, 2010)

Other symptoms that rhinologic patients often experience, in addition to nasal congestion, are nasal discharge, loss of sense of smell and facial pain. These are considered to be the primary symptoms of rhinosinusitis. Moreover, these symptoms can be accompanied with different secondary symptoms, such as sneezing, cough, sore throat, voice changes, epiphora, fever and fatigue. (Eccles, 2011b)

2.4 Examination of a rhinologic patient

2.4.1 Objective methods

2.4.1.1 Patient history and status

The examination of a rhinologic patient includes an encompassing anamnesis in order to fully understand the nature of the illness behind the symptoms. Typical symptoms of acute and chronic rhinosinusitis often include bilateral nasal congestion, facial stuffiness or pain, rhinorrhoea, postnasal drip, sneezing and fever. Patients with allergic symptoms often have these similar symptoms enhanced with itchy red eyes, watery eyes and swollen eyelids. Nonallergic rhinitis or vasomotor rhinitis often mimics allergic rhinitis, although the inflammation in the nasal mucosa in this case is caused by, for example, spicy food, hormonal changes during pregnancy or temperature changes. The prolonged or excess use of topical decongestants can lead to rhinitis medicamentosa, which causes similar symptoms.

Continuous unilateral nasal congestion without other typical rhinosinusitis symptoms is a possible sign of nasal cavity blockage due to septal deviation, turbinate hypertrophy, nasal polyposis or tumour. Further, the unilateral leak of clear liquid from the nasal cavity could be a sign of a liquor fistula in the roof of the nasal cavity. A history of head or nasal trauma can support the possibility of a liquor fistula.

Careful assessment of the clinical status of a rhinologic patient consists of anterior rhinoscopy and mirror aided posterior rhinoscopy. Nasendoscopy of the nasal cavity with either a rigid or flexible endoscope is also performed.

For a more comprehensive examination, X-rays or MRI can be used. In order to achieve good perception on the bony structures and a coarse but often adequate resolution on the soft tissues of the nasal cavity, imaging modalities using X-rays,

such as conventional CT and CBCT, are chosen nowadays. If better resolution is needed to study the bony and especially the soft tissues, MRI is used. (Fokkens et al., 2020) A more encompassing description of the different imaging modalities can be found in chapter 2.5.

In assessing the resistance and dimensions of the nasal airway, rhinomanometry and acoustic rhinometry are among the most used outpatient methods. These methods are comprehensively discussed in chapters 2.4.1.2 and 2.4.1.3. Less frequently used outpatient methods for nasal patency assessment include peak nasal inspiratory flow (PNIF) measurement, which is a direct measurement method to measure nasal airflow during inspiration using a Youlten peak flow meter (Holmström, Scadding, Lund, & Darby, 1990). The method consists of using a portable inspiratory flow meter and a tight-fitting anaesthetic mask. During the measurements, the patients are asked to keep their mouth closed while inhaling via the nose as fast and as forcefully as possible through the mask. The highest flow rates measured by the flow meter in litres per minute are then recorded.

Peak nasal expiratory flow (PNEF) measurement, a method that precedes PNIF, uses a Wright's mini peak flow meter from which the Youlten peak flow meter was developed (Wright, 1978). Both PNIF and PNEF methods have been previously studied to find out possible potential for diagnostics and follow-up of nasal diseases in primary care but the methods did not show sufficient practicality or repeatability (Blomgren, Simola, Hytönen, & Pitkäranta, 2003). Other previous and rarely used rhinometric methods are rhinostereometry (Juto & Lundberg, 1982), forced oscillation (Lorino et al., 1998) manometric rhinometry (Porter, Williamson, Kerridge, & Maw, 1995) and nasal spirometry (Harar, Kalan, & Kenyon, 2001).

2.4.1.2 Rhinomanometry

Rhinomanometry is used to quantitatively measure nasal airway resistance, and thus assess nasal patency. The most commonly used method of rhinomanometry is active anterior rhinomanometry. In this method, the patient is actively breathing through one side of the nasal cavity while, at the same time, the pressure difference and airflow rate in inspiration and expiration between the posterior and anterior parts of the contralateral nasal air route is measured with a sensing tube inserted in to the nostril with an airtight seal (Clement, Gordts, & Standardisation Committee on Objective Assessment of the Nasal Airway, IRS, 2005; Eccles, 2011a). The measurements are performed separately for both sides of the nasal cavity and the results are presented in a diagram of the pressure flow curve (Figure 1).

Another anterior method is passive anterior rhinomanometry. In this method, the pressure is separately measured from each nasal cavity at a given airflow of 250 cm^3/s. A third method that measures the pressure difference between the anterior and posterior nasal regions and also the pressure difference in the nasopharynx is posterior rhinomanometry. This method uses a test tube which is placed in the mouth and the airflow of both sides of the nasal cavity is measured simultaneously. (Clement et al., 2005; Eccles, 2011a)

Rhinomanometry is mainly used to assess anatomical (Pirilä & Tikanto, 2009) and mucosal (Ciprandi, Cirillo, Vizzaccaro, Pallestrini, & Tosca, 2006) nasal obstruction prior to treatment decisions. In study settings, rhinomanometry has also been used before and after medical or operative treatment to assess treatment results (Bizaki, Numminen, Taulu, & Rautiainen, 2016; Haavisto & Sipilä, 2013; Thulesius, Cervin, & Jessen, 2014). However, rhinomanometric measurements have not been shown to correlate with patients' symptoms of nasal congestion or changes in them (Kim, C. S. et al., 1998).

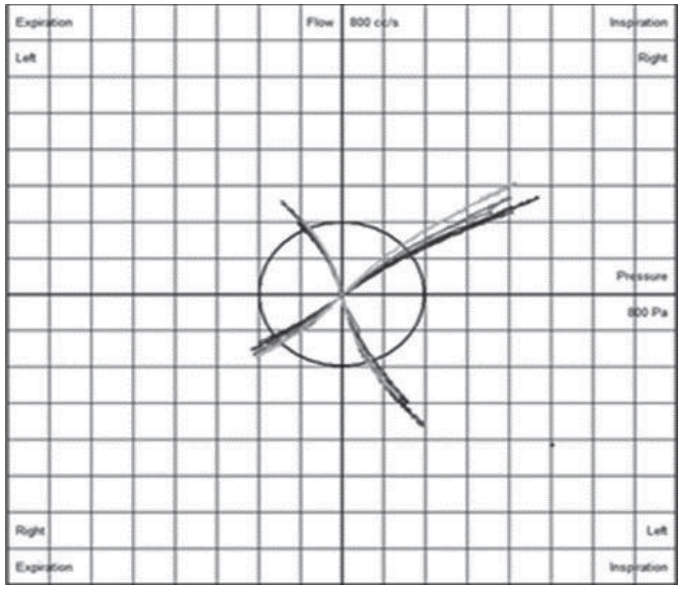

Figure 1. Standard presentation of active anterior rhinomanometry results. Airflow rate is presented in the y axis and pressure difference in the x axis. Inspiratory and expiratory results on the left and right nasal cavities are presented in the opposite quadrants of the graph.

2.4.1.3 Acoustic rhinometry

Acoustic rhinometry is a method used to assess the cross-sectional area and volume of the nasal cavity as a function of the distance from the nostrils into the nasal cavity using acoustic reflections (Clement et al., 2005). In this method, the test device creates an acoustic pulse which is transmitted to the nose via a tube. The pulse is then reflected back to a microphone according to the changes in the local acoustic impedance associated with the cross-sectional area of the nasal cavity. The acquired reflections are then analysed using computer software and processed to create a graph of the area and distance. This method provides clinicians with a two-dimensional estimate of the dimensions of the nasal cavity. Moreover, the method is non-invasive, fast to carry out and requires only a limited amount of co-operation from the patient.

Acoustic rhinometry, first described by Hilberg et al. (1989), is mainly used in the pre-treatment assessment of the nasal cavity and as support for clinical decision-making. Nowadays, the repertoire of both the clinical problems that are analysed with acoustic rhinometry and its clinical pre-operative use covers, for example, turbinoplasty, septal deviation, sinus surgery, nonallergic rhinitis and sleep disorders (Corey, 2006). The method has also been performed prior to and after medical or operative treatment in order to study the results of the given treatment (Bizaki et al., 2016; Harju, Numminen, Kivekäs, & Rautiainen, 2018; Ragab, Lund, & Scadding, 2004).

Acoustic rhinometry has been found to be reliable in measuring the anterior nasal cavity diameters. However, when it comes to the middle and posterior regions of the nasal cavity, the measurements overestimate the diameters significantly. In a previous study, the cross-sectional area measurements between acoustic rhinometry and CT measurements correlated well in the anterior nasal cavity regions with a mean error of 4.5%. In the posterior regions, however, the mean error of the acoustic rhinometry was more than twice that of the measurements from CT scans (Terheyden, Maune, Mertens, & Hilberg, 2000). Similar results have been reported in other studies (Hilberg et al., 1989; Numminen, Dastidar, Heinonen, Karhuketo, & Rautiainen, 2003). In addition, according to a study by Cankurtaran et al. (2007), acoustic rhinometry can overestimate the volume of the nasal cavity by more than 20%. Furthermore, when compared to patients' subjective symptoms of nasal congestion and changes in them, acoustic rhinometry has not shown correlative results (Kim, C. S. et al., 1998).

2.4.2 Subjective measurements

2.4.2.1 Visual analogue scale

The visual analogue scale (VAS) is used in questionnaires to study the psychometric responses of patients. The scale measures a patient's subjective experiences, which cannot be directly measured. VAS uses a continuous 10 cm horizontal line and a scale from 0 to 10 between the two end-points. The end-points represent the extremes of the measured feeling.

Today, VAS is one of the most common scales used to assess the level of pain (Williamson & Hoggart, 2005). The scale has been found to be highly effective and relatively simple to use (Klimek et al., 2017). Moreover, according to the findings of previous studies, the VAS scale has been found to be highly reliable in the assessment of acute pain (Bijur, Silver, & Gallagher, 2001) and the pain experienced by patients with osteoarthritic knee (Alghadir, Anwer, Iqbal, & Iqbal, 2018), the VAS scale has been found to be highly reliable. In rhinologic patients, it is recommended that the VAS scale be used in the subjective assessment of the severity of symptoms (Fokkens et al., 2020).

2.4.2.2 Sino-nasal outcome test 22

The 22-item sinonasal outcome test (SNOT-22), first validated in 2009, is a disease-specific health related questionnaire used to assess the quality of life of patients with chronic rhinosinusitis (CRS) (Hopkins, C., Gillett, Slack, Lund, & Browne, 2009). It is the most modern version of the SNOT questionnaires and contains 22 questions covering different CRS symptoms and health related quality of life problems. Each question has an answer scale from 0 to 5 representing the severity of each problem. In total, the questionnaire gives points from 0 to 110, which can be used to reflect the severity of CRS. The use of SNOT-22 is included in the guidelines concerning the examination of patients with CRS and has been shown to be the best pre-operative predictor of sinus surgery outcome (Fokkens et al., 2020). When used to compare the severity of CRS symptom in a timespan or pre- and posttreatment results, the minimal important change has been found to be approximately 9 points (Hopkins, C. et al., 2009). The SNOT-22 questionnaire has also been recently validated in Finnish (Koskinen et al., 2021).

2.4.2.3 Other subjective measurement methods

Along with the SNOT-22 questionnaire, the Questionnaire of Olfactory Disorders (QOD) and the Sinusitis Control Test (SCT) were reported to have provided the highest quality CRS-specific symptom assessment in a systematic review (Rudmik et al., 2015). The same review along with another study (Remenschneider et al., 2015) found the EuroQol 5 Dimension (EQ-5D) questionnaire to be a high-quality method for assessing the general quality of life of patients with CRS. Another general health related quality of life questionnaire used in CRS studies is the Medical Outcomes Study Short Form-36 (SF-36), which has been mainly used in a descriptive instrument role but also to some extent in economic valuations (Remenschneider et al., 2015).

Nasal congestion severity can be assessed with the Nasal Obstruction Symptom Evaluation (NOSE) questionnaire (Stewart et al., 2004). The NOSE questionnaire has been shown to have good correlation with VAS results, and it has been reported to be effective in evaluating nasal surgery responses (Shukla, Nemade, & Shinde, 2020). The all-purpose, health related quality of life questionnaires designed for otorhinolaryngologic conditions, the Glasgow Benefit Inventory (GBI) as a change questionnaire and the Glasgow Health Status Inventory (GHSI) as a state questionnaire, have also been widely used (Hendry, Chin, Swan, Akeroyd, & Browning, 2016; van Egmond, M M H T, van Heerbeek, Ter Haar, E L M, & Rovers, 2017).

2.4.3 Treatments

2.4.3.1 Intranasal medical treatments

The most used topical decongestants are xylometazoline and oxymetazoline. These are imidazole derivative medication molecules which mimic the molecular shape of adrenaline. They can therefore bind to the adrenergic receptors (α_1 and α_2) of the lamina propria of the blood vessels in the nasal mucosa and function as α-adrenoceptor agonists. They then cause the blood vessels to constrict, which leads to a reduction in swelling of the nasal mucosa (Haenisch et al., 2010). Xylometazoline or oxymetazoline-based nasal sprays are commonly used to ease the symptoms of nasal congestion caused by the common cold, rhinosinusitis and allergic rhinitis. However, it is recommended that the role of topical decongestants are limited to

being a short-term additional treatment option in treating nasal congestion (Fokkens et al., 2020). Furthermore, prolonged use of topical decongestants can lead to rebound congestion, also called rhinitis medicamentosa (Ramey, Bailen, & Lockey, 2006).

Intranasal corticosteroids are used in the form of nasal sprays to reduce the inflammation in the nasal mucosa. They are used in medical conditions, such as chronic rhinosinusitis, nasal polyposis and allergic rhinitis, to ease rhinorrhoea, nasal congestion, sneezing and nasal itching (Fokkens et al., 2020; Trangsrud, Whitaker, & Small, 2002). The most commonly used intranasal corticosteroids are mometasone and fluticasone (Bensch, 2016). Intranasal corticosteroids have been proven to be safe to use for many intranasal medical conditions, although prolonged or misuse of these substances can have a role in causing adverse events, such as epistaxis, nasal irritation or septal perforation (Bensch, 2016).

2.4.3.2 Surgical treatments

The surgical treatment of a rhinologic patient varies according to the underlying reasons behind the nasal symptoms. The decision to use surgical procedures for rhinologic patients is usually made after unsuccessful medical treatment or due to the presence of clear structural causes. For example, after topical or systematic treatments, a variety of endoscopic sinus surgery procedures can be performed when treating CRS with or without nasal polyposis (Fokkens et al., 2020). Nowadays, the surgical procedure performed varies from widening only the maxillary sinus ostia operatively or with balloon sinuplasty, when treating moderate CRS, to the comprehensive surgical opening of all the paranasal sinuses and, if needed, removal of the excess soft tissues in cases of severe CRS with widespread polyposis.

The presence of structural deviations or other structures that narrow the air space can be operated individually or as an auxiliary operation to paranasal sinus operations. Typical examples of structural causes of nasal discomfort in adult patients are septal deviation and inferior turbinate hypertrophy. Nasal septal deviation can be congenital by nature or caused by trauma. If the deviation causes apparent nasal breathing problems, septoplasty can be performed to straighten the septum and widen the nasal passage (Most & Rudy, 2017).

Inferior turbinate surgery can be performed in different ways. One of the most commonly used ambulatory and mini-invasive methods is radiofrequency thermal ablation (Li, Powell, Riley, Troell, & Guilleminault, 1998). The method can be performed under local anaesthesia, does not require nasal packing, is suitable for out-

patient clinics and can be repeated if necessary (Bäck, Hytönen, Malmberg, & Ylikoski, 2002). Other possible mini-invasive inferior nasal hypertrophy operations include laser cautery, cryocautery, electrocautery and the fairly new but somewhat more invasive microdebrider-assisted inferior turbinoplasty (MAIT) (Willatt, 2009). For all mini-invasive inferior turbinate operations, it is common that the benefits of the surgery are often ceded in several years of follow-up (Janda, Sroka, Baumgartner, Grevers, & Leunig, 2001; Liu, C. M., Tan, Lee, Lin, & Huang, 2009; Passàli, Passàli, Damiani, Passali, & Bellussi, 2003; Sinno et al., 2016). Additionally, different inferior turbinate surgery techniques have been shown to be equally efficient in reducing inferior turbinate volume (Harju et al., 2018). The more invasive inferior turbinate hypertrophy operations include outfracture, partial turbinectomy and total turbinectomy techniques. However, these operations are rarely used nowadays and have been replaced by less invasive operative methods (Sinno et al., 2016; Willatt, 2009).

2.5 Imaging in rhinology

2.5.1 In general

Sinus X-ray represents the oldest method used for the imaging of the anatomy of the nasal cavity and the paranasal sinuses. Nowadays, imaging modalities used to examine rhinologic patients include different applications of CT and to some extent MRI. Both of these imaging methods provide scans in three plains: coronal, axial and sagittal. CT modalities are the mainstream of rhinology imaging, providing good information on the bony structures and drainage pathways. MRI scans are mainly used to evaluate tumours and examine infectious processes that have extended beyond the paranasal sinuses into proximate soft tissues. (Fatterpekar et al., 2008)

In clinical use, the anatomy of the nasal cavity and the paranasal sinuses are traditionally assessed from consecutive 2D scans in different planes produced by CT modalities (Figure 2) or MRI. This requires good perception from the clinicians, as the actual 3D anatomy of the nasal cavity and the paranasal sinuses is very complicated. In addition, perceiving the relation of different sinonasal structures and drainage routes from scans can be challenging. This has led to the development of different methods aimed at improving 3D perception of the anatomy and for surgery planning. For instance, a building block method (Wormald, 2005) has been

introduced to ease the perception of the frontal sinus drainage pathway and to help surgery planning. Moreover, image guided surgery has been widely used in sinonasal surgery to help navigate in the most complex anatomical conditions, especially in secondary or tertiary operations in the nasal cavity (Prulière-Escabasse & Coste, 2010).

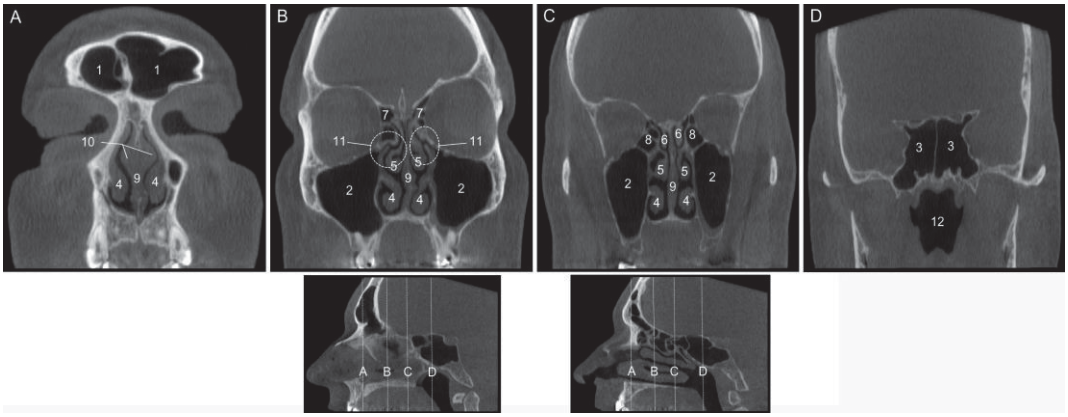

Figure 2. Radiological nasal cavity anatomy in CT scans. Above: four coronal planes from anterior to posterior, below: two sagittal planes from the septal midline (left) and nasal cavity midline (right) with lines representing the locations of the coronal planes above (A-D). 1=frontal sinuses, 2=maxillary sinuses, 3=sphenoid sinuses, 4=inferior turbinates, 5=middle turbinates, 6=superior turbinates, 7=anterior ethmoid sinuses, 8=posterior ethmoid sinuses, 9=nasal septum, 10=intumescentia septi nasi anterior, 11=ostiomeatal complex, 12=nasopharynx.

2.5.2 Sinus X-ray

First described by Schüller in 1905 and later studied and improved by Waters in 1915 and by Caldwell in 1918, the sinus X-ray was the first clinical method used for imaging the paranasal sinuses (Burke et al., 1994). Sinus X-ray is a cheap and very simple transillumination method for imaging the nasal cavity and the paranasal sinuses. However, this imaging method only provides a single plain-film radiography image of the skull in which the nasal cavity and the paranasal sinuses are shown one upon the other. There are four commonly used projections in sinus X-ray imaging: anteroposterior view at a 15º angle (Caldwell view), occipitomental (Waters view), and lateral and submental vertex views (Yousem, 1993). Sinus X-rays are, to some extent, still used in primary healthcare, although studies have shown that this method

is less sensitive in demonstrating radiological changes in acute rhinosinusitis when compared to CT scans (Burke et al., 1994). Moreover, the routine use of sinus X-ray is no longer recommended in diagnosing acute rhinosinusitis (Marple, Brunton, & Ferguson, 2006).

2.5.3 Computed tomography

CT is an imaging technique that uses X-rays to produce multiple topographical slices of the scanned body parts. During this procedure, the patient is placed in a supine position on a motorized table which is moved according to the scanning protocol. Simultaneously, a source of X-rays, producing a fan-shaped X-ray beam, is rotated within a circular opening while a set of X-ray detectors are rotated in synchrony on the far side of the patient. The beam width ranges from 1 mm to 20 mm. Modern CT machines, called multidetector CT (MDCT) scanners, have multiple adjacent rows of detectors (up to 64) in order to produce multiple images simultaneously, and thereby reducing overall scanning time. After scanning, the information acquired by the detectors is then moved to a processing computer to produce multiple consecutive image slices, representing the scanned body part. (Brenner & Hall, 2007) The image data are collected and presented by the CT imaging system in an axial plane. The other two planes, coronal and sagittal, are produced afterwards by a radiologist. Different tissues, fluids and air space in CT scans are presented with gray scale images based on a quantitative radiodensity descriptive scale called the Hounsfield scale. In this scale, different tissues and air have different gray scale values called the Hounsfield units (HU).

CT scanning is performed using either the axial or helical CT method. Axial CT is commonly used for head scans and helical CT is typically used for body scans. In axial CT, the patient table is stationary during a scanning rotation. Thereafter, it is moved along for the next slice. Helical CT is performed by continuously moving the table while the X-ray source and the detectors rotate, producing a spiral or helical scan. (Brenner & Hall, 2007)

2.5.3.1 Computed tomography in rhinology

Traditional, also called standard or clinical, CT imaging in rhinology uses the axial CT imaging method, as described in section 2.5.3. This method provides accurate image data of the anatomy of the nasal cavity and the paranasal sinuses. The imaging

region includes approximately an area that ranges anteroposterior from the tip of the nose to the mid regions of the vertebrae and superoinferior from the level of the upper teeth to the level of the upper margin of the frontal sinuses.

CT imaging has been the gold standard of nasal cavity and paranasal sinus imaging since the 1990s (Abul-Kasim, Strömbeck, & Sahlstrand-Johnson, 2011). CT imaging is recommended to be used as part of the diagnosis of nasal cavity and paranasal sinus pathologies after proper clinical examination and case-by-case consideration (Fokkens et al., 2020; Jones, N. S., 2002). Although good resolution of the bony and soft tissue structures is achieved with CT imaging, radiation exposure to the patient has to be taken into account. In a previous study, the mean effective radiation dose of standard paranasal MDCT scans in paranasal imaging was 0.48 mSv, whereas the effective radiation dose of low-dose MDCT was 0.39 mSv (Al Abduwani, ZilinSkiene, Colley, & Ahmed, 2016). In another study, an effective sinonasal radiation dose as low as 0.078 mSv was experimentally achieved by low-dose MDCT, which in this study setup proved to be ten times smaller than in a standard CT protocol (Fraczek, Guzinski, Morawska-Kochman, & Krecicki, 2017).

2.5.3.2 Cone beam computed tomography

CBCT was introduced during the late 1990s, and it was first used in dental imaging (Arai, Tammisalo, Iwai, Hashimoto, & Shinoda, 1999; Mozzo et al., 1998). Nowadays, CBCT imaging is widely used for the imaging of the oral and maxillofacial regions. This imaging technique is based on the principle of a moving X-ray source and a detector method, as in clinical CT, but the difference is that a round or rectangular cone shaped X-ray beam with a single 360° scan is used. CBCT devices usually use a rotation arc or C-arm to rotate the X-ray source and detector around the patient, and thus patient movement is not required in CBCT imaging. Most CBCT devices use a 360° angle, but 180° angles can also be used. During the rotation which typically lasts from 10 to 40 seconds, CBCT devices acquire several hundred 2D X-ray projections. These projections are then processed using computer software which incorporates sophisticated image reconstruction algorithms to produce a 3D presentation or standard 2D visualization (axial, coronal, and sagittal) of the scanned object. (Kumar, Shanavas, Sidappa, & Kiran, 2015; Pauwels, Araki, Siewerdsen, & Thongvigitmanee, 2015)

CBCT has many beneficial features compared to traditional CT. In a previous study, the mean effective radiation dose in sinonasal imaging was found to be 0.27 mSv, which was lower than the effective dose from standard MDCT (0.48 mSv) and

low-dose MDCT (0.39 mSv) (Al Abduwani et al., 2016). In addition, the same study indicated that the clear delineation of principal surgically relevant osseous structures in CBCT scans was comparable to standard CT scans. However, soft tissue visibility was found to be limited. In a recent review based on information from the International Commission on Radiation Protection, the median effective dose of modern CBCT to the facial area was found to vary from 0.03 mSv to 0.11 mSv, depending on the field of view and the imaging device used (Al-Okshi, Lindh, Sale, Gunnarsson, & Rohlin, 2015). In another review, the benefits of CBCT over clinical CT were said to be, for example, 3D dataset, high resolution, lower radiation, less disturbance from metal artefacts, reduced costs, easy accessibility, in-office imaging and energy saving (De Vos, Casselman, & Swennen, 2009). The same review found limitations in CBCT considering, for instance, low contrast range, limited detector size, limited inner soft tissue information, increased noise from scatter radiation and dataset artefacts caused by patient movement. In addition to these limitations, Hounsfield units have a limited use in CBCT-derived tissue density measurements (Pauwels, Jacobs, Singer, & Mupparapu, 2015).

2.5.4 Magnetic resonance imaging

MRI is based on nuclear magnetic resonance and uses strong magnetic fields, magnetic field gradients and radio waves to produce three planar (axial, coronal and sagittal) images of the desired region of the body. In order to produce accurate images of the nasal cavity and the paranasal sinuses, both high-resolution T1- and T2-weighted images must be acquired. Contrast-enhanced T1-weighted images, with gadolinium chelate as the contrast agent, are also routinely acquired when imaging the nasal cavity and paranasal sinuses. Fat-saturated T1-weighted images are often included to nasal cavity and paranasal sinus imaging in order to improve detection of the extent of local disease and diseases outside the paranasal sinuses. (Fatterpekar et al., 2008)

In sinonasal imaging, MRI is mainly used to identify tumours and assess the extent of these pathologies. However, tumours can in some cases be challenging to separate from inflammatory processes, such as granulation tissue. Nasal polyps and their extent can be more precisely distinguished from normal mucous membrane with MRI than with CT imaging methods, although nasal polyps are not primarily imaged with MRI. (Fatterpekar et al., 2008)

2.5.5 Disease severity assessment based on patient imaging

The Lund-MacKay (LM) staging method (Lund & Mackay, 1993) is used for the assessment of the degree of CRS severity. Today, it is a widely used CRS staging system due to its simplicity and ease of use. The staging method bilaterally classifies the mucous membrane thickness of the maxillary, anterior ethmoid, posterior ethmoid, sphenoid and frontal sinuses together with the regions of the ostiomeatal complexes. All these regions are classified on a scale from 0 to 2 (0 = no abnormalities, 1 = partial opacification, 2 = total opacification) (Figure 3). The maximum score in LM staging is 24. The LM staging method has been shown to have only minute correlation with patient symptoms when compared to the results of symptom questionnaires (Bradley & Kountakis, 2005; Hopkins, C., Browne, Slack, Lund, & Brown, 2007; Pallanch et al., 2013). However, the LM staging method has shown correlation with other markers of disease severity, the nature of surgical treatment offered and the outcome of each treatment (Hopkins, C. et al., 2007).

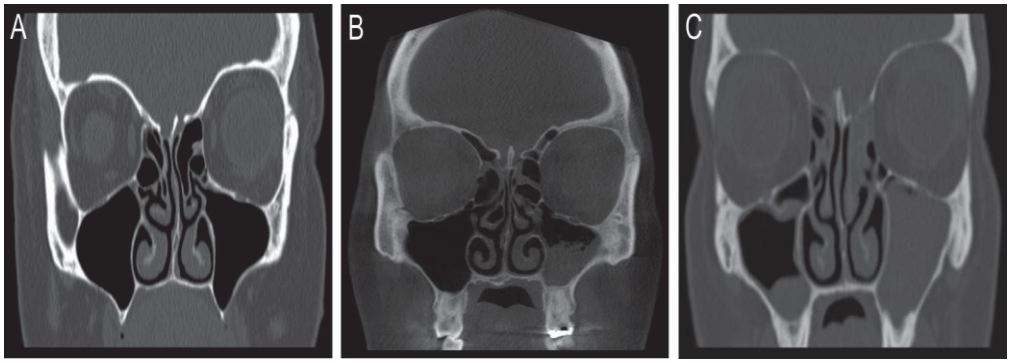

Figure 3. Lund-MacKay staging method in maxillary sinuses. A: LM score 0 in both of the maxillary sinuses, B: LM score 1 in the left maxillary sinus and C: LM score 2 in the left maxillary sinus.

Zinreich's modified LM staging, used for the first time in a study by Kennedy et al. (2005), is a CRS staging system that is a modification of the LM staging system. This staging system classifies the mucous membrane inflammation of the maxillary, anterior ethmoid, posterior ethmoid, sphenoid and frontal sinuses bilaterally as a portion of the mucous membrane volume of the respective sinus volume on a scale from 0 to 5 (0 = no inflammation, 1 = 1%-25% inflammation, 2 = 26%-50% inflammation, 3 = 51%-75% inflammation, 4 = 76%-99% inflammation, 5 = 100%

inflammation). The ostiomeatal complexes are not assessed in this method, and the maximum score is 50.

Okushi et al. (2013) proposed a staging system in which the mucous membrane inflammation of the maxillary, anterior ethmoid, posterior ethmoid, sphenoid and frontal sinus is bilaterally assessed on a scale from 0 to 4 (0 = no inflammation, 1 = 1%-33% inflammation, 2 = 34%-66% inflammation, 3 = 67%-99% inflammation, 4 = 100% inflammation) and the ostiomeatal complexes on a scale from 0 to 2 (0 = not occluded, 2 = occluded). Thus, on this scale, the maximum score is 44.

Several other staging systems have been proposed to classify rhinology findings (Lund & Kennedy, 1997). Many of these proposed staging systems (Friedman, Katsantonis, Sivore, & Kay, 1990; Gliklich & Metson Ralph, 1994; Kennedy, 1992) are based on staging the findings on a scale from 0 to 4, depending on the visual depiction of the inflammation in the nasal cavity and the paranasal sinuses. Other proposed staging systems (Jorgensen, 1991; Newman, Platts-Mills, Phillips, Hazen, & Gross, 1994) are based on similar numerical scoring of the paranasal sinuses as that used in LM staging.

2.6 3D modelling and printing

3D modelling and printing have become more common along with the development of computer software capabilities and computer-aided design (CAD). 3D modelling means creating a representation of a physical object using a collection of points in 3D space. These points are connected to each other with different geometrical entities, for example, lines, curves and curved surfaces. Generally, 3D modelling can be performed manually, by scanning or algorithmically. (Crafts et al., 2017)

2.6.1 3D modelling

3D models are formed from CT or MRI scans in which the raw data are stored in digital imaging and communications in medicine (DICOM) file format. Image analysis software is then used to edit and segment the DICOM files, after which the DICOM files are converted to one of the CAD file formats: standard tessellation language (STL) file format or the newer additive manufacturing file (AMF) format. If necessary, the STL or AMF files can be further meshed, edited and segmented with CAD software. 3D printers then use these prepared STL or AMF files to

produce 3D models which, if required, are finally postprocessed to finalise the object (Crafts et al., 2017).

In medical use, virtual 3D modelling has become more common in various specialties due to enhanced computer software capabilities (Tack, Victor, Gemmel, & Annemans, 2016). Both clinical CT and MRI scans have been widely used to produce virtual and printed 3D models in different applications, for example, in orthopaedics (Chen, C. et al., 2019; Samaila et al., 2020), maxillofacial surgery (Louvrier et al., 2017), cardiovascular diseases (Giannopoulos et al., 2016), neurosurgery (Randazzo, Pisapia, Singh, & Thawani, 2016) and dentistry (Dawood et al., 2015). The main use of 3D modelling includes the production of surgical guides, surgery planning models and custom implants (Tack et al., 2016). 3D modelling has also been found to be of great interest regarding human anatomy and surgery education, although higher quality of evidence is needed to prove that 3D modelling is superior to traditional cadaver models (Langridge et al., 2018). Furthermore, 3D modelling is reported to reduce surgical time and total radiation exposure as well as improve medical outcome, even though further statistical evidence is required to make conclusive statements (Tack et al., 2016). CBCT has also been used in 3D modelling to produce tooth replicas (Sokolowski et al., 2019), in virtual dental treatment planning (Yilmaz, 2015) and as a tool for endodontic education (Reymus et al., 2019). A recent study compared the use of clinical CT and CBCT scans in 3D nasal cavity modelling and modelling flow calculations (Tretiakow, Tesch, Meyer-Szary, Markiet, & Skorek, 2020). Both imaging methods were found to be useful for 3D modelling, but CT produced better quality 3D models, although with higher radiation dose.

2.6.2 3D printing

3D printing is an additive manufacturing process in which a virtual 3D model is printed into a physical three-dimensional model by printing consecutive layers of printing material on top of each other. Different materials can be used according to the set requirements. The main methods of 3D printing are fused deposition modelling (FDM), stereolithography (SLA), powder bed fusion as well as material and binder jetting printing. In addition, inkjet printing, liquid binding in three-dimensional printing (3DP), contour crafting, direct energy deposition (DED) and laminated object manufacturing (LOM) are all widely used. More novel 3D printing methods include two-photon polymerization (TPP), electrohydrodynamic printing

(EHDP), projection micro stereolithography (PμSLA) as well as non-contact micro and nano-printing methods. (Ngo, Kashani, Imbalzano, Nguyen, & Hui, 2018)

2.6.3 3D printing methods

2.6.3.1 Fused deposition modelling

FDM or fused filament fabrication uses a continuous filament of a thermoplastic polymer to print layers of materials to produce a printed 3D model. The used filament is heated at the nozzle of the printer to reach a semi-liquid state, after which the filament is extruded on the printing platform or on the already printed layer. The layers are fused together due to the thermoplasticity of the filaments, and, after printing, the 3D model is solidified at room temperature. (Ngo et al., 2018)

The benefits of this method are its low cost compared to other 3D printing methods, practicality and suitability for consumer use. The disadvantages are the low resolution of the end product, weak mechanical properties and the limited number of thermoplastic materials available. (Crafts et al., 2017; Ngo et al., 2018) In addition to traditional 3D printing, a recent review found FDM to be a very promising technique for producing oral drug forms for precision medicine, especially for children, the elderly and rare disease treatments (Cailleaux, Sanchez-Ballester, Gueche, Bataille, & Soulairol, 2020).

2.6.3.2 Stereolithography

SLA is one of the earliest methods of 3D printing and uses ultraviolet (UV) light to initiate a chain reaction on a layer of liquid resin or monomer (acrylic or epoxy-based) solution. These monomers are UV-active and instantaneously convert to polymer chains after activation. A pattern inside the resin layer is solidified after polymerization to hold the following layers. After printing, the unreacted resin is removed, and post-processing heating or photo-curing can be used to achieve the desired mechanical performance. (Ngo et al., 2018)

Stereolithography produces high-quality 3D objects with a resolution as low as 10 μm. However, this method is time-consuming, expensive and the reactions in the printing material are complex. Also, printer maintenance is expensive, and the

method requires postprocessing which is complex and includes using strong solvents. (Crafts et al., 2017; Ngo et al., 2018)

2.6.3.3 Powder bed fusion

Powder bed fusion uses thin layers of very fine powder which are spread and closely packed on a printing platform. To fuse the layers of powder to each other, a laser beam or a binder is used. This process is repeated for each new layer of powder until the 3D model is ready. Excess powder is removed by a vacuum. When needed, postprocessing and detailing by sintering, coating and infiltrating can be done. Two different methods, selective laser sintering (SLS) and selective laser melting (SLM), can be used, depending on the printing material. SLS is suitable for a variety of polymers, metals and alloy powders. SLM is, however, only suitable for specific metals, such as aluminium and steel. (Ngo et al., 2018)

Powder bed fusion generates 3D models with good quality and mechanical properties, which makes this method suitable for the printing of complex structures. The drawbacks of this method are the cost of the printer and printing materials, the need for highly experienced operators and special facilities as well as the porosity of the end product when the powder is fused with the binder. (Crafts et al., 2017; Ngo et al., 2018)

2.6.3.4 Material jetting printing

Material jetting printing (MJP) produces 3D models using liquid resin which is dropped on the platform either continuously or on demand during the printing process. After being dropped, the photosensitive resin is solidified by UV light, after which the next layer can be dropped on top of the first one. Although this method is expensive, it offers good resolution in the 3D model and reduced postprocessing is required. Less printer maintenance is also needed, and it is possible to print heterogeneous objects with MJP. (Crafts et al., 2017)

2.6.3.5 Binder jetting printing

Binder jetting printing (BJP) uses a powdered material that is sprayed into a layer and selectively joined into the targeted layer shape with a binder. Typically, a polymeric

liquid is used as the binder material. When consecutive layers are being printed on top of each other, the layers are bonded together, creating a 3D model which requires a substantial amount of postprocessing in order to be finalised. This postprocessing includes de-powdering, sintering, additional material infiltration and annealing. Still, the resolution of the end product may be less accurate. BJP printers are, however, affordable compared to other printers and also produce less noise. Although excess postprocessing is required, the printer itself can produce multiple 3D models in a period of 24 hours. (Crafts et al., 2017; Mostafaei et al., 2020)

2.6.4 3D printing materials

The most common materials used for 3D printing today include plastics, thermoplastics, metal and polymeric powders, ceramics, photopolymers and solutions (Jamroz, Szafraniec, Kurek, & Jachowicz, 2018). In a recent review, previous developments and potential future trends to replace oil-based plastics by naturally-derived biopolymers, such as cellulose, hemicellulose and the derivatives or composites of these polysaccharides, have been discussed (Liu, J. et al., 2019). 3D printing materials used or studied today for producing biomaterials can be divided by their properties. Melt-cure polymers, such as polylactic acid (PLA), polycaprolactone (PCL) and polyurethane (PU), have high mechanical strength and durability, although they require high process temperatures or toxic solvents. Hydrogels are divided into two groups: natural hydrogels, such as collagen, gelatin and alginate, and synthetic hydrogels, for example, polyethylene glycol (PEG) and poly(lactic-glycolic) acid (PLGA). These hydrogels have good swelling features but lack mechanical strength and shape fidelity. However, the synthetic hydrogels can be photo-crosslinked with polyvinyl alcohol (PVA) to provide higher mechanical strength. To better use the advantages of the two hydrogel groups, combinations have been developed that are called hybrid hydrogels. Decellularized extracellular matrix (dECM), derived from living tissues and organs, has been studied to better recreate the complexity of the natural extracellular matrix. (Tetsuka & Shin, 2020)

2.7 Use of 3D in otorhinolaryngology

2.7.1 Rhinology

3D technology has been used for analysing and treating nasal cavity and paranasal sinus pathologies. Moreover, intraoperative 3D navigation has been widely used in endoscopic sinus surgery (ESS) operations, which has significantly improved patient safety in the operative treatments of the paranasal sinuses and frontal skull base (Freysinger, Gunkel, & Thumfart, 1997). Maxillary sinus volumetric measurements of the air space and the mucous membrane in CRS patients have been previously studied, although the results were not compared to other CRS assessment methods (Deeb et al., 2011). 3D volumetric measurements of the nasal cavity have been used to assess postoperative results compared to preoperative conditions after septorhinoplasty, showing increased nasal cavity air space volume along with improved symptom relief (Tugrul et al., 2019). In addition, 3D printed models of septal perforations, ranging from 1.2 cm to 3.5 cm, have been used to fabricate fitting prostheses for adequate closure of the perforations, with good results in symptoms relief (Onerci Altunay et al., 2016).

2.7.2 Traumatology, oncology and reconstructive surgery

In tumour surgery and maxillofacial reconstruction, the use of 3D modelling has been studied mainly in the planning of endoscopic skull base surgery (Haerle et al., 2013). Preoperative 3D planning for tumour resection has also been studied in mandibular pathologies (Yusa, Yamanochi, Takagi, & Iino, 2017). In midface forming, mandibular reconstruction and orthognathic surgery, 3D technology has been widely used in preoperative planning, modelling and implant applications (Steinbacher, 2015).

Traumatic injuries of the maxillofacial region are often presented in 3D reconstructions, in addition to the traditional three planar view, to ease treatment planning. Complicated or large orbital floor fractures have increasingly been operated using preoperative 3D planning, 3D modelling of the orbital floor for perioperative orbital plate adjustment and preformed orbital plates based on 3D modelling (Park et al., 2015). Moreover, 3D modelling has also been used in the

preoperative planning of osteotomy guides when treating complex posttraumatic facial injuries with facial transplantation (Lassus et al., 2018).

3D modelling and printing have been used to produce auricular 3D models for preoperative planning with microtia patients (Jeon et al., 2016; Zhu & Chen, 2016). Moreover, the same studies have found the use of 3D template reduce excess work during surgery and produce better postoperative results. 3D planning has also been reported to simplify implant surgery for the insertion of craniofacial implants to support a nasal prosthesis (Ciocca, Fantini, De Crescenzio, Persiani, & Scotti, 2011).

2.7.3 Education and training

In otorhinolaryngology, 3D modelling and printing have been found to be useful in many fields of education and training. In otology, the use of 3D printed temporal bones have been found beneficial in temporal bone surgery training (Hochman et al., 2015). However, 3D models were not found to clearly outperform the use of cadavers. In treating microtia, the 3D printing of a representative paediatric costal cartilage model for auricular framework reconstruction simulations was found to be inexpensive and potentially beneficial for trainees and more experienced microtia surgeons (Berens et al., 2016). 3D modelling and printing have also shown potential in endoscopic endonasal surgery training (Chan et al., 2015). Additionally, 3D technology has been used to produce 3D models for rigid bronchoscopy foreign body removal (Al-Ramahi et al., 2016) and epistaxis treatment (Chiesa Estomba, Gonzalez Fernandez, & Iglesias Otero, 2018) training.

2.8 Measuring flow from computed tomography based models

2.8.1 Flow and breathing resistance in general

Measuring flow and breathing resistance in the nasal cavity is a complicated procedure. First, the bony anatomy causes difficulties by being complicated in itself. In addition, added difficulty is caused by the different appearance of the mucous membrane which, additionally, changes its form according to the nasal cycle. Second, the airflow in the nasal cavity is not constant, as the velocity of the airflow accelerates and decreases during the breathing cycles. Modelling all these factors precisely in a reliable way would not be realistic due to the time and resources required. Thus,

studies have concentrated on finding the optimal mathematical model that would represent airflow mechanics. The real airflow in the nasal cavity is not steady, but it has been debated whether the mean airflow could be sufficiently modelled as steady or as a series of quasi-steady flows. It also has to be considered whether the flow should be modelled laminar or turbulent. (Doorly, Taylor, & Schroter, 2008)

In a previous study, the airflow in the nasal cavity was treated solely as steady and laminar (Keyhani, Scherer, & Mozell, 1995). Similarly, another study used flow rates of both 7.5 l/min and 15 l/min while treating the airflow as steady and laminar (Wen, Inthavong, Tu, & Wang, 2008). These study setups were based on a preceding study which indicated the flow in a half nasal cavity model to be laminar with the flow rate of 180 ml/s (21.6 l/min with bilateral flow) or lower when measured with hot wire anemometry (Hahn, Scherer, & Mozell, 1993). Thus, in modelling calm breathing the steady flow assumption is applicable. However, turbulent models are needed along with the steady flow model when studying, for instance, odorant transfer (Zhao et al., 2006), heat transfer (Ishikawa, Nakayama, Watanabe, & Matsuzawa, 2006) as well as nanoparticle transport and deposition (Shi, Kleinstreuer, & Zhang, 2006). In addition, both the laminar and turbulent models have been recently used to assess the nasal flow resistance in comparison to rhinomanometric measurements (Cherobin et al., 2021; Kimbell et al., 2019; Osman et al., 2016).

2.8.2 Particle image velocimetry

PIV is a flow measuring method that uses a sheet of laser light to illuminate and thus measure the movement of tracer particles in a water current flowing through an optically transparent object. The laser light is pulsed twice in rapid succession which enables the recording of two subsequent positions for each particle with a charge-coupled device (CCD) camera. Depending on the use of cameras and postprocessing, two- or three-dimensional velocity vectors are produced within the illuminated plane. (Adrian, 1991; Prasad & Adrian, 1993)

The setup basis for PIV nasal cavity flow measurements, using a 3D silicone model of the nasal cavity, was first demonstrated by Hopkins et al. (2000). In a previous study that compared nasal cavity PIV measurements representing airflow to corresponding CFD calculations, the mainstream of the airflow was found to shift downward, when a single-sided turbinectomy in different extent was performed to a 3D model (Na et al., 2012). However, the study was done only with models and did not compare the results to clinical patient results. Further studies have developed

this PIV setup by using stereoscopic particle image velocimetry (SPIV) (Spence et al., 2011; Spence, Buchmann, & Jermy, 2012). SPIV measurements have also been compared to CFD measurements, although the comparison has usually only been done with visual assessment (Cozzi, Felisati, & Quadrio, 2017). An experimental PIV setup, digital particle image velocimetry (DPIV), has also been discussed in a recent review (Chung & Kim, 2008).

2.8.3 Computational fluid dynamics

CFD is a branch of fluid mechanics and a computational way of analysing and solving complex fluid flow phenomena and mechanics. The basis of almost all CFD problems is in the Navier-Stokes (NS) partial differential equations. These NS equations define many single-phase fluid flows, in other words, either gas or liquid but not both. When studying CFD models, a choice between laminar and more complicated turbulent CFD models has to be made prior to calculations. Typically, CFD calculation studies dealing with turbulent flows solve simplified versions of the NS equations, most usually the Reynolds-averaged Navies-Stokes (RANS) equations which rely on Reynolds averaging of turbulent fluctuations. The most usual approach to turbulent flow calculations is to use two-equation RANS models that introduce the Boussinesq linear eddy viscosity assumption, where turbulent viscosity is assumed to be isotropic and is a property of the flow. These two-equation models, such as k-ε, k-ω and Menter's shear stress transport (k-ω SST) turbulence models, are reasonably good for most cases. (Quadrio et al., 2014)

In a previous study, 3D model CFD calculations were used to assess nasal airflow characteristics with different flow rates when inferior turbinate hypertrophy is present (Chen, X. B. et al., 2010). The study showed that the average turbulent intensity of the flow in the 3D modelled nasal cavity was low when modelling calm breathing but increased notably with a more blocked nasal cavity. In addition, the most intensive turbulent flow was shown to be in the functional nasal valve region and the surface of the inferior turbinate in a wider model. However, more hypertrophic inferior turbinates caused the intensity of the flow to move upwards while not passing through the lower regions of the nasal cavity.

In a recent study, it was noted that CFD calculations have become more precise and produce results that are closer to real life circumstances, although some development areas still remain, for example, in user-friendliness and the lack of proper clinical tests (Lintermann & Schröder, 2019). Another recent study found

CFD calculations have a weak correlation with rhinomanometric measurements in nasal resistance, although the correlation was somewhat better with lower pressure values (Cherobin et al., 2021). The study also showed that CFD calculations underestimate nasal resistance compared to rhinomanometric measurements, a finding that was in line with a previous study by Osman et al. (2016). Additionally, another earlier study with patients who were undergoing deviated nasal septum operation showed as high as a 10-fold discrepancy between the CFD calculations and rhinomanometric measurements, with CFD underestimating the level of nasal resistance compared to rhinomanometry (Hemtiwakorn, Mahasitthiwat, Tungjitkusolmun, Hamamoto, & Pintavirooj, 2015). However, a very recent study found that CFD calculated nasal pressure values correlate well with rhinomanometric measurements in less obstructed nasal cavities (Berger et al., 2021). Additionally, in the same study, CFD calculated nasal resistance values were found to have moderate correlation with rhinomanometric values. Moreover, it has been found that the CFD calculations of nasal resistance have good agreement with rhinomanometric results when using a plastic nasal cavity model, although this was found with a single 3D print (Kimbell et al., 2019).

3 AIMS OF THE STUDY

1. To study whether CBCT is applicable and accurate enough for virtual sinonasal 3D modelling. (I-IV)

2. To study whether patient scan-based volumetric and cross-sectional area measurements of the sinonasal region can produce more accurate and less subjective results compared to current examination methods. (I, IV)

3. To evaluate the applicability of patient imaging in the production of printed sinonasal 3D models. (II, III)

4. To evaluate whether patient imaging-based 3D models are accurate enough for sinonasal airflow modelling. (II, III)

4 MATERIALS AND METHODS

4.1 3D volumetry and modelling

4.1.1 Patient selection

The present studies are based on patients having either CRS or chronic nasal congestion as their main rhinologic condition.

In study I, 72 adult CRS patients with a previous operation of either uncinectomy (n=37) or ostial balloon dilation (n=35) were included along with pre- and postoperative CBCT scans. All patients chosen for study I had their main radiological findings in the maxillary sinuses. By the end of the study, ten patients had opted out and one patient was excluded due to extensive artefacts in CBCT scans. For the purposes of this study, a total of 61 patients (42 female and 19 male), and thus 122 maxillary sinuses, were analysed. The study population comprised 30 patients from the uncinectomy group and 31 patients from the ostial balloon dilation group. The range of the age of the patients was from 20 to 63 years, with the mean age of 38.4 (± 11.3 years).

For study II, the preoperative CBCT scans of five adult patients with symptoms of chronic nasal congestion were included. Thus, ten individual nasal cavities were studied. Exclusion criteria were chronic rhinosinusitis, nasal polyps and tumours. Study III included the preoperative CBCT scans of one adult patient with chronic nasal congestion without chronic rhinosinusitis, nasal polyps or other pathology.

A total of 26 patients with chronic nasal obstruction were included to study IV. These patients had enlarged inferior turbinates and had been treated with radiofrequency thermal ablation. One patient was excluded from the study due to extensive artefacts in the CBCT scans caused by dental fillings, which prevented 3D measurements. Therefore, 25 patients were included in the data analysis of study IV. In addition, with regard to only the correlation analysis, one patient had to be excluded due to missing acoustic rhinometry measurements. This resulted in a total of 24 patients being included in the correlation analysis.

All the patients in the present studies had been CBCT scanned preoperatively and at twelve months postoperatively. In studies I and IV, both the pre- and postoperative CBCT scans were used, whereas in studies II and III, only the preoperative CBCT scans were used.

4.1.2 3D modelling and volumetric measurements from CBCT scans (I-IV)

The CBCT data were saved in DICOM format and downloaded to OnDemand3D™ (version 1.0, CyberMed, Inc., Yuseong-gu, Daejeon, South Korea) software to perform the virtual 3D modelling. 3D modelling was performed to produce volumetric measurements of the air space in the nasal cavities (II, IV) and the maxillary sinuses (I, II). A similar method was used to measure the volumes of the inferior turbinates (IV). In addition, 3D modelling was used to produce printed 3D models of the nasal cavities for the experiments (II, III). Initially in study II, we used Matlab® (MathWorks, Inc., Natick, Massachusetts, United States) software, which is widely used by engineers, to produce virtual 3D models for 3D printing, after which we proceeded solely with OnDemand3D™.

Since no definitive HU values have previously been set for different tissues or air in CBCT scans, the OnDemand3D™ software's own threshold scaling function was used to define the proper HU threshold values for air and inferior turbinate soft tissue. The HU threshold values for air space in patient CBCT scans was defined to be from -1000 to -430 (I-IV). The same HU threshold values were also found to be applicable for the virtual modelling of the air space of the 3D silicone model (III). The HU threshold values representing air in plastic 3D models was defined with the software's own scaling function to be from -1000 to -800 (II). The HU threshold values for inferior turbinate soft tissue were defined to be from -429 to 400 (IV).

In studies I and IV, one patient was excluded from the studies due to extensive artefacts. These were caused by dental filling and we observed they led to widespread radial break lines in the CBCT scans, making it impossible to produce 3D models in these cases. Thus, 3D modelling from CBCT scans is sensitive to artefacts that break the anatomical lines.

4.1.3 3D printing (II, III)

The virtual 3D models produced with Matlab® and OnDemand3D™ software were translated to STL file formats. These STL files were then post-processed with open-

source Slic3r (II) or Blender v2.76b (Blender Foundation) (III) software to generate the toolpaths for the 3D printer. In both studies II and III, the FDM 3D printing technique was used.

In study II, the printed 3D plastic models (Figure 4) were produced with a Lulzbot® Taz 4 3D printer (Aleph Objects, Inc., Loveland, Colorado, United States) with a nozzle size of 0.4 mm and a layer thickness of 0.25 mm. Polylactic acid (PLA), a commonly used corn-based thermoplastic material for 3D printing, was used as the raw material

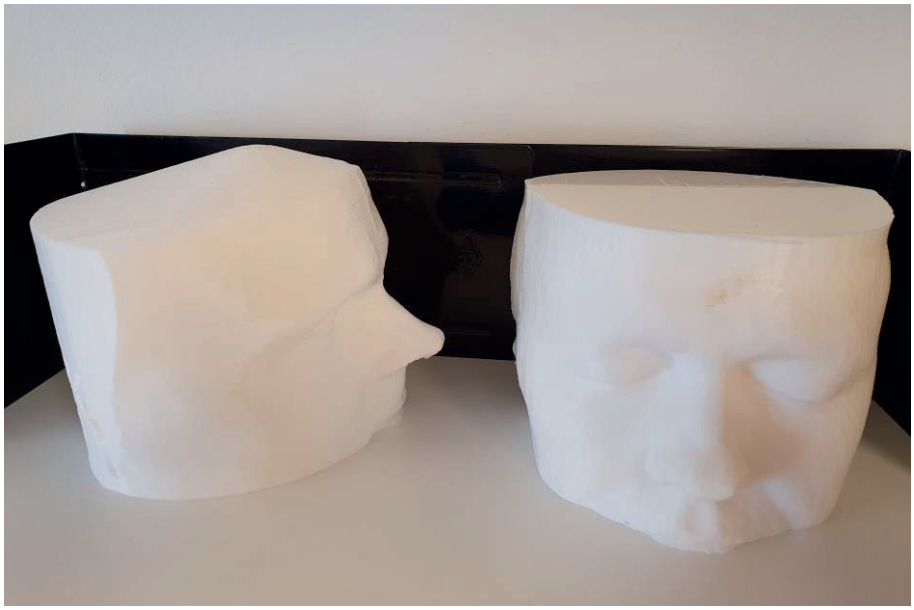

Figure 4. Examples of the printed 3D plastic models. (II)

The plastic 3D prints, including the nasal cavities and the paranasal sinuses, were printed from the level of the nasopharynx to the level of the frontal sinus in 1:1 size. To reduce the risk of artefacts, the printing was performed by manufacturing the 3D prints upside down in order to provide better fixation support for the sinonasal structures, which are mainly attached to the roof of the nasal cavity. Since it would have been challenging to remove the supporting structures afterwards, no supporting structures were generated for the 3D prints. The printing of one plastic 3D print took approximately 48 hours. No additional clean-up of the printed objects was required. However, some printing artefacts were left in the cavities after printing due to the lack of supporting structures for the overhanging parts. When all five 3D

prints had been printed, CBCT images were taken of each print for further analysis and to confirm that the prints corresponded with the data of the real patients.

In study III, one 3D print of the nasal cavity in silicone was produced. Initially, the Ultimaker 2.0 (Ultimaker B.V., Netherlands) 3D printer was used to produce a water-soluble 3D printed model of the air space in the nasal cavity (Figure 5), thereby functioning as the negative of the nasal cavity structures. In preparation for the PIV measurements, the final 3D print size was increased by a factor of 1.85. In addition, a supplemental passage of a round tube was fitted downstream of the nasopharynx to help experimental setup assembly. A water-soluble PVA filament called Ultimaker PVA was used in this 3D printing phase. The total printing time was approximately 57 hours.

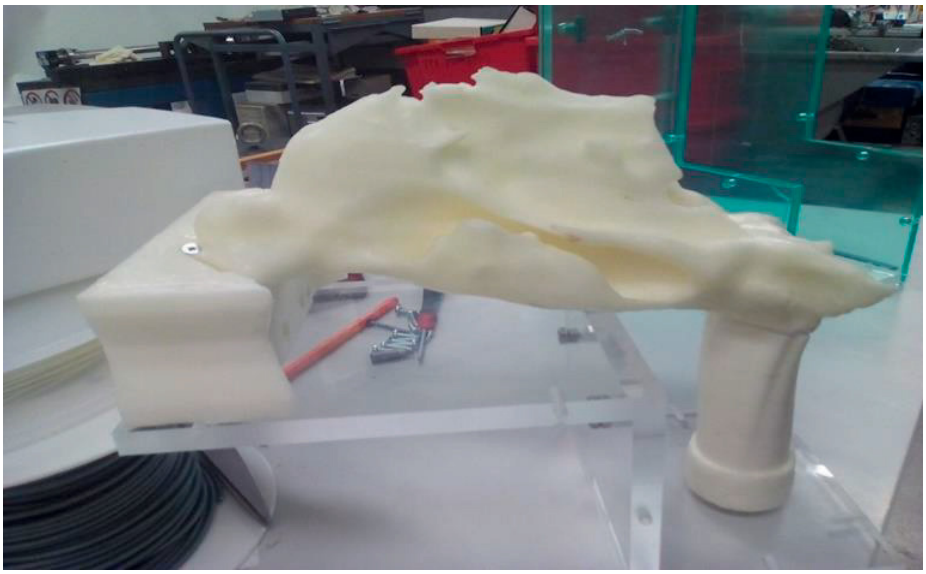

Figure 5. 3D printed water-soluble model of the nasal cavity air space used in the production of the silicone nasal cavity model. (III)

In the second phase, the silicone 3D model was produced. After sealing the surface of the PVA 3D print with glue (Bostik AB, Sweden), the printed PVA negative of the nasal cavity was positioned in a Plexiglas box. Uncured Dow Corning Sylgard 184 (Dow Corning, USA) silicone was then poured into a Plexiglas box to cover the printed nasal cavity. The box was then placed in a vacuum chamber to ensure the removal of air. The PVA was later dissolved with 55 °C water and afterwards, in some parts, the manual removal of PVA was necessary. The dissolving of the PVA took several months and could not be successfully accelerated with solvents.

4.1.4 Maxillary sinus 3D volumetry from CBCT scans (I)

In study I, the air space 3D volume of the maxillary sinuses was measured from pre- and postoperative CBCT scans (Figure 6). The combined volume of the left and right maxillary sinuses, representing the total maxillary sinus volume in each patient, was used in the comparison between pre- and postoperative conditions. The CBCT scans were also used to evaluate the thickness of the mucous membrane. The evaluation was performed only in the region of the maxillary sinuses since the patients did not have any notable radiological findings outside the maxillary sinuses. LM stages were evaluated for the maxillary sinuses and the ostiomeatal complexes. Zinreich's modified LM stages were evaluated only for the maxillary sinuses because this staging system does not note the ostiomeatal complexes. In addition, the patients had filled out the SNOT-22 questionnaire pre- and postoperatively. The 3D measured total volumetric changes from pre- to postoperative conditions were compared with the changes in both the LM and Zinreich's modified LM staging as well as the SNOT-22 results.

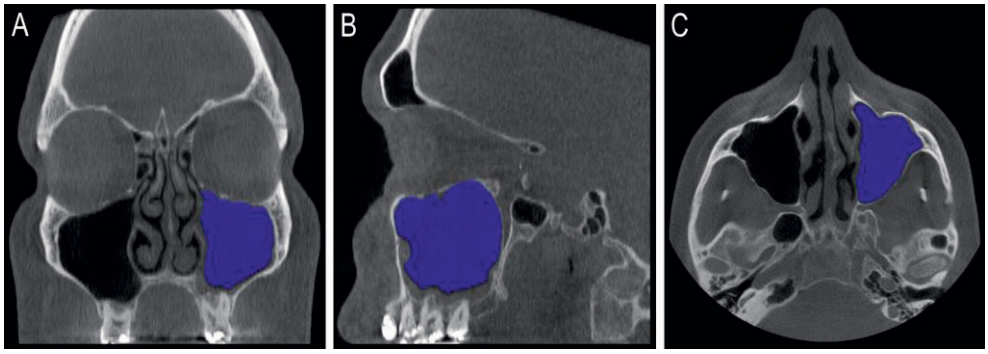

Figure 6. Measurement setup in patient CBCT scans for the 3D volumetric measurement of the air space of a single maxillary sinus in all three planes (A = coronal, B = sagittal, C = axial). (I)

4.1.5 Printing nasal cavities in plastic 3D models using CBCT scans (II)

In study II, five preoperative patient CBCT scans were used to produce plastic 3D prints of the nasal cavities. These plastic 3D prints were also CBCT scanned for volumetric and linear measurements. 3D volume measurements of the maxillary sinuses and the nasal cavities in both the patient and 3D print CBCT scans were performed. Additionally, linear measurements were taken in the following ways to

lower the risk of artefacts: septum length from the tip of the nose to the closest endpoint of the nasal septum, nasal cavity height at the same endpoint of the nasal septum and the width of the nasal cavity at the same location (Figure 7).

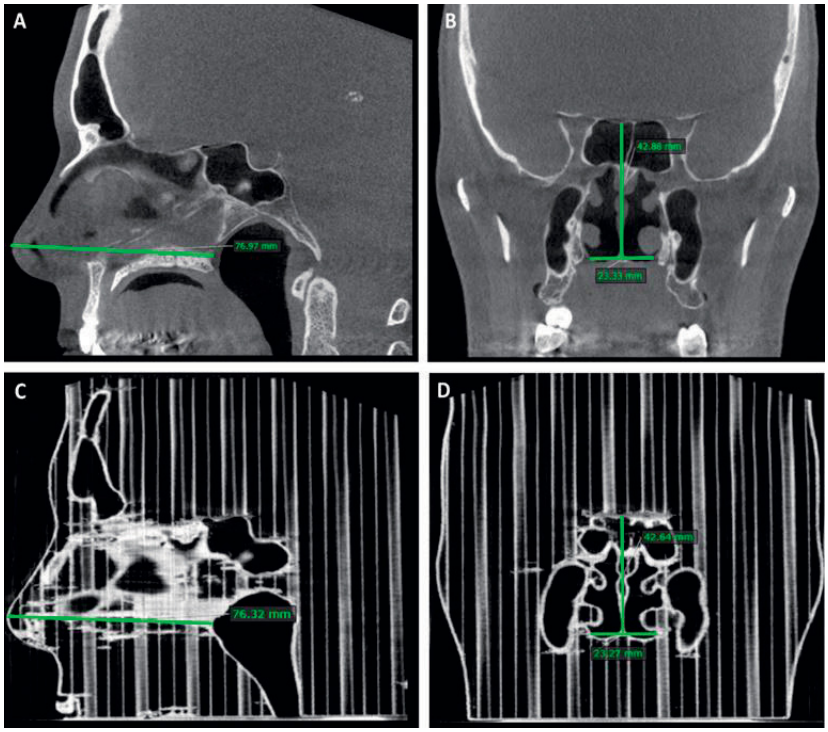

Figure 7. Measurement setup for the linear measurements of the nasal cavity dimensions in both patient (A and B) and plastic 3D print (C and D) CBCT scans. (II)

Rhinomanometric measurements had been performed preoperatively for the patients by a nurse in the otorhinolaryngology clinic. The measurements were done by using anterior rhinomanometry with an NR6 Rhinomanometer (GM Instruments Ltd, Kilwinning, Scotland, United Kingdom) and Nasal Acoustic Rhinomanometer Information System (NARIS) version 3.2 software (GM Instruments Ltd, Kilwinning, Scotland, United Kingdom). The same measurements were performed with the same instruments with the plastic 3D prints and the airflow was produced by one of the investigators breathing through a plastic tube connected to the nasopharynx of the 3D prints. The results were measured from the airflow rates by using the Broms method. Finally, one patient was excluded from the rhinomanometric data analysis due to technically failed measurements in

rhinomanometry. Thus, a total of eight individual nasal cavities and maxillary sinuses were studied with rhinomanometry.

All the measurements were performed to assess the congruence of the results *in vivo* and *in vitro*. We observed a small difference between the patient and plastic 3D model volumetric and linear measurements. Therefore, as an additional analysis, we also used a scaling formula to make the rhinomanometric results *in vitro* comparable with the results *in vivo*. With the assumption of flow in the nasal cavities being laminar, the scaling was based on an analogy from the laminar tube flow Hagen-Poiseuille equation by taking into account nasal cavity volumes and septum lengths. The scaling for the unilateral rhinomanometric results *in vitro* was calculated by using the following formula derived from the Hagen-Poiseuille equation: results *in vitro* multiplied by nasal septum length ratio (*in vivo*/*in vitro*) to the power of three divided by nasal cavity volume ratio (*in vivo*/*in vitro*) squared.

Due to the small number of patients and the deviation in the rhinomanometric results in study II, the use of geometric mean instead of arithmetic mean was found to be more illustrative in presenting the rhinomanometric results. The geometric standard deviation (GSD) was calculated using the following formula: $GSD(X) = e^{SD(\ln X)}$, in which e is Euler number, SD is arithmetic standard deviation, ln is natural logarithm and X is measurements.

4.1.6 PIV performance in validating CFD models based on nasal cavity CBCT scans (III)

In study III, preoperative patient CBCT scans of a single patient were used. The CBCT scans were used to produce a silicone 3D model of the nasal cavity. This 3D model was used in PIV measurements in which the movement of the tracing particles in a water flow of 0.225 l/s (equivalent to 13.53 l/min) was measured in two dimensions, which corresponded to the longitudinal and vertical axis of the nasal cavity of the patient. On average, one whole horizontal measurement cross-section of 2 mm was measured in one working day.

CFD calculations were conducted assuming the flow to be incompressible. The studied CFD models comprised a laminar model and two turbulent models (k-ω and k-ω SST). In addition to calculating and measuring with the flow rate of 10 l/min *in vivo*, CFD calculations representing human breathing of 20 l/min were also studied.

Four coronal cross-sections were chosen for the data analysis: the anterior tip of the inferior turbinate, the anterior tip of the middle turbinate, the posterior part of

the inferior turbinate and the nasopharynx (Figure 8). The first three coronal cross-sections of the nasal cavity were divided into three vertical parts and further divided into left and right sides in order to better illustrate the route of the flow. The fourth cross-section was only divided into left and right sides.

Time averaged axial mean flow velocity and axial volume flow rate ratios were measured from PIV and calculated from CFD in these four cross-sections. These parameters represent the velocity and the distribution of the flow in the nasal cavity. Axial volume flow rate ratios were calculated by dividing local flow rates over summarised total flow rates. To assess the stress caused by the flow to the boundary of the flow and the nasal cavity surface, median wall shear stresses were calculated in the same cross-sections from CFD. The numerical post-processing was made with the open-source visualisation and data analysis software ParaView 5.0.1.

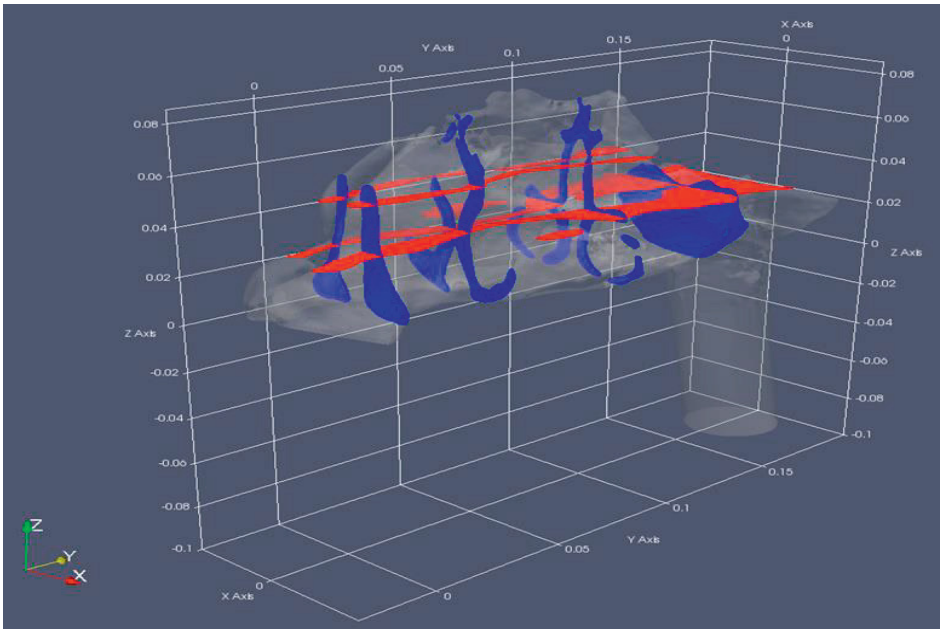

Figure 8. The four coronal cross-sections on both the left and right nasal cavities chosen for the data analysis (blue planes). The horizontal planes (red) divide the first three coronal cross-sections into three vertical parts. (III)

4.1.7 3D volumetric and cross-section area measurements from CBCT scans in assessing the results of inferior turbinate surgery (IV)

In total, the pre- and postoperative CBCT scans of 26 patients were used to virtually 3D model the inferior turbinates for volumetric measurements. Similar 3D modelling was performed for the operated anterior part of the inferior turbinates and the surrounding air space. The anterior part consisted of an area from 5 mm to 20 mm posterior from the anterior peak of the inferior turbinate.

In addition, coronal cross-sectional areas from both the inferior turbinates and the air spaces surrounding the inferior turbinates were measured. The measurement of the cross-sectional areas started 5 mm and ended 50 mm posterior from the anterior peak of the inferior turbinate. The distance between each measuring point was 5 millimetres. For these measurements, we used the Smart Pen function of OnDemand3D™ with some manual corrections.

The uppermost limit of the region of interest (ROI) for both the volumetric and cross-sectional area measurements was set at the lowest level of the middle turbinates. The nasal cavity floor was used as the lowest level of the ROI. Using the OnDemand3D™ software, the combined time for the volumetric and cross-sectional area measurements of the pre- and postoperative CBCT scans took approximately 7 to 10 hours per patient.

The correlation of the volumetric and cross-sectional area measurements were compared with results gained from pre- and postoperative acoustic rhinometry, performed by a nurse in the otorhinolaryngology clinic, as well as VAS and GHSI questionnaires. Acoustic rhinometry tests without adrenaline and the results from both MCA2 and V2-5 were included in the study.

4.2 Ethics

In studies I and IV, the study protocols were approved by the Ethics Committee of Pirkanmaa Hospital District. In studies II and III, all patient data were acquired from the medical records database of Tampere University Hospital, and the study protocol approvals were obtained from the Science Centre of Tampere University Hospital.

4.3 Statistics

In study I, all data were analysed with SPSS 22 software. The mean results of the volumetric measurements were analysed with Wilcoxon's One-Sample test. The correlation of the 3D volumetric measures, LM staging, Zinreich's modified LM staging, and SNOT-22 were analysed with Spearman's correlation test.

In studies II and III, no statistical analysis was performed due to the small sample size and the experimental study design.

In study IV, all data were analysed with SPSS 26 software. The median results of the volumetric and cross-sectional area measurements were analysed with Wilcoxon signed-rank test. The correlation analysis between the 3D volumetric, cross-sectional area and the acoustic rhinometry measurements as well as the VAS and GHSI results were performed with Spearman's correlation test.

5 RESULTS

5.1 Maxillary sinus 3D volumetry from CBCT scans (I)

Changes in the pneumatized volume were detected in every maxillary sinus with the volumetric method. The smallest observed change in pneumatized volume per individual maxillary sinus with the volumetric method was 0.0017 cm^3. The smallest observed pneumatized volume change per individual maxillary sinus using LM staging was 0.49 cm^3, and for Zinreich´s staging system the similar result was 0.53 cm^3. These results were obtained by gathering all the maxillary sinuses that had a change in the staging system scores in question, and the smallest volume change in these sinuses was then observed.

With a minimum change in total volumetric measurements of 5%, both the LM and Zinreich´s staging systems failed to detect changes in 18 out of 43 patients (42%) (Table 1). For 10% volumetric change, LM failed to detect changes in 8 out of 28 patients (29%) and Zinreich´s staging system in 10 out of 28 patients (36%). With a 20% change in volume, the LM showed no change in 3 out of 17 patients (18%) and Zinreich´s staging system failed to detect changes in 2 out of 17 patients (12%). When it comes to all of the patients in our study, both the LM and Zinreich's modified LM staging systems showed no change in 32 out of 61 patients (53%).

The alterations in the maxillary sinuses measured with the 3D volumetric method correlated well with changes in Zinreich's modified LM staging (Figure 9) and to some extent with changes in LM staging. A moderate correlation of the volumetric change to the SNOT-22 change was observed (Figure 10). Additionally, a moderate negative correlation between the SNOT-22 score and Zinreich's modified LM staging was observed, while the LM staging did not show correlation with SNOT-22.

Table 1. The number of patients detected with volumetric method in different volume change scales (both negative and positive). Additionally, the number and percentage of cases that were not detected by Lund-MacKay staging (LM) or Zinreich's modified LM staging methods with the volumetric method number serving as the baseline. (I)

Volumetric change	< 5%	≥ 5%	≥ 10%	≥ 15%	≥ 20%	≥ 25%
Volumetric method	18/61 (30%)	43/61 (70%)	28/61 (46%)	21/61 (34%)	17/61 (29%)	11/61 (18%)
Lund-MacKay	14/18 (78%)	18/43 (42%)	8/28 (29%)	4/21 (19%)	3/17 (18%)	2/11 (18%)
Zinreich's modified LM staging	14/18 (78%)	18/43 (42%)	10/28 (36%)	5/21 (24%)	2/17 (12%)	0/11 (0%)

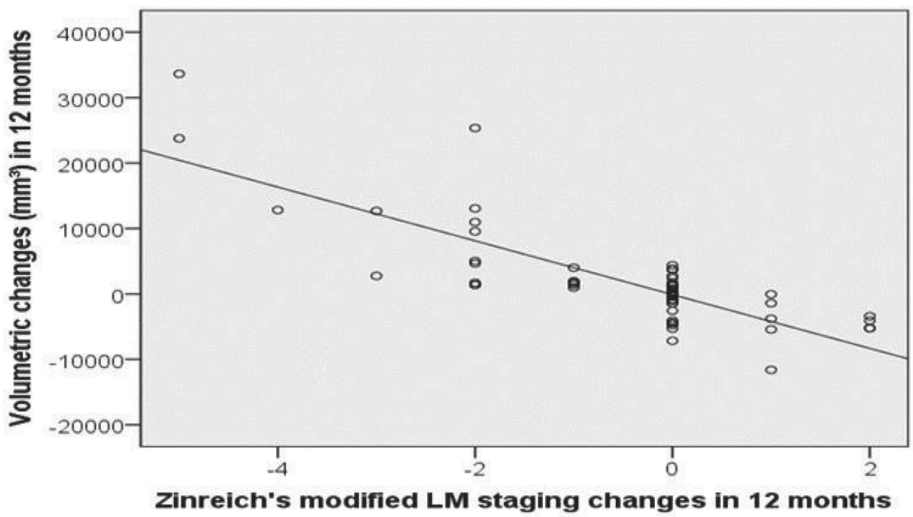

Figure 9. The correlation between the 3D volumetric changes and Zinreich's modified LM staging change (Spearman's rho -0.77, $p \leq 0.01$). The volumetric changes are presented in cubic millimetres. (I)

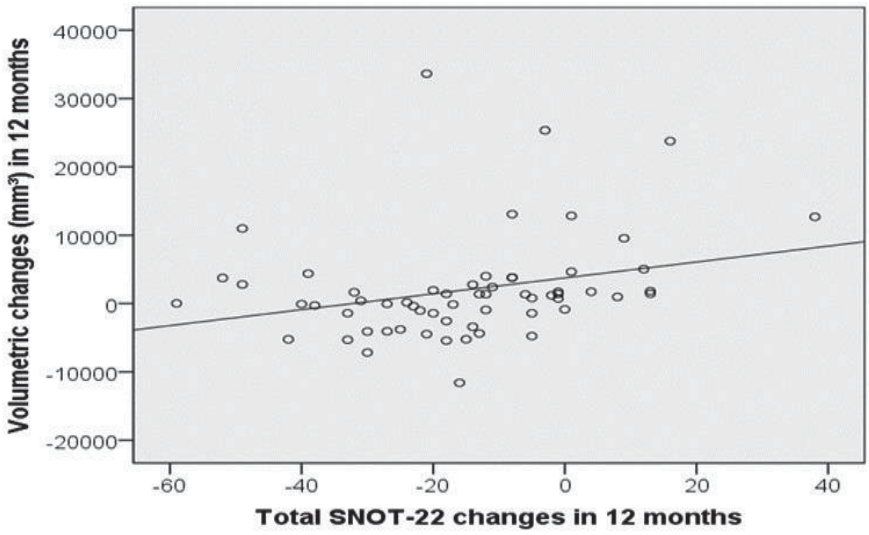

Figure 10. The correlation between the 3D volumetric changes and SNOT-22 changes (Spearman's rho 0.38, $p \leq 0.01$). The volumetric changes are presented in cubic millimetres. (I)

5.2 Printing nasal cavities in plastic 3D models using CBCT scans (II)

In the volumes of the maxillary sinuses, the results *in vivo* were higher with a ratio of 1.05 ± 0.01 (mean ± SD) compared with the volumetric results *in vitro*. In the nasal cavities, the volumetric measurements were higher *in vivo* with a ratio of 1.20 ± 0.1 (mean ± SD) when compared with the results *in vitro*. In the linear measurement, the results were higher in the measurements *in vivo*: 1.03 ± 0.02 (mean ± SD) in nasal septum length, 1.04 ± 0.03 (mean ± SD) in the height of the nasal cavity and 1.06 ± 0.1 (mean ± SD) in the width of the nasal cavity.

The resistance *in vivo*, measured with rhinomanometry, was less in inspiration with a geometric mean ratio of 0.77 and in expiration with a ratio of 0.71. Respectively, standard deviation factors were 2.78 and 2.32. When the results *in vitro* were scaled based on nasal cavity volume and septum length differences, the similar ratios were 1.03 and 0.95 with standard deviation factors of 2.86 and 2.39, respectively. The total resistance results obtained with rhinomanometry were analogous to the unilateral measurement results. The graphs *in vitro* generated by the rhinomanometric software were close to the graphs *in vivo* (Figure 11).

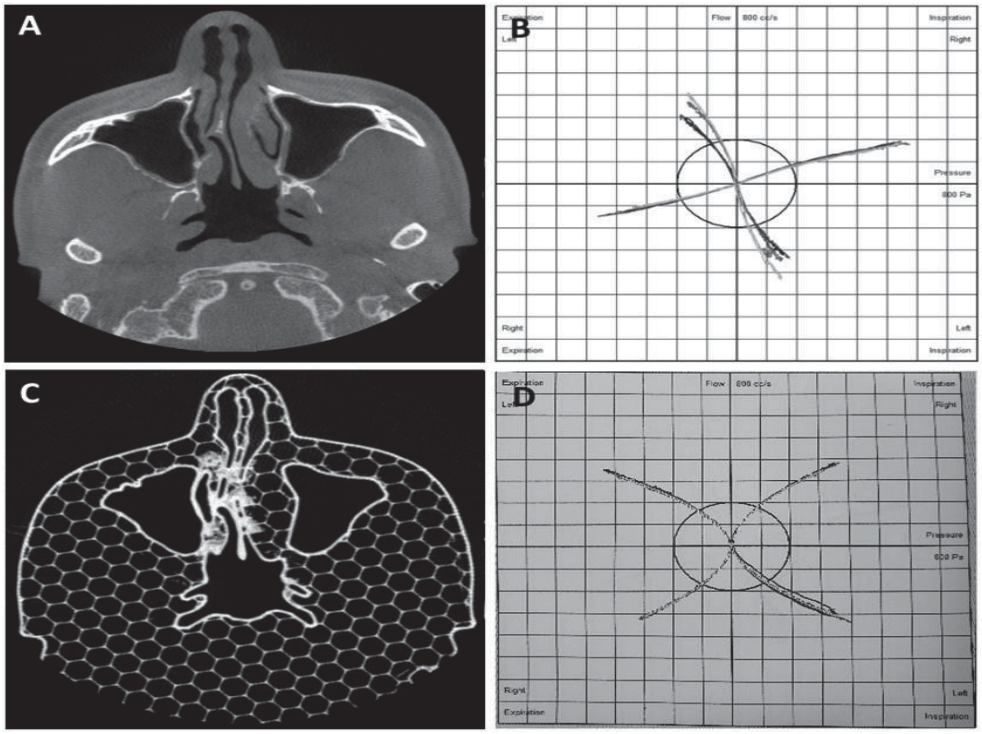

Figure 11. Above: Axial CBCT image (A) from a patient and rhinomanometry (B) from the same patient. Below: Corresponding CBCT image (C) and rhinomanometry (D) from the 3D print. Rhinomanometric graphs are close to each other. Small divergences from the original can be observed in the plastic 3D print. (II)

5.3 PIV performance in validating CFD models based on nasal cavity CBCT scans (III)

Axial mean flow velocities calculated from laminar CFD showed the highest results in the left nasal cavity's lower third in the first cross-section and in the middle third in the second cross-section (Figure 12a). This corresponded with the PIV measurements (Figure 12b). In the right nasal cavity, the calculated axial mean flow velocities in laminar CFD were highest in the lower third of the first cross-section and in the lower third of the third cross-section. The CFD calculations corresponded with the PIV measurements. In the fourth cross-section, the axial mean velocities were equal between laminar CFD and PIV in both the left and right sides. The differences in axial mean velocities between the laminar and turbulent (k-ω and k-ω SST) CFD models were small.

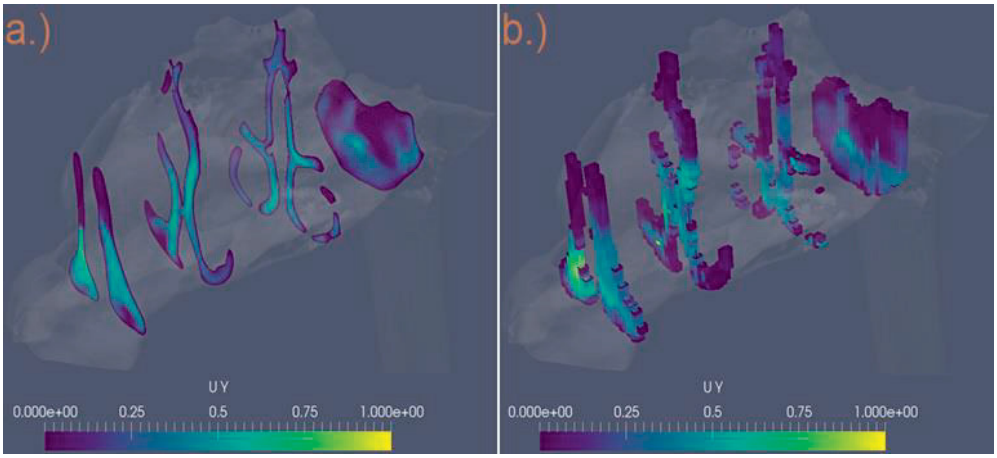

Figure 12. The velocities in the four analysed coronal cross-sections (UY=velocity in y axis). The lowest values are presented in violet and the highest in yellow. a.) Axial mean flow velocities (m/s) from laminar CFD results. b.) Axial mean flow velocities (m/s) from PIV measurements. (III)

The main volume of the flow calculated from CFD in the left nasal cavity's first cross-section was in the lower third with a ratio of 0.47. The PIV measurement in the same location was 0.48. In the right nasal cavity, the main volume of the flow calculated from laminar CFD was in the lower third of the nasal cavity in all three most anterior cross-sections with ratios ranging from 0.35 to 0.42. Corresponding PIV measurements were from 0.35 to 0.41. In the fourth cross-section, the volume of the flow was equal between laminar CFD and PIV for the left (0.42) and right sides (0.58). The differences in axial volume flow rate ratios between the laminar and turbulent (k-ω and k-ω SST) CFD models were minute.

Median wall shear stress was highest in the lower third of the first cross-section at 7.76 Pa (Figure 13). In the second cross-section, median wall shear stress varied from 2.07 Pa to 6.55 Pa and in the third cross-section from 4.02 Pa to 5.97 Pa. In the whole fourth cross-section, median wall shear stress was 2.92 Pa.

CFD calculations with the calculated flow corresponding to the flow of 20 l/min *in vivo* did not show any notable differences between the CFD models. However, median wall shear stress results showed observable differences between the flows corresponding to human breathing of 10 l/min and 20 l/min.

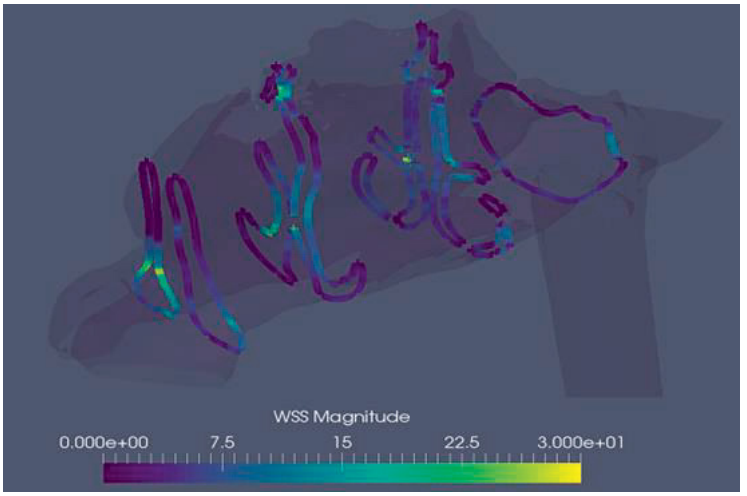

Figure 13. Mean wall shear stresses (Pa) in the four analysed coronal cross-sections. The lowest values are presented in violet and the highest in yellow. (III)

5.4 3D volumetric and cross-sectional area measurements from CBCT scans in assessing the results of inferior turbinate surgery (IV)

The preoperative median total volume from the combined left and right inferior turbinates was 11.7 cm^3, while the median total volume postoperatively was 9.3 cm^3 ($p<0.01$). In the anterior 5 mm to 20 mm of the inferior turbinate, the preoperative inferior turbinate total volume of 4.2 cm^3 decreased postoperatively to 3.0 cm^3 ($p<0.001$). Corresponding volumetric results for the pneumatized area in the anterior part increased from 2.3 cm^3 to 3.4 cm^3 ($p<0.001$).

When the preoperative and postoperative measurements were analysed together, comprising 48 cases in total, the volumetric measurements of the pneumatized nasal cavity in the anterior part of the measured region correlated with V2-5 results from acoustic rhinometry and with VAS scores (Figure 14). Moreover, turbinate volume correlated with VAS and QOL scores in the anterior part of its volume. However, the measurements of the whole length of the inferior turbinate or the changes in it did not show correlation with the other parameters. In addition, the volume changes in the anterior part of the inferior turbinate or the air space surrounding it did not correlate with changes in the other parameters.

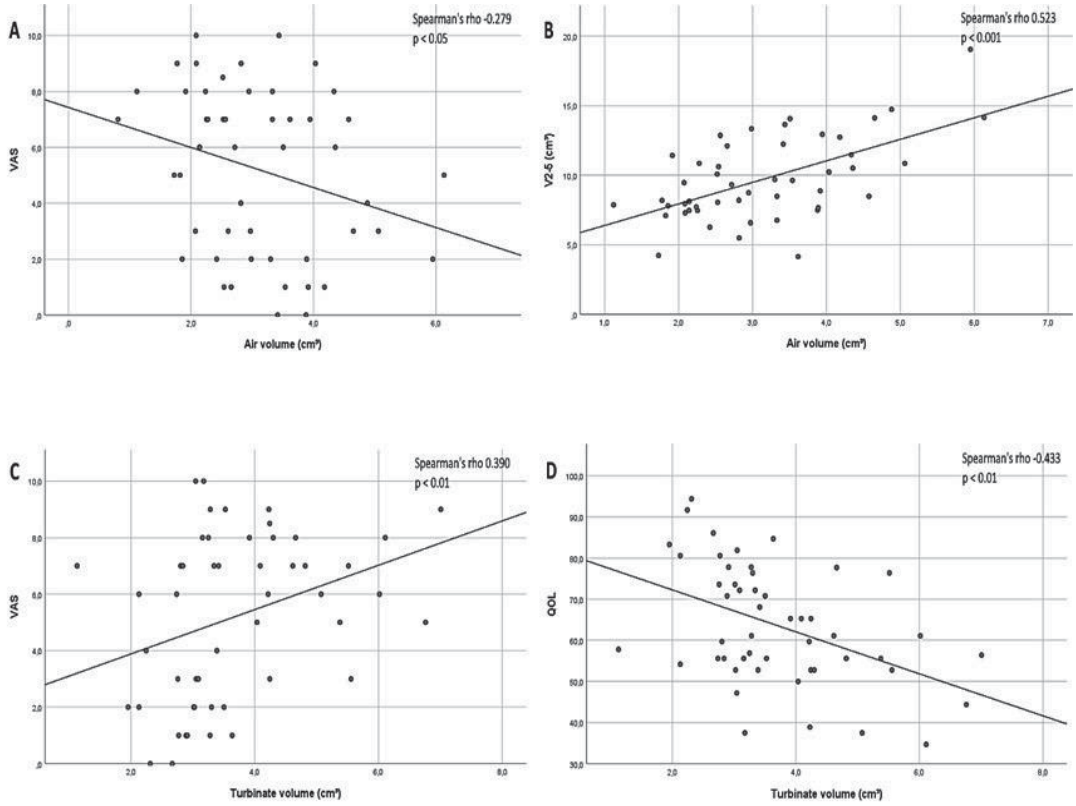

Figure 14. Correlation graphs for the 3D volumetric measurements of the individual anterior parts of the inferior turbinates (n = 48). The air volume (cm^3) correlations between VAS score and V2-5 (cm^3) are presented in graphs A and B. The turbinate volume (cm^3) correlations between VAS and QOL scores are presented in graphs C and D. Spearman's rho number and R^2 correlation line are included in the graphs. (IV)

The main changes in cross-sectional area from pre- to postoperative measurements were found in the region of the operated anterior part of the inferior turbinate and the pneumatized area surrounding it (Figure 15). The changes were also statistically significant. Some smaller cross-sectional area changes with a statistical significance were also found in the posterior regions of the inferior turbinate. The cross-sectional area measurements correlated with VAS and QOL scores in the most anterior measurement points when the pre- and postoperative measurements were analysed together (Table 2). However, the results did not correlate with the results from acoustic rhinometry, and in addition, the cross-sectional area changes did not correlate with changes in the other parameters.

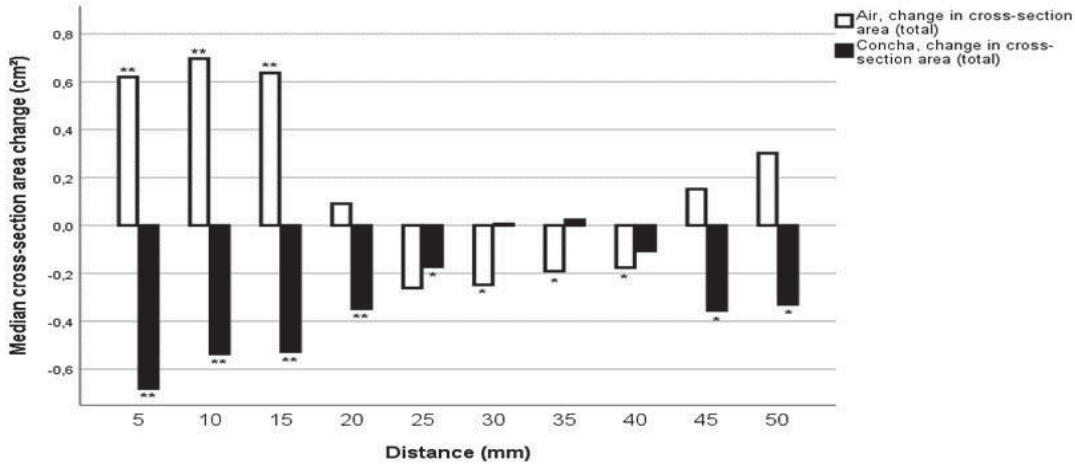

Figure 15. Cross-sectional area change in both inferior turbinate (concha) and surrounding air in every measuring point (n = 25). The results have been calculated from the median total cross-sectional area measurements. The distance represents the measuring point distance from the anterior peak of the inferior turbinate. Statistically significant changes, analysed with Wilcoxon signed-rank test, are marked with an asterisk (** for p<0.01 and * for p<0.05). (IV)

Table 2. Cross-sectional area correlation with VAS and QOL scores in the area of the anterior part of the inferior turbinate for both pre- and postoperative results (n = 48). The correlation coefficient with VAS and QOL is shown for each cross-sectional area measuring point from the anterior part (5-20 mm) of the inferior turbinate. The statistically significant results, analysed with Spearman's rho test, are presented with an asterisk (** for p<0.01 and * for p<0.05). (IV)

Cross-sectional area correlation with VAS and QOL

	Air				Turbinate			
	5 mm	**10 mm**	**15 mm**	**20 mm**	**5 mm**	**10 mm**	**15 mm**	**20 mm**
VAS	-0.408**	-0.411**	-0.261	0.006	0.539**	0.439**	0.379**	0.242
QOL	0.280*	0.323*	0.242	-0.031	-0.400**	-0.377**	-0.411**	-0.251

6 DISCUSSION

6.1 Present patient imaging and unused potential

Today, the use of patient scans in clinical work is still based on analysing consecutive 2D slices, and many clinicians are prone to use only one of the three available image plains. Furthermore, when using image staging methods, the subjective opinion of the clinician can affect the results (Basu, Georgalas, Kumar, & Desai, 2005). At present, the predictions of medical treatment or surgery results in the nasal cavity and the paranasal sinuses, especially when treating nasal congestion, are directional. In order to better understand the reasons underlying patient symptoms and to improve the predictions of the effects of different medical and surgical treatments on the symptoms, a more sophisticated method is required.

As presented in the studies of this dissertation, changes in the mucous membrane of the maxillary sinuses, nasal turbinate size and nasal cavity air space can be assessed and measured with greater objectivity and accuracy compared to the staging methods being used today. The present studies also indicate that CT scans are able to provide more valuable information on the conditions in the nasal cavity by functioning as a basis for 3D modelling and CFD analyses. In addition, CBCT-based 3D models were observed to be sufficiently close to the quality of the previously presented sinonasal clinical CT-based 3D modelling (Hopkins, L. M. et al., 2000; Spence et al., 2011) and CFD (Na et al., 2012) utilizations. Thus, it is possible to achieve sufficient additional information on the conditions in the nasal cavity with less radiation exposure to patients than is induced with clinical CT. The use of the methods presented in this dissertation have the potential to increase our understanding of the airflow and mucous membrane conditions in the nasal cavity, and thus could provide a basis for more sophisticated analysis and treatment planning tools for clinical decision making.

3D modelling has potential in predicting the results of the chosen nasal cavity and paranasal sinus treatment. Previous studies have contributed to this subject by assessing the effects of different surgical procedures on nasal cavity airflow mechanics in calculated CFD 3D models. These studies showed that nasal cavity operations in calculated models cause the airflow in the nasal cavity to alter its

distribution (Zhao et al., 2006) and more aggressive surgery can cause disturbances in the physiological intranasal air conditioning due to disturbed airflow patterns added with an increase of nasal cavity volume in relation to the surface area (Lindemann et al., 2005). However, it should be born in mind that these studies are based solely on single model experiments and that comprehensive studies comparing the CFD calculations and actual patient results with a large group of patients are still lacking.

6.2 Patient scan-based 3D assessment and measurements of the nasal cavity

6.2.1 CT-based measurements and staging

Nowadays, LM staging and other staging methods are used as objective methods to assess the severity of chronic rhinosinusitis from CT scans. These methods are easy and simple to use. The downside of these methods is that the produced results are only visual estimates of the mucous membrane conditions and the results can be affected by the subjective opinion of the clinician (Basu et al., 2005). Compared to LM staging and its derivative, the actual measurement of maxillary sinus air space volume in study II was shown to be more accurate in detecting even the smallest changes in the maxillary sinus air space, and thus inversely in mucous membrane thickness. In turn, the change in volume has to be notable in order to be detected by the staging methods, as can be seen in study II.

These results are in line with previous studies in which CRS patients were treated with single-dose triamcinolone (Likness et al., 2014; Pallanch et al., 2013). These studies found the 3D volume measurements to be more comprehensive and sensitive compared to LM in assessing mucous membrane change and to correlate better with patient symptoms. Moreover, the 3D measurements in the present studies are based on fixed HU values. Therefore, in addition to increased accuracy, the 3D measurements could decrease the subjectivity of the results when assessing sinonasal conditions.

It has to be taken into consideration, however, that neither the 3D volumetric measurement nor the staging method changes had strong correlation with the patients' symptom experience in study II. This finding is in line with previous studies reporting a lack of correlation between objective assessments with CT scan staging

methods and patient symptoms (Bradley & Kountakis, 2005; Hopkins, C. et al., 2007; Pallanch et al., 2013). Therefore, our results further strengthen the previous findings that visual assessments are not enough to evaluate the effects of paranasal mucous membrane changes on patient experiences of nasal symptoms. However, the 3D measurement method used in our studies can be further utilized as a basis for 3D modelling and flow calculations.

CBCT scans are known to produce more rugged boundary layers between different anatomical structures than clinical CT scans. In addition, CBCT scans have been shown to be less precise in differing tissue divergences (Al Abduwani et al., 2016). However, as previously described, these observations do not cause significant differences in anatomical landmark measurements between clinical CT and CBCT (Guyader et al., 2018; Peltonen et al., 2007). In these earlier studies, both imaging methods proved to have the same level of accuracy in revealing clinically and surgically significant middle ear structures as well as producing 3D reconstructions of human temporal bone. As reported in the present studies, defining the boundary layer between air and soft tissue with patient CBCT scans is possible with reasonable accuracy and repeatability with constant HU threshold values.

6.2.2 CT measurements and acoustic rhinometry

When it comes to assessing the nasal symptoms caused by nasal cavity structures, such as hypertrophied inferior turbinates, the clinical visual examination functions as the basis and is supported by outpatient measurements, such as acoustic rhinometry and rhinomanometry. The downside of visual examination-based evaluation is that it is always, to some extent, dependant on the subjective opinion of the clinician. Additionally, acoustic rhinometry and rhinomanometry, although informative and relatively easy to use, have not shown correlating results with patient symptoms (Kim, C. S. et al., 1998). What is more, acoustic rhinometry, although quite accurate in the anterior regions with a mean error of 4.5%, overestimates the dimensions of the nasal cavity in the middle and posterior regions of the nasal cavity by 20% in volume and by more than twice in cross-sectional areas (Cankurtaran et al., 2007; Numminen et al., 2003; Terheyden et al., 2000).

Actual cross-sectional area and 3D volume measurements could decrease the subjectivity and uncertainty factors that are present in clinical visual examination and outpatient measurements. In studies II and IV, the CBCT scans were shown to be applicable in measuring nasal cavity volumes in 3D, and, as presented in study IV,

the cross-sectional area measurements were performed with good accuracy. For cross-sectional area measurements, the identification of the border between the air space and soft tissue in CBCT scans caused minor challenges. The identification of the exact border sometimes confused the measuring software, and thus required some manual correction.

As shown in study IV, the actual cross-sectional area measurements did not correlate with the results gained from acoustic rhinometry, although the V2-5 results correlated with 3D volume measurements. This is in line with the previously mentioned findings that acoustic rhinometry has uncertainties in providing accurate dimensional measurements. In addition, the cross-sectional area measurements in study IV, especially in the operated areas, were shown to have correlation with the results from the VAS and the QOL questionnaire. Compared to the results presented in a previous study showing no correlation between VAS and rhinometric tests (Kim, C. S. et al., 1998), the results of the present study are promising in the targeting of better objective rhinologic patient assessment methods.

6.3 Patient imaging applicability for 3D modelling and assessment of nasal function

Patient scans proved to be an applicable basis for 3D modelling of the nasal cavity in the present studies. The virtual 3D models created from the CBCT scans were suitable for converting to STL files, and these were sufficient for further use in 3D printing and flow calculations. The produced virtual 3D models were observed to have slight surface roughness due to the resolution quality of the CBCT scans. However, this was compensated for in the convergence to STL files phase in which the surface was very slightly smoothened without notably affecting the volume or structure of the virtual 3D model.

Compared to previous studies that have used clinical CT scans for the virtual (Lintermann & Schröder, 2019; Na et al., 2012) and printed (Hopkins, L. M. et al., 2000; Kim, J. K. et al., 2006; Na et al., 2012) 3D modelling of the nasal cavity, the 3D models produced in the present studies were observed to be visually comparable. The main anatomical differences emerged in the narrow structures, where the resolution of the CBCT scans is lower than in clinical CT scans.

Based on the present and previous studies, patient imaging is applicable for PIV measurements and CFD calculations. Previous studies modelling nasal cavity airflow with PIV measurements and CFD calculations have used clinical CT scans as the

basis for the experiments. These experimental studies have produced good visual presentations of the flows with different flow velocities (Lintermann & Schröder, 2019; Na et al., 2012). The visual results with both PIV and CFD in the present CBCT studies are close to the previous visual presentations. Both the previous and present studies showed the main flow routing mainly in the region of the inferior turbinates in the anterior part of the nasal cavity and in the region of the middle turbinates in the middle parts of the nasal cavity.

However, the numerical PIV and CFD results of the present studies are not fully comparable with those of previous studies. This is because previous study setups have varied, and the results have mainly been presented with visual presentations without comprehensive numerical results. It also has to be taken into consideration that there are no constant measurement locations for PIV measurements and CFD calculations. In study III, the visual presentations are accompanied by numerical results in order to increase the comparability of the results for future studies. The presented locations of the numerical results could also function as the reference locations for additional studies.

6.4 Patient scan-based 3D print applicability for the 3D modelling of the nasal cavity

The manufacture of 3D prints of the nasal cavities both in plastic and silicone produced visually realistic end products compared to the original anatomy of the patient nasal cavities. Also, the FDM 3D printing technique used in our studies was shown to be useful for the presented use. The most distinct anatomical structures, such as maxillary sinuses as well as the lower and middle regions of the nasal cavities, turned out to be most convenient to print into 3D models. Moreover, in the present studies, these regions suffered the least risk of artefact. The small and narrow structures, mainly representing upper nasal cavity regions and narrow meatuses, were more vulnerable during 3D printing. These structures were at risk of collapsing when the printing was performed starting from below. Additionally, the structures representing inferior turbinates were at risk of bending under weight in the traditional 3D printing orientation. This problem was solved by altering the 3D printing orientation of the virtual model upside down and starting the printing process from the upper regions. Thus, the problematic structures were provided with better fixation support, as the insertions of these structures were printed first.

In study II, the nasal cavity structures were, for the first time, printed in plastic 3D models for study purposes. During the production of these 3D models, no support structures were used. These could help to fine-tune the 3D printing results in plastic 3D prints of the nasal cavity. However, the concern was that the removal of these support structures either manually or by dissolving could be very challenging from the narrow structures. The removal of excess supporting structures could also cause an additional risk of producing post-processing artefacts in the end products.

In study III, following closely the process presented in a study by Hopkins et al. (2000), the 3D printing was started with the production of a water-soluble 3D model of the air space, thereby functioning as the negative for the nasal cavity structures before using it to produce the actual end product with poured silicone. In this method, the removal of the water-soluble air space model from inside the hardened silicone model proved to be challenging and laborious. Despite the use of a water-soluble material, some additional manual removal of the excess material was required.

In both studies II and III, the 3D prints produced were based on patient CBCT scans. In addition, the 3D prints were also CBCT scanned for comparison with the original anatomy and for the verification of the resemblance. The produced 3D prints in both plastic and silicone were found to be very close to the original anatomy. In the plastic 3D models, the resemblance to the original was over 94%. The measured linear and 3D volume measurements were close to the original, especially in the well-defined areas. Small and narrow structures proved to be challenging to print in 3D. This was also found in the nasal cavity volumetric measurements, where the difference between the original and printed structures was 20% in mean results. These results are in line with the results of a previous study in which the mean dimensional error of the clinical CT-based 3D print was from 2.10% to 2.67% when compared to the original dry skull measurements (Silva et al., 2008). The same study also pointed out that small foramina, thin bones and acute bone projections are problematic to print which is a coaxial observation to the findings in study II.

In study III, the resemblance of the produced 3D silicone model to the original anatomy was visually inspected from the respective CBCT scans. Since no comparative measures or surface structure analysis could be found from the literature concerning nasal cavity printing, the 3D silicone model was visually compared to previous clinical CT-based silicone models. With visual comparison, the accuracy of the CBCT-based 3D silicone model in study III was close to the

accuracy of the previous CT-based 3D silicone models illustrated in studies by Hopkins et al. (2000), Spence et al. (2011) and Na et al. (2012)

In study II, the 3D printing of the nasal cavity was performed in plastic for the first time, and rhinomanometric measurements were done with the produced plastic 3D prints to compare the results with patient measurements. The plastic 3D prints were applicable for producing rhinomanometric measurements and the graphs gained from these tests were comparable to the original patient rhinomanometric graphs. Although some challenges were encountered with the rhinomanometric results due to the challenges in printing narrow structures, the 3D prints turned out to be promising for modelling human rhinomanometric results, and thus nasal airflow characteristics.

The present studies showed that different printing materials can have different HU thresholds when defining the boundary layer between air and the printing material in question. This has to be taken into consideration when studying and comparing 3D prints to patient measurements and scans. In the present studies, the use of both plastic and silicone were found applicable for the intended use in each study in which they were used. However, these materials are inflexible, and this can have an effect on the rhinometric and PIV measurements. In future, it would be reasonable to experiment on and study materials that would have a more flexible surface structure. These materials could possibly perform as better representatives of the surface properties of the nasal mucosa, and thus improve the possibility of producing a realistic printed nasal 3D model.

6.5 Strengths and limitations

The strength of the present studies is the interdisciplinary implementation, including both the medical and fluid mechanical engineering sciences. The present studies comprehensively used sinonasal patient scans in 3D print studies for the first time. Moreover, the sinonasal patient scan-based virtual and printed sinonasal 3D models as well as the flow calculations were studied in comparison to clinical assessment methods of the nasal cavity and patient symptoms that included acoustic rhinometry, rhinomanometry, SNOT-22 and VAS.

The results of the present pilot studies are, however, limited by the relatively small sample size in the virtual 3D modelling and measurement studies and, in part, the experimental setup of the 3D print and flow calculation studies. Thus, from a clinical point of view, a more extensive sample size will be needed in future, especially to

verify our flow mechanical findings and to fine-tune the nasal cavity airflow model as well as the phases of the nasal cavity 3D printing.

6.6 Future aspects

Due to their capabilities, CBCT, as presented in this dissertation, and both clinical CT and MRI, as presented in previous studies, can be used for enhanced three-dimensional applications. In future, patient imaging-based CFD studies should concentrate on finding and illustrating the local and universal nasal airflow characteristics that are affecting the symptoms of both nasal congestion and patency. Furthermore, following the previous study setups by Lindemann et al. (2005), Zhao et al. (2006) and Chen et al. (2010), the aim of future studies ought to be to further study the effects of different sinonasal treatments on nasal airflow characteristics and also on patient symptoms. As a continuum, more studies that compare the sinonasal symptom relief gained after surgery, which is based on surgery planning using both conventional clinical assessment and CFD 3D calculations, should be performed in future. The imaging-based 3D modelling and CFD studies should also be expanded to include the naso- and hypopharynx, and thereby widening the assessed upper airway region. In doing so, medical conditions, such as sleep apnoea, that concern wider upper airway regions could be studied more comprehensively.

For future studies and software innovators, the aim should be to develop a more automated 3D modelling and computation software package to speed up the 3D analysis of both the sinonasal structures and the airflow conditions. This could provide clinicians with a more comprehensive understanding of the reasons behind different nasal symptoms. Moreover, fully automated 3D modelling and CFD software could have potential in functioning as a pre-treatment planning tool for clinicians, as tentatively presented in a recent study (Hemtiwakorn et al., 2015). In order to achieve these goals, different computational models should be comprehensively studied and compared to the measurements achieved with patients and patient modelling 3D prints.

7 CONCLUSIONS

1. CBCT was proven to have sufficient accuracy for virtual sinonasal 3D modelling.

2. Volumetric measurements of the maxillary sinuses taken from patient scans were found to be more accurate and objective than conventional mucous membrane thickness staging systems. Nasal cavity volume and cross-sectional area measurements taken from patient scans were found to provide objective results and also had a promising correlation with patient symptoms.

3. Patient imaging was found to provide sufficiently accurate scans that can be used to print sinonasal 3D models with acceptable congruence with the original patient anatomy.

4. Patient imaging-based 3D models can be used with sufficient accuracy for studies modelling nasal airflow properties.

8 REFERENCES

Abul-Kasim, K., Strömbeck, A., & Sahlstrand-Johnson, P. (2011). Low-dose computed tomography of the paranasal sinuses: Radiation doses and reliability analysis. *American Journal of Otolaryngology, 32*(1), 47-51. doi:10.1016/j.amjoto.2009.08.004

Adrian, R. J. (1991). Particle-imaging techniques for experimental fluid mechanics. *Annual Review of Fluid Mechanics, 23*(1), 261-304. doi:10.1146/annurev.fl.23.010191.001401

Al Abduwani, J., ZilinSkiene, L., Colley, S., & Ahmed, S. (2016). Cone beam CT paranasal sinuses versus standard multidetector and low dose multidetector CT studies. *American Journal of Otolaryngology, 37*(1), 59-64. doi:10.1016/j.amjoto.2015.08.002

Alghadir, A. H., Anwer, S., Iqbal, A., & Iqbal, Z. A. (2018). Test-retest reliability, validity, and minimum detectable change of visual analog, numerical rating, and verbal rating scales for measurement of osteoarthritic knee pain. *Journal of Pain Research, 11*, 851-856. doi:10.2147/JPR.S158847

Al-Okshi, A., Lindh, C., Sale, H., Gunnarsson, M., & Rohlin, M. (2015). Effective dose of cone beam CT (CBCT) of the facial skeleton: A systematic review. *The British Journal of Radiology, 88*(1045), 20140658. doi:10.1259/bjr.20140658

Al-Ramahi, J., Luo, H., Fang, R., Chou, A., Jiang, J., & Kille, T. (2016). Development of an innovative 3D printed rigid bronchoscopy training model. *The Annals of Otology, Rhinology, and Laryngology, 125*(12), 965-969. doi:0003489416667742

Arai, Y., Tammisalo, E., Iwai, K., Hashimoto, K., & Shinoda, K. (1999). Development of a compact computed tomographic apparatus for dental use. *Dentomaxillofacial Radiology, 28*(4), 245-248. doi:10.1038/sj/dmfr/4600448

Bäck, L. J., Hytönen, M. L., Malmberg, H. O., & Ylikoski, J. S. (2002). Submucosal bipolar radiofrequency thermal ablation of inferior turbinates: A long-term follow-up with subjective and objective assessment. *The Laryngoscope, 112*(10), 1806-1812. doi:10.1097/00005537-200210000-00019

Baraniuk, J. N., & Merck, S. J. (2009). New concepts of neural regulation in human nasal mucosa. *Acta Clinica Croatica, 48*(1), 65-73.

Basu, S., Georgalas, C., Kumar, B. N., & Desai, S. (2005). Correlation between symptoms and radiological findings in patients with chronic rhinosinusitis: An evaluation study using the sinonasal assessment questionnaire and lund-mackay grading system. *European Archives of Oto-Rhino-Laryngology : Official*

Journal of the European Federation of Oto-Rhino-Laryngological Societies (EUFOS) : Affiliated with the German Society for Oto-Rhino-Laryngology - Head and Neck Surgery, 262(9), 751-754. doi:10.1007/s00405-004-0891-0

Becquemin, M. H., Swift, D. L., Bouchikhi, A., Roy, M., & Teillac, A. (1991). Particle deposition and resistance in the noses of adults and children. *European Respiratory Journal, 4*(6), 694-702. Retrieved from https://www.ncbi.nlm.nih.gov/pubmed/1889496

Bensch, G. W. (2016). Safety of intranasal corticosteroids. *Annals of Allergy, Asthma & Immunology : Official Publication of the American College of Allergy, Asthma, & Immunology, 117*(6), 601-605. doi:S1081-1206(16)30332-5

Berens, A. M., Newman, S., Bhrany, A. D., Murakami, C., Sie, K. C., & Zopf, D. A. (2016). Computer-aided design and 3D printing to produce a costal cartilage model for simulation of auricular reconstruction. *Otolaryngology--Head and Neck Surgery : Official Journal of American Academy of Otolaryngology-Head and Neck Surgery, 155*(2), 356-359. doi:10.1177/0194599816639586

Berger, M., Giotakis, A. I., Pillei, M., Mehrle, A., Kraxner, M., Kral, F., . . . Freysinger, W. (2021). Agreement between rhinomanometry and computed tomography-based computational fluid dynamics. *International Journal of Computer Assisted Radiology and Surgery, 16*(4), 629-638. doi:10.1007/s11548-021-02332-1

Beule, A. G. (2010). Physiology and pathophysiology of respiratory mucosa of the nose and the paranasal sinuses. *GMS Current Topics in Otorhinolaryngology, Head and Neck Surgery, 9*, Doc07. doi:10.3205/cto000071

Bijur, P. E., Silver, W., & Gallagher, E. J. (2001). Reliability of the visual analog scale for measurement of acute pain. *Academic Emergency Medicine : Official Journal of the Society for Academic Emergency Medicine, 8*(12), 1153-1157. doi:10.1111/j.1553-2712.2001.tb01132.x

Bizaki, A. J., Numminen, J., Taulu, R., & Rautiainen, M. (2016). Decrease of nasal airway resistance and alleviations of symptoms after balloon sinuplasty in patients with isolated chronic rhinosinusitis: A prospective, randomised clinical study. *Clinical Otolaryngology : Official Journal of ENT-UK ; Official Journal of Netherlands Society for Oto-Rhino-Laryngology & Cervico-Facial Surgery, 41*(6), 673-680. doi:10.1111/coa.12583

Blomgren, K., Simola, M., Hytönen, M., & Pitkäranta, A. (2003). Peak nasal inspiratory and expiratory flow measurements--practical tools in primary care? *Rhinology, 41*(4), 206-210.

Bradley, D. T., & Kountakis, S. E. (2005). Correlation between computed tomography scores and symptomatic improvement after endoscopic sinus surgery. *The Laryngoscope, 115*(3), 466-469. doi:00005537-200503000-00014

Brenner, D. J., & Hall, E. J. (2007). Computed tomography--an increasing source of radiation exposure. *The New England Journal of Medicine, 357*(22), 2277-2284. doi:357/22/2277

Buck, L., & Axel, R. (1991). A novel multigene family may encode odorant receptors: A molecular basis for odor recognition. *Cell, 65*(1), 175-187. doi:0092-8674(91)90418-X

Burke, T. F., Guertler, A. T., & Timmons, J. H. (1994). Comparison of sinus X-rays with computed tomography scans in acute sinusitis. *Academic Emergency Medicine : Official Journal of the Society for Academic Emergency Medicine, 1*(3), 235-239. doi:10.1111/j.1553-2712.1994.tb02437.x

Cailleaux, S., Sanchez-Ballester, N. M., Gueche, Y. A., Bataille, B., & Soulairol, I. (2020). Fused deposition modeling (FDM), the new asset for the production of tailored medicines. *Journal of Controlled Release : Official Journal of the Controlled Release Society,* doi:S0168-3659(20)30637-4

Cankurtaran, M., Celik, H., Coşkun, M., Hizal, E., & Cakmak, O. (2007). Acoustic rhinometry in healthy humans: Accuracy of area estimates and ability to quantify certain anatomic structures in the nasal cavity. *Annals of Otology, Rhinology & Laryngology, 116*(12), 906-916. doi:10.1177/000348940711601207

Chan, H. H., Siewerdsen, J. H., Vescan, A., Daly, M. J., Prisman, E., & Irish, J. C. (2015). 3D rapid prototyping for otolaryngology-head and neck surgery: Applications in image-guidance, surgical simulation and patient-specific modeling. *PloS One, 10*(9), e0136370. doi:10.1371/journal.pone.0136370

Chen, C., Cai, L., Zheng, W., Wang, J., Guo, X., & Chen, H. (2019). The efficacy of using 3D printing models in the treatment of fractures: A randomised clinical trial. *BMC Musculoskeletal Disorders, 20*(1), 65-9. doi:10.1186/s12891-019-2448-9

Chen, X. B., Lee, H. P., Chong, V. F., & Wang de, Y. (2010). Impact of inferior turbinate hypertrophy on the aerodynamic pattern and physiological functions of the turbulent airflow - a CFD simulation model. *Rhinology, 48*(2), 163-168. doi:10.4193/Rhin09.093

Cherobin, G. B., Voegels, R. L., Pinna, F. R., Gebrim, E M M S, Bailey, R. S., & Garcia, G. J. M. (2021). Rhinomanometry versus computational fluid dynamics: Correlated, but different techniques. *American Journal of Rhinology & Allergy, 35*(2), 245-255. doi:10.1177/1945892420950157

Chiesa Estomba, C. M., Gonzalez Fernandez, I., & Iglesias Otero, M. A. (2018). How we do it: Anterior and posterior nosebleed trainer, the 3D printing epistaxis project. *Clinical Otolaryngology : Official Journal of ENT-UK ; Official Journal of Netherlands Society for Oto-Rhino-Laryngology & Cervico-Facial Surgery, 43*(2), 765-766. doi:10.1111/coa.12711

Chung, S., & Kim, S. K. (2008). Digital particle image velocimetry studies of nasal airflow. *Respiratory Physiology & Neurobiology, 163*(1), 111-120. doi:https://doi.org/10.1016/j.resp.2008.07.023

Ciocca, L., Fantini, M., De Crescenzio, F., Persiani, F., & Scotti, R. (2011). Computer-aided design and manufacturing construction of a surgical template for craniofacial implant positioning to support a definitive nasal prosthesis.

Clinical Oral Implants Research, 22(8), 850-856. doi:10.1111/j.1600-0501.2010.02066.x

Ciprandi, G., Cirillo, I., Vizzaccaro, A., Pallestrini, E., & Tosca, M. A. (2006). Decongestion test in patients with allergic rhinitis: Functional evaluation of nasal airflow. *American Journal of Rhinology, 20*(2), 224-226.

Clement, P. A., Gordts, F., & Standardisation Committee on Objective Assessment of the Nasal Airway, IRS. (2005). Consensus report on acoustic rhinometry and rhinomanometry. *Rhinology, 43*(3), 169-179.

Corey, J. P. (2006). Acoustic rhinometry: Should we be using it? *Current Opinion in Otolaryngology & Head and Neck Surgery, 14*(1), 29-34. doi:10.1097/01.moo.0000193166.57129.80

Cozzi, F., Felisati, G., & Quadrio, M. (2017). Velocity measurements in nasal cavities by means of stereoscopic PIV - preliminary tests. *Journal of Physics: Conference Series,* , 882. doi:10.1088/1742-6596/882/1/012010

Crafts, T. D., Ellsperman, S. E., Wannemuehler, T. J., Bellicchi, T. D., Shipchandler, T. Z., & Mantravadi, A. V. (2017). Three-dimensional printing and its applications in otorhinolaryngology-head and neck surgery. *Otolaryngology--Head and Neck Surgery, 156*(6), 999-1010. doi:10.1177/0194599816678372

Dahl, R., & Mygind, N. (1998). Anatomy, physiology and function of the nasal cavities in health and disease. *Advanced Drug Delivery Reviews, 29*(1-2), 3-12. doi:S0169-409X(97)00058-6

Dawood, A., Marti Marti, B., Sauret-Jackson, V., & Darwood, A. (2015). 3D printing in dentistry. *British Dental Journal, 219*(11), 521-529. doi:10.1038/sj.bdj.2015.914

De Vos, W., Casselman, J., & Swennen, G. R. (2009). Cone-beam computerized tomography (CBCT) imaging of the oral and maxillofacial region: A systematic review of the literature. *International Journal of Oral and Maxillofacial Surgery, 38*(6), 609-625. doi:10.1016/j.ijom.2009.02.028

Deeb, R., Malani, P. N., Gill, B., Gil, B., Jafari-Khouzani, K., Soltanian-Zadeh, H., . . . Zacharek, M. A. (2011). Three-dimensional volumetric measurements and analysis of the maxillary sinus. *Am J Rhinol Allergy, 25*(3), 152-156. doi:10.2500/ajra.2011.25.3605

Doorly, D. J., Taylor, D. J., & Schroter, R. C. (2008). Mechanics of airflow in the human nasal airways. *Respiratory Physiology & Neurobiology, 163*(1-3), 100-110. doi:10.1016/j.resp.2008.07.027

Eccles, R. (2000). Nasal airflow in health and disease. *Acta Oto-Laryngologica, 120*(5), 580-595. doi:10.1080/000164800750000388

Eccles, R. (2011a). A guide to practical aspects of measurement of human nasal airflow by rhinomanometry. *Rhinology, 49*(1), 2-10. doi:10.4193/Rhino10.065

Eccles, R. (2011b). Mechanisms of the symptoms of rhinosinusitis. *Rhinology, 49*(2), 131-138.

Eccles, R., & Jones, A. S. (1983). The effect of menthol on nasal resistance to air flow. *The Journal of Laryngology and Otology, 97*(8), 705-709. doi:10.1017/s002221510009486x

Fatterpekar, G. M., Delman, B. N., & Som, P. M. (2008). Imaging the paranasal sinuses: Where we are and where we are going. *Anatomical Record (Hoboken, N.J.: 2007), 291*(11), 1564-1572. doi:10.1002/ar.20773

Fokkens, W. J., Lund, V. J., Hopkins, C., Hellings, P. W., Kern, R., Reitsma, S., . . . Zwetsloot, C. P. (2020). European position paper on rhinosinusitis and nasal polyps 2020. *Rhinology, 58*(Suppl S29), 1-464. doi:10.4193/Rhin20.600

Fokkens, W. J., & Scheeren, R. A. (2000). Upper airway defence mechanisms. *Paediatric Respiratory Reviews, 1*(4), 336-341. doi:10.1053/prrv.2000.0073

Fraczek, M., Guzinski, M., Morawska-Kochman, M., & Krecicki, T. (2017). Investigation of sinonasal anatomy via low-dose multidetector CT examination in chronic rhinosinusitis patients with higher risk for perioperative complications. *European Archives of Oto-Rhino-Laryngology : Official Journal of the European Federation of Oto-Rhino-Laryngological Societies (EUFOS) : Affiliated with the German Society for Oto-Rhino-Laryngology - Head and Neck Surgery, 274*(2), 787-793. doi:10.1007/s00405-016-4268-y

Freysinger, W., Gunkel, A. R., & Thumfart, W. F. (1997). Image-guided endoscopic ENT surgery. *European Archives of Oto-Rhino-Laryngology : Official Journal of the European Federation of Oto-Rhino-Laryngological Societies (EUFOS) : Affiliated with the German Society for Oto-Rhino-Laryngology - Head and Neck Surgery, 254*(7), 343-346. doi:10.1007/BF02630726

Friedman, W. H., Katsantonis, G. P., Sivore, M., & Kay, S. (1990). Computed tomography staging of the paranasal sinuses in chronic hyperplastic rhinosinusitis. *The Laryngoscope, 100*(11), 1161-1165. doi:10.1288/00005537-199011000-00005

Giannopoulos, A. A., Mitsouras, D., Yoo, S. J., Liu, P. P., Chatzizisis, Y. S., & Rybicki, F. J. (2016). Applications of 3D printing in cardiovascular diseases. *Nature Reviews.Cardiology, 13*(12), 701-718. doi:10.1038/nrcardio.2016.170

Gliklich, R. D., & Metson Ralph. (1994). A comparison of sinus computed tomography (CT) staging systems for outcomes research. *American Journal of Rhinology, 8*(6), 291-298. doi:https://doi.org/10.2500/105065894781874197

Guyader, E., Savean, J., Clodic, C., Letellier, P., Meriot, P., & Marianowski, R. (2018). Three-dimensional reconstruction of the temporal bone: Comparison of in situ, CT, and CBCT measurements. *European Annals of Otorhinolaryngology, Head and Neck Diseases, 135*(6), 393-398. doi:S1879-7296(18)30131-5

Haavisto, L. E., & Sipilä, J. I. (2013). Acoustic rhinometry, rhinomanometry and visual analogue scale before and after septal surgery: A prospective 10-year follow-up. *Clinical Otolaryngology : Official Journal of ENT-UK ; Official Journal of Netherlands Society for Oto-Rhino-Laryngology & Cervico-Facial Surgery, 38*(1), 23-29. doi:10.1111/coa.12043

Haenisch, B., Walstab, J., Herberhold, S., Bootz, F., Tschaikin, M., Ramseger, R., & Bonisch, H. (2010). Alpha-adrenoceptor agonistic activity of oxymetazoline and xylometazoline. *Fundamental & Clinical Pharmacology, 24*(6), 729-739. doi:10.1111/j.1472-8206.2009.00805.x

Haerle, S. K., Daly, M. J., Chan, H. H., Vescan, A., Kucharczyk, W., & Irish, J. C. (2013). Virtual surgical planning in endoscopic skull base surgery. *The Laryngoscope, 123*(12), 2935-2939. doi:10.1002/lary.24004

Hahn, I., Scherer, P. W., & Mozell, M. M. (1993). Velocity profiles measured for airflow through a large-scale model of the human nasal cavity. *Journal of Applied Physiology (Bethesda, Md.: 1985), 75*(5), 2273-2287. doi:10.1152/jappl.1993.75.5.2273

Harar, R. P., Kalan, A., & Kenyon, G. S. (2001). Assessing the reproducibility of nasal spirometry parameters in the measurement of nasal patency. *Rhinology, 39*(4), 211-214.

Hariri, B. M., & Cohen, N. A. (2016). New insights into upper airway innate immunity. *American Journal of Rhinology & Allergy, 30*(5), 319-323. doi:10.2500/ajra.2016.30.4360

Harju, T., Numminen, J., Kivekäs, I., & Rautiainen, M. (2018). A prospective, randomized, placebo-controlled study of inferior turbinate surgery. *The Laryngoscope, 128*(9), 1997-2003. doi:10.1002/lary.27103

Hasegawa, M., & Kern, E. B. (1977). The human nasal cycle. *Mayo Clinic Proceedings, 52*(1), 28-34.

Hemtiwakorn, K., Mahasitthiwat, V., Tungjitkusolmun, S., Hamamoto, K., & Pintavirooj, C. (2015). Patient-specific aided surgery approach of deviated nasal septum using computational fluid dynamics. *IEEJ Transactions on Electrical and Electronic Engineering, 10*(3), 274-286. doi:10.1002/tee.22084

Hendry, J., Chin, A., Swan, I. R., Akeroyd, M. A., & Browning, G. G. (2016). The glasgow benefit inventory: A systematic review of the use and value of an otorhinolaryngological generic patient-recorded outcome measure. *Clinical Otolaryngology : Official Journal of ENT-UK ; Official Journal of Netherlands Society for Oto-Rhino-Laryngology & Cervico-Facial Surgery, 41*(3), 259-275. doi:10.1111/coa.12518

Hilberg, O., Jackson, A. C., Swift, D. L., & Pedersen, O. F. (1989). Acoustic rhinometry: Evaluation of nasal cavity geometry by acoustic reflection. *Journal of Applied Physiology (Bethesda, Md.: 1985), 66*(1), 295-303. doi:10.1152/jappl.1989.66.1.295

Hochman, J. B., Rhodes, C., Wong, D., Kraut, J., Pisa, J., & Unger, B. (2015). Comparison of cadaveric and isomorphic three-dimensional printed models in temporal bone education. *The Laryngoscope, 125*(10), 2353-2357. doi:10.1002/lary.24919

Holmström, M., Scadding, G. K., Lund, V. J., & Darby, Y. C. (1990). Assessment of nasal obstruction. A comparison between rhinomanometry and nasal inspiratory peak flow. *Rhinology, 28*(3), 191-196.

Hopkins, C., Browne, J. P., Slack, R., Lund, V., & Brown, P. (2007). The lund-mackay staging system for chronic rhinosinusitis: How is it used and what does it predict? *Otolaryngology--Head and Neck Surgery : Official Journal of American Academy of Otolaryngology-Head and Neck Surgery, 137*(4), 555-561. doi:S0194-5998(07)00138-6

Hopkins, C., Gillett, S., Slack, R., Lund, V. J., & Browne, J. P. (2009). Psychometric validity of the 22-item sinonasal outcome test. *Clinical Otolaryngology : Official Journal of ENT-UK ; Official Journal of Netherlands Society for Oto-Rhino-Laryngology & Cervico-Facial Surgery, 34*(5), 447-454. doi:10.1111/j.1749-4486.2009.01995.x

Hopkins, L. M., Kelly, J. T., Wexler, A. S., & Prasad, A. K. (2000). Particle image velocimetry measurements in complex geometries. *Experiments in Fluids, 29*(1), 91-95. doi:10.1007/s003480050430

Ishikawa, S., Nakayama, T., Watanabe, M., & Matsuzawa, T. (2006). Visualization of flow resistance in physiological nasal respiration: Analysis of velocity and vorticities using numerical simulation. *Archives of Otolaryngology--Head & Neck Surgery, 132*(11), 1203-1209. doi:132/11/1203

Jamroz, W., Szafraniec, J., Kurek, M., & Jachowicz, R. (2018). 3D printing in pharmaceutical and medical applications - recent achievements and challenges. *Pharmaceutical Research, 35*(9), 176-x. doi:10.1007/s11095-018-2454-x

Janda, P., Sroka, R., Baumgartner, R., Grevers, G., & Leunig, A. (2001). Laser treatment of hyperplastic inferior nasal turbinates: A review. *Lasers in Surgery and Medicine, 28*(5), 404-413. doi:10.1002/lsm.1068

Jankowski, R., Nguyen, D. T., Poussel, M., Chenuel, B., Gallet, P., & Rumeau, C. (2016). Sinusology. *European Annals of Otorhinolaryngology, Head and Neck Diseases, 133*(4), 263-268. doi:10.1016/j.anorl.2016.05.011

Jeon, B., Lee, C., Kim, M., Choi, T. H., Kim, S., & Kim, S. (2016). Fabrication of three-dimensional scan-to-print ear model for microtia reconstruction. *The Journal of Surgical Research, 206*(2), 490-497. doi:S0022-4804(16)30264-5

Jones, N. (2001). The nose and paranasal sinuses physiology and anatomy. *Advanced Drug Delivery Reviews, 51*(1-3), 5-19. doi:S0169-409X(01)00172-7

Jones, N. S. (2002). CT of the paranasal sinuses: A review of the correlation with clinical, surgical and histopathological findings. *Clinical Otolaryngology and Allied Sciences, 27*(1), 11-17. doi:525

Jorgensen, R. A. (1991). Endoscopic and computed tomographic findings in ostiomeatal sinus disease. *Archives of Otolaryngology--Head & Neck Surgery, 117*(3), 279-287. doi:10.1001/archotol.1991.01870150047005

Juto, J. E., & Lundberg, C. (1982). An optical method for determining changes in mucosal congestion in the nose in man. *Acta Oto-Laryngologica, 94*(1-2), 149-156. doi:10.3109/00016488209128899

Keh, S. M., Facer, P., Yehia, A., Sandhu, G., Saleh, H. A., & Anand, P. (2011). The menthol and cold sensation receptor TRPM8 in normal human nasal mucosa and rhinitis. *Rhinology, 49*(4), 453-457. doi:10.4193/Rhin11.089

Kennedy, D. W. (1992). Prognostic factors, outcomes and staging in ethmoid sinus surgery. *The Laryngoscope, 102*(12 Pt 2 Suppl 57), 1-18.

Kennedy, D. W., Kuhn, F. A., Hamilos, D. L., Zinreich, S. J., Butler, D., Warsi, G., . . . Tavakkol, A. (2005). Treatment of chronic rhinosinusitis with high-dose oral terbinafine: A double blind, placebo-controlled study. *The Laryngoscope, 115*(10), 1793-1799. doi:00005537-200510000-00015

Kennedy, D. W., Zinreich, S. J., Kumar, A. J., Rosenbaum, A. E., & Johns, M. E. (1988). Physiologic mucosal changes within the nose and ethmoid sinus: Imaging of the nasal cycle by MRI. *The Laryngoscope, 98*(9), 928-933. doi:10.1288/00005537-198809000-00005

Keyhani, K., Scherer, P. W., & Mozell, M. M. (1995). Numerical simulation of airflow in the human nasal cavity. *Journal of Biomechanical Engineering, 117*(4), 429-441. doi:10.1115/1.2794204

Kim, C. S., Moon, B. K., Jung, D. H., & Min, Y. G. (1998). Correlation between nasal obstruction symptoms and objective parameters of acoustic rhinometry and rhinomanometry. *Auris, Nasus, Larynx, 25*(1), 45-48. doi:S0385-8146(97)10011-6

Kim, J. K., Yoon, J. H., Kim, C. H., Nam, T. W., Shim, D. B., & Shin, H. A. (2006). Particle image velocimetry measurements for the study of nasal airflow. *Acta Oto-Laryngologica, 126*(3), 282-287. doi:W332764821452243

Kimbell, J. S., Basu, S., Garcia, G. J. M., Frank-Ito, D. O., Lazarow, F., Su, E., . . . Wong, B. J. (2019). Upper airway reconstruction using long-range optical coherence tomography: Effects of airway curvature on airflow resistance. *Lasers in Surgery and Medicine, 51*(2), 150-160. doi:10.1002/lsm.23005

Klimek, L., Bergmann, K., Biedermann, T., Bousquet, J., Hellings, P., Jung, K., . . . Pfaar, O. (2017). Visual analogue scales (VAS): Measuring instruments for the documentation of symptoms and therapy monitoring in cases of allergic rhinitis in everyday health care: Position paper of the german society of allergology (AeDA) and the german society of allergy and clinical immunology (DGAKI), ENT section, in collaboration with the working group on clinical immunology, allergology and environmental medicine of the german society of otorhinolaryngology, head and neck surgery (DGHNOKHC). *Allergo Journal International, 26*(1), 16-24. doi:10.1007/s40629-016-0006-7

Koskinen, A., Hammaren-Malmi, S., Myller, J., Makela, M., Penttila, E., Pessi, T., . . . Hytonen, M. (2021). Translation, cross-cultural adaptation, and validation of the sino-nasal outcome test (snot)-22 for finnish patients. *European Archives of Oto-Rhino-Laryngology : Official Journal of the European Federation of Oto-Rhino-Laryngological Societies (EUFOS) : Affiliated with the German Society for Oto-Rhino-Laryngology - Head and Neck Surgery, 278*(2), 405-410. doi:10.1007/s00405-020-06297-w

Kumar, M., Shanavas, M., Sidappa, A., & Kiran, M. (2015). Cone beam computed tomography - know its secrets. *Journal of International Oral Health : JIOH, 7*(2), 64-68.

Langridge, B., Momin, S., Coumbe, B., Woin, E., Griffin, M., & Butler, P. (2018). Systematic review of the use of 3-dimensional printing in surgical teaching and assessment. *Journal of Surgical Education, 75*(1), 209-221. doi:https://doi.org/10.1016/j.jsurg.2017.06.033

Lassus, P., Lindford, A., Vuola, J., Back, L., Suominen, S., Mesimaki, K., . . . Tornwall, J. (2018). The helsinki face transplantation: Surgical aspects and 1-year outcome. *Journal of Plastic, Reconstructive & Aesthetic Surgery : JPRAS, 71*(2), 132-139. doi:S1748-6815(17)30413-8

Lee, H. Y., Kim, H. U., Kim, S. S., Son, E. J., Kim, J. W., Cho, N. H., . . . Yoon, J. H. (2002). Surgical anatomy of the sphenopalatine artery in lateral nasal wall. *The Laryngoscope, 112*(10), 1813-1818. doi:10.1097/00005537-200210000-00020

Lee, R. J., & Cohen, N. A. (2015). Taste receptors in innate immunity. *Cellular and Molecular Life Sciences, 72*(2), 217-236. doi:10.1007/s00018-014-1736-7

Lee, R. J., Xiong, G., Kofonow, J. M., Chen, B., Lysenko, A., Jiang, P., . . . Cohen, N. A. (2012). T2R38 taste receptor polymorphisms underlie susceptibility to upper respiratory infection. *Journal of Clinical Investigation, 122*(11), 4145-4159. doi:10.1172/JCI64240

Li, K. K., Powell, N. B., Riley, R. W., Troell, R. J., & Guilleminault, C. (1998). Radiofrequency volumetric tissue reduction for treatment of turbinate hypertrophy: A pilot study. *Otolaryngology--Head and Neck Surgery : Official Journal of American Academy of Otolaryngology-Head and Neck Surgery, 119*(6), 569-573. doi:10.1016/S0194-5998(98)70013-0

Likness, M. M., Pallanch, J. F., Sherris, D. A., Kita, H., Mashtare, T. L., & Ponikau, J. U. (2014). Computed tomography scans as an objective measure of disease severity in chronic rhinosinusitis. *Otolaryngology--Head and Neck Surgery : Official Journal of American Academy of Otolaryngology-Head and Neck Surgery, 150*(2), 305-311. doi:10.1177/0194599813513881

Lindemann, J., Brambs, H. J., Keck, T., Wiesmiller, K. M., Rettinger, G., & Pless, D. (2005). Numerical simulation of intranasal airflow after radical sinus surgery. *American Journal of Otolaryngology, 26*(3), 175-180. doi:S0196070905000396

Lintermann, A., & Schröder, W. (2019). A hierarchical numerical journey through the nasal cavity: From nose-like models to real anatomies. *Flow, Turbulence and Combustion, 102*(1), 89-116. doi:10.1007/s10494-017-9876-0

Liu, C. M., Tan, C. D., Lee, F. P., Lin, K. N., & Huang, H. M. (2009). Microdebrider-assisted versus radiofrequency-assisted inferior turbinoplasty. *The Laryngoscope, 119*(2), 414-418. doi:10.1002/lary.20088

Liu, J., Sun, L., Xu, W., Wang, Q., Yu, S., & Sun, J. (2019). Current advances and future perspectives of 3D printing natural-derived biopolymers. *Carbohydrate Polymers, 207*, 297-316. doi:S0144-8617(18)31410-3

Liu, S. C., Lu, H. H., Cheng, L. H., Chu, Y. H., Lee, F. P., Wu, C. C., & Wang, H. W. (2015). Identification of the cold receptor TRPM8 in the nasal mucosa.

American Journal of Rhinology & Allergy, 29(4), 112. doi:10.2500/ajra.2015.29.4202

Lorino, A. M., Lofaso, F., Abi-Nader, F., Drogou, I., Dahan, E., Zerah, F., . . . Lorino, H. (1998). Nasal airflow resistance measurement: Forced oscillation technique versus posterior rhinomanometry. *The European Respiratory Journal, 11*(3), 720-725.

Louvrier, A., Marty, P., Barrabe, A., Euvrard, E., Chatelain, B., Weber, E., & Meyer, C. (2017). How useful is 3D printing in maxillofacial surgery? *Journal of Stomatology, Oral and Maxillofacial Surgery, 118*(4), 206-212. doi:S2468-7855(17)30119-2

Lund, V. J., & Kennedy, D. W. (1997). Staging for rhinosinusitis. *Otolaryngology--Head and Neck Surgery : Official Journal of American Academy of Otolaryngology-Head and Neck Surgery, 117*(3 Pt 2), 35. doi:a83514

Lund, V. J., & Mackay, I. S. (1993). Staging in rhinosinusitus. *Rhinology, 31*(4), 183-184. Retrieved from https://www.ncbi.nlm.nih.gov/pubmed/8140385

MacArthur, F. J., & McGarry, G. W. (2017). The arterial supply of the nasal cavity. *European Archives of Oto-Rhino-Laryngology : Official Journal of the European Federation of Oto-Rhino-Laryngological Societies (EUFOS) : Affiliated with the German Society for Oto-Rhino-Laryngology - Head and Neck Surgery, 274*(2), 809-815. doi:10.1007/s00405-016-4281-1

Maniscalco, M., Sofia, M., & Pelaia, G. (2007). Nitric oxide in upper airways inflammatory diseases. *Inflammation Research, 56*(2), 58-69. doi:10.1007/s00011-006-6111-1

Marple, B. F., Brunton, S., & Ferguson, B. J. (2006). Acute bacterial rhinosinusitis: A review of U.S. treatment guidelines. *Otolaryngology--Head and Neck Surgery : Official Journal of American Academy of Otolaryngology-Head and Neck Surgery, 135*(3), 341-348. doi:S0194-5998(05)02321-1

Moss, W. J., Faraji, F., Jafari, A., & DeConde, A. S. (2019). A systematic review of the nasal septal turbinate: An overlooked surgical target. *American Journal of Otolaryngology, 40*(6), 102188. doi:S0196-0709(19)30071-7

Most, S. P., & Rudy, S. F. (2017). Septoplasty: Basic and advanced techniques. *Facial Plastic Surgery Clinics of North America, 25*(2), 161-169. doi:S1064-7406(16)30146-8

Mostafaei, A., Elliott, A. M., Barnes, J. E., Li, F., Tan, W., Cramer, C. L., . . . Chmielus, M. (2020). Binder jet 3D printing—Process parameters, materials, properties, modeling, and challenges. *Progress in Materials Science,* , 100707. doi:https://doi.org/10.1016/j.pmatsci.2020.100707

Mozzo, P., Procacci, C., Tacconi, A., Martini, P. T., & Andreis, I. A. (1998). A new volumetric CT machine for dental imaging based on the cone-beam technique: Preliminary results. *European Radiology, 8*(9), 1558-1564. doi:10.1007/s003300050586

Na, Y., Chung, K. S., Chung, S. K., & Kim, S. K. (2012). Effects of single-sided inferior turbinectomy on nasal function and airflow characteristics. *Respiratory Physiology & Neurobiology, 180*(2-3), 289-297. doi:10.1016/j.resp.2011.12.005

Naclerio, R. M., Bachert, C., & Baraniuk, J. N. (2010). Pathophysiology of nasal congestion. *International Journal of General Medicine, 3*, 47-57. doi:10.2147/ijgm.s8088

Naclerio, R. M., Pinto, J., Assanasen, P., & Baroody, F. M. (2007). Observations on the ability of the nose to warm and humidify inspired air. *Rhinology, 45*(2), 102-111. Retrieved from https://www.ncbi.nlm.nih.gov/pubmed/17708456

Netter, F. H. (2018). *Atlas of human anatomy* (7th ed.) Elsevier Ltd.

Newman, L. J., Platts-Mills, T. A., Phillips, C. D., Hazen, K. C., & Gross, C. W. (1994). Chronic sinusitis. relationship of computed tomographic findings to allergy, asthma, and eosinophilia. *Jama, 271*(5), 363-367. doi:10.1001/jama.271.5.363

Ng, B. A., Ramsey, R. G., & Corey, J. P. (1999). The distribution of nasal erectile mucosa as visualized by magnetic resonance imaging. *Ear, Nose, & Throat Journal, 78*(3), 159, 163-6.

Ngo, T. D., Kashani, A., Imbalzano, G., Nguyen, K. T. Q., & Hui, D. (2018). Additive manufacturing (3D printing): A review of materials, methods, applications and challenges. *Composites Part B: Engineering, 143*, 172-196. doi:https://doi.org/10.1016/j.compositesb.2018.02.012

Numminen, J., Dastidar, P., Heinonen, T., Karhuketo, T., & Rautiainen, M. (2003). Reliability of acoustic rhinometry. *Respiratory Medicine, 97*(4), 421-427. doi:10.1053/rmed.2002.1465

Okushi, T., Nakayama, T., Morimoto, S., Arai, C., Omura, K., Asaka, D., . . . Otori, N. (2013). A modified lund-mackay system for radiological evaluation of chronic rhinosinusitis. *Auris, Nasus, Larynx, 40*(6), 548-553. doi:10.1016/j.anl.2013.04.010

Onerci Altunay, Z., Bly, J. A., Edwards, P. K., Holmes, D. R., Hamilton, G. S., O'Brien, E. K., . . . Pallanch, J. F. (2016). Three-dimensional printing of large nasal septal perforations for optimal prosthetic closure. *American Journal of Rhinology & Allergy, 30*(4), 287-293. doi:10.2500/ajra.2016.30.4324

Osman, J., Großmann, F., Brosien, K., Kertzscher, U., Goubergrits, L., & Hildebrandt, T. (2016). Assessment of nasal resistance using computational fluid dynamics. *Current Directions in Biomedical Engineering, 2*(1), 617-621. doi:10.1515/cdbme-2016-0136

Pallanch, J. F., Yu, L., Delone, D., Robb, R., Holmes, D. R., Camp, J., . . . Kita, H. (2013). Three-dimensional volumetric computed tomographic scoring as an objective outcome measure for chronic rhinosinusitis: Clinical correlations and comparison to lund-mackay scoring. *International Forum of Allergy & Rhinology, 3*(12), 963-972. doi:10.1002/alr.21219

Park, S. W., Choi, J. W., Koh, K. S., & Oh, T. S. (2015). Mirror-imaged rapid prototype skull model and pre-molded synthetic scaffold to achieve optimal

orbital cavity reconstruction. *Journal of Oral and Maxillofacial Surgery : Official Journal of the American Association of Oral and Maxillofacial Surgeons, 73*(8), 1540-1553. doi:10.1016/j.joms.2015.03.025

Parker, D., & Prince, A. (2011). Innate immunity in the respiratory epithelium. *American Journal of Respiratory Cell and Molecular Biology, 45*(2), 189-201. doi:10.1165/rcmb.2011-0011RT

Passàli, D., Passàli, F. M., Damiani, V., Passali, G. C., & Bellussi, L. (2003). Treatment of inferior turbinate hypertrophy: A randomized clinical trial. *The Annals of Otology, Rhinology, and Laryngology, 112*(8), 683-688. doi:10.1177/000348940311200806

Pauwels, R., Araki, K., Siewerdsen, J. H., & Thongvigitmanee, S. S. (2015). Technical aspects of dental CBCT: State of the art. *Dentomaxillofacial Radiology, 44*(1), 20140224. doi:10.1259/dmfr.20140224

Pauwels, R., Jacobs, R., Singer, S. R., & Mupparapu, M. (2015). CBCT-based bone quality assessment: Are hounsfield units applicable? *Dentomaxillofacial Radiology, 44*(1), 20140238. doi:10.1259/dmfr.20140238

Peltonen, L. I., Aarnisalo, A. A., Kortesniemi, M. K., Suomalainen, A., Jero, J., & Robinson, S. (2007). Limited cone-beam computed tomography imaging of the middle ear: A comparison with multislice helical computed tomography. *Acta Radiologica (Stockholm, Sweden : 1987), 48*(2), 207-212. doi:772611501

Pirilä, T., & Tikanto, J. (2009). Acoustic rhinometry and rhinomanometry in the preoperative screening of septal surgery patients. *American Journal of Rhinology & Allergy, 23*(6), 605-609. doi:10.2500/ajra.2009.23.3372

Porter, M., Williamson, I., Kerridge, D., & Maw, R. (1995). Manometric rhinometry: A new method of measuring nasal volume. *Rhinology, 33*(2), 86-88.

Prasad, A. K., & Adrian, R. J. (1993). Stereoscopic particle image velocimetry applied to liquid flows. *Experiments in Fluids, 15*(1), 49-60. doi:10.1007/BF00195595

Prulière-Escabasse, V., & Coste, A. (2010). Image-guided sinus surgery. *European Annals of Otorhinolaryngology, Head and Neck Diseases, 127*(1), 33-39. doi:10.1016/j.anorl.2010.02.009

Quadrio, M., Pipolo, C., Corti, S., Lenzi, R., Messina, F., Pesci, C., & Felisati, G. (2014). Review of computational fluid dynamics in the assessment of nasal air flow and analysis of its limitations. *Eur Arch Otorhinolaryngol, 271*(9), 2349-2354. doi:10.1007/s00405-013-2742-3

Ragab, S. M., Lund, V. J., & Scadding, G. (2004). Evaluation of the medical and surgical treatment of chronic rhinosinusitis: A prospective, randomised, controlled trial. *The Laryngoscope, 114*(5), 923-930. doi:00005537-200405000-00027

Ramey, J. T., Bailen, E., & Lockey, R. F. (2006). Rhinitis medicamentosa. *Journal of Investigational Allergology & Clinical Immunology, 16*(3), 148-155.

Randazzo, M., Pisapia, J. M., Singh, N., & Thawani, J. P. (2016). 3D printing in neurosurgery: A systematic review. *Surgical Neurology International, 7*(Suppl 33), S801-S809. doi:10.4103/2152-7806.194059

Remenschneider, A. K., D'Amico, L., Gray, S. T., Holbrook, E. H., Gliklich, R. E., & Metson, R. (2015). The EQ-5D: A new tool for studying clinical outcomes in chronic rhinosinusitis. *The Laryngoscope, 125*(1), 7-15. doi:10.1002/lary.24715

Reymus, M., Fotiadou, C., Kessler, A., Heck, K., Hickel, R., & Diegritz, C. (2019). 3D printed replicas for endodontic education. *International Endodontic Journal, 52*(1), 123-130. doi:10.1111/iej.12964

Rudmik, L., Hopkins, C., Peters, A., Smith, T. L., Schlosser, R. J., & Soler, Z. M. (2015). Patient-reported outcome measures for adult chronic rhinosinusitis: A systematic review and quality assessment. *The Journal of Allergy and Clinical Immunology, 136*(6), 1532-1540.e2. doi:S0091-6749(15)01513-4

Sahin, G., Klimek, L., Mullol, J., Hörmann, K., Walther, L. E., & Pfaar, O. (2011). Nitric oxide: A promising methodological approach in airway diseases. *International Archives of Allergy Immunology, 156*(4), 352-361. doi:10.1159/000324678

Samaila, E. M., Negri, S., Zardini, A., Bizzotto, N., Maluta, T., Rossignoli, C., & Magnan, B. (2020). Value of three-dimensional printing of fractures in orthopaedic trauma surgery. *The Journal of International Medical Research, 48*(1), 300060519887299. doi:10.1177/0300060519887299

Sarin, S., Undem, B., Sanico, A., & Togias, A. (2006). The role of the nervous system in rhinitis. *The Journal of Allergy and Clinical Immunology, 118*(5), 999-1016. doi:S0091-6749(06)01935-X

Scott, J. R., Psaltis, A. J., & Wormald, P. J. (2020). Vascular anatomy of the inferior turbinate and its clinical implications. *American Journal of Rhinology & Allergy, 34*(5), 604-609. doi:10.1177/1945892420914185

Shi, H., Kleinstreuer, C., & Zhang, Z. (2006). Laminar airflow and nanoparticle or vapor deposition in a human nasal cavity model. *Journal of Biomechanical Engineering, 128*(5), 697-706. doi:10.1115/1.2244574

Shukla, R. H., Nemade, S. V., & Shinde, K. J. (2020). Comparison of visual analogue scale (VAS) and the nasal obstruction symptom evaluation (NOSE) score in evaluation of post septoplasty patients. *World Journal of Otorhinolaryngology - Head and Neck Surgery, 6*(1), 53-58. doi:10.1016/j.wjorl.2019.06.002

Silva, D. N., Gerhardt de Oliveira, M., Meurer, E., Meurer, M. I., Lopes da Silva, J V, & Santa-Barbara, A. (2008). Dimensional error in selective laser sintering and 3D-printing of models for craniomaxillary anatomy reconstruction. *Journal of Cranio-Maxillo-Facial Surgery : Official Publication of the European Association for Cranio-Maxillo-Facial Surgery, 36*(8), 443-449. doi:10.1016/j.jcms.2008.04.003

Sinno, S., Mehta, K., Lee, Z. H., Kidwai, S., Saadeh, P. B., & Lee, M. R. (2016). Inferior turbinate hypertrophy in rhinoplasty: Systematic review of surgical

techniques. *Plastic and Reconstructive Surgery, 138*(3), 419e-429e. doi:10.1097/PRS.0000000000002433

Sokolowski, A. A., Sokolowski, A. A., Kammerhofer, J., Madreiter-Sokolowski, C. T., Payer, M., Koller, M., . . . Wegscheider, W. A. (2019). Accuracy assessment of 3D-printed tooth replicas. *International Journal of Computerized Dentistry, 22*(4), 321-329. doi:43782

Spence, C. J. T., Buchmann, N. A., & Jermy, M. C. (2012). Unsteady flow in the nasal cavity with high flow therapy measured by stereoscopic PIV. *Experiments in Fluids, 52*(3), 569-579. doi:10.1007/s00348-011-1044-z

Spence, C. J. T., Buchmann, N. A., Jermy, M. C., & Moore, S. M. (2011). Stereoscopic PIV measurements of flow in the nasal cavity with high flow therapy. *Experiments in Fluids, 50*(4), 1005-1017. doi:10.1007/s00348-010-0984-z

Steinbacher, D. M. (2015). Three-dimensional analysis and surgical planning in craniomaxillofacial surgery. *Journal of Oral and Maxillofacial Surgery : Official Journal of the American Association of Oral and Maxillofacial Surgeons, 73*(12 Suppl), 40. doi:10.1016/j.joms.2015.04.038

Stewart, M. G., Witsell, D. L., Smith, T. L., Weaver, E. M., Yueh, B., & Hannley, M. T. (2004). Development and validation of the nasal obstruction symptom evaluation (NOSE) scale. *Otolaryngology--Head and Neck Surgery : Official Journal of American Academy of Otolaryngology-Head and Neck Surgery, 130*(2), 157-163. doi:10.1016/j.otohns.2003.09.016

Tack, P., Victor, J., Gemmel, P., & Annemans, L. (2016). 3D-printing techniques in a medical setting: A systematic literature review. *Biomedical Engineering Online, 15*(1), 115-4. doi:10.1186/s12938-016-0236-4

Tai, C. F., & Baraniuk, J. N. (2002). Upper airway neurogenic mechanisms. *Current Opinion in Allergy and Clinical Immunology, 2*(1), 11-19. doi:10.1097/00130832-200202000-00003

Terheyden, H., Maune, S., Mertens, J., & Hilberg, O. (2000). Acoustic rhinometry: Validation by three-dimensionally reconstructed computer tomographic scans. *Journal of Applied Physiology (1985), 89*(3), 1013-1021. doi:10.1152/jappl.2000.89.3.1013

Tetsuka, H., & Shin, S. R. (2020). Materials and technical innovations in 3D printing in biomedical applications. *Journal of Materials Chemistry.B, 8*(15), 2930-2950. doi:10.1039/d0tb00034e

Thulesius, H. L., Cervin, A., & Jessen, M. (2014). Treatment with a topical glucocorticoid, budesonide, reduced the variability of rhinomanometric nasal airway resistance. *Rhinology, 52*(1), 19-24. doi:10.4193/Rhin12.180

Trangsrud, A. J., Whitaker, A. L., & Small, R. E. (2002). Intranasal corticosteroids for allergic rhinitis. *Pharmacotherapy, 22*(11), 1458-1467. doi:10.1592/phco.22.16.1458.33692

Tretiakow, D., Tesch, K., Meyer-Szary, J., Markiet, K., & Skorek, A. (2020). Three-dimensional modeling and automatic analysis of the human nasal cavity and

paranasal sinuses using the computational fluid dynamics method. *European Archives of Oto-Rhino-Laryngology,* doi:10.1007/s00405-020-06428-3

Tugrul, S., Dogan, R., Hassouna, H., Sharifov, R., Ozturan, O., & Eren, S. B. (2019). Three-dimensional computed tomography volume and physiology of nasal cavity after septhorhinoplasty. *Journal of Craniofacial Surgery, 30*(8), 2445-2448. doi:10.1097/SCS.0000000000005730

van Egmond, M M H T, van Heerbeek, N., Ter Haar, E L M, & Rovers, M. M. (2017). Clinimetric properties of the glasgow health status inventory, glasgow benefit inventory, peak nasal inspiratory flow, and 4-phase rhinomanometry in adults with nasal obstruction. *Rhinology, 55*(2), 126-134. doi:10.4193/Rhin16.296

von Arx, T., Lozanoff, S., & Bornstein, M. M. (2019). Extraoral anatomy in CBCT - a literature review. part 1: Nasoethmoidal region. *Swiss Dental Journal, 129*(10), 804-815. doi:sdj-2019-10-01

Wen, J., Inthavong, K., Tu, J., & Wang, S. (2008). Numerical simulations for detailed airflow dynamics in a human nasal cavity. *Respiratory Physiology & Neurobiology, 161*(2), 125-135. doi:10.1016/j.resp.2008.01.012

Wheatley, J. R., Amis, T. C., & Engel, L. A. (1991). Nasal and oral airway pressure-flow relationships. *Journal of Applied Physiology, 71*(6), 2317-2324. doi:10.1152/jappl.1991.71.6.2317

White, D. E., Bartley, J., & Nates, R. J. (2015). Model demonstrates functional purpose of the nasal cycle. *Biomedical Engineering Online, 14*, 38-4. doi:10.1186/s12938-015-0034-4

Willatt, D. (2009). The evidence for reducing inferior turbinates. *Rhinology, 47*(3), 227-236. doi:10.4193/Rhin09.017

Williams, M., & Eccles, R. (2016). A model for the central control of airflow patterns within the human nasal cycle. *The Journal of Laryngology and Otology, 130*(1), 82-88. doi:10.1017/S0022215115002881

Williamson, A., & Hoggart, B. (2005). Pain: A review of three commonly used pain rating scales. *Journal of Clinical Nursing, 14*(7), 798-804. doi:JCN1121 [pii]

Wormald, P. J. (2005). Surgery of the frontal recess and frontal sinus. *Rhinology, 43*(2), 82-85.

Wright, B. M. (1978). A miniature wright peak-flow meter. *British Medical Journal, 2*(6152), 1627-1628. doi:10.1136/bmj.2.6152.1627

Yilmaz, B. (2015). Incorporating digital scans of diagnostic casts into computed tomography for virtual implant treatment planning. *The Journal of Prosthetic Dentistry, 114*(2), 178-181. doi:10.1016/j.prosdent.2015.03.009

Yousem, D. M. (1993). Imaging of sinonasal inflammatory disease. *Radiology, 188*(2), 303-314. doi:10.1148/radiology.188.2.8327669

Yusa, K., Yamanochi, H., Takagi, A., & Iino, M. (2017). Three-dimensional printing model as a tool to assist in surgery for large mandibular tumour: A case report. *Journal of Oral & Maxillofacial Research, 8*(2), e4. doi:10.5037/jomr.2017.8204

Zhao, K., Pribitkin, E. A., Cowart, B. J., Rosen, D., Scherer, P. W., & Dalton, P. (2006). Numerical modeling of nasal obstruction and endoscopic surgical intervention: Outcome to airflow and olfaction. *American Journal of Rhinology, 20*(3), 308-316. doi:10.2500/ajr.2006.20.2848

Zhu, P., & Chen, S. (2016). Clinical outcomes following ear reconstruction with adjuvant 3D template model. *Acta Oto-Laryngologica, 136*(12), 1236-1241. doi:10.1080/00016489.2016.1206967

ORIGINAL PUBLICATIONS

PUBLICATION I

Three-Dimensional Volumetric Evaluation of the Maxillary Sinuses in Chronic Rhinosinusitis Surgery

Valtonen O, Bizaki A, Kivekäs I, Rautiainen M

Annals of Otology, Rhinology & Laryngology. 127(12):931-936, 2018
doi: 10.1177/0003489418801386

Article

Three-Dimensional Volumetric Evaluation of the Maxillary Sinuses in Chronic Rhinosinusitis Surgery

Annals of Otology, Rhinology & Laryngology
2018, Vol. 127(12) 931–936

DOI: 10.1177/0003489418801386
journals.sagepub.com/home/aor
SAGE

Olli Valtonen, MD[1], Argyro Bizaki, MD, PhD[1], Ilkka Kivekäs, MD, PhD[1], and Markus Rautiainen, MD, PhD[1]

Abstract

Introduction: The objective of this study was to ascertain whether the 3-dimensional volumetric measurement method could be used for the evaluation of operative treatment results in patients with chronic rhinosinusitis.

Methods: A total of 61 adult patients with chronic rhinosinusitis were analyzed. Cone-beam computed tomographic images of the paranasal sinuses were examined preoperatively and at 12 months postoperatively. The results were compared using the Sino-Nasal Outcome Test (SNOT-22) and the Lund-Mackay (LM) and Zinreich modified staging systems.

Results: The mean change in pneumatized volumes in the maxillary sinuses after operative treatment per patient was 2.0 $\pm$ 7.5 cm^3 ($P = .146$). The median for volumetric change was 0.97 cm^3 (range, −11.6 to 33.6 cm^3). Both the LM and Zinreich modified LM staging systems showed no change in 32 of 61 patients (53%). The alterations in patients' maxillary sinuses measured using the volumetric measurement method correlated well with changes in Zinreich's modified LM staging (−0.77, $P < .01$).

Conclusions: The 3D volumetric method is more sensitive in detecting small alterations in pneumatized volumes of the maxillary sinuses than Zinreich's modified LM staging and LM staging. The method correlates better with Zinreich's modified LM staging than with LM staging.

Keywords

volumetry, 3D, Lund-Mackay, Zinreich's modified LM, SNOT-22, chronic rhinosinusitis

Introduction

Several different assessment methods have been developed for the evaluation of chronic rhinosinusitis (CRS) findings. In addition, subjective symptom-based questionnaires such as the Sino-Nasal Outcome Test (SNOT-22), which is among the most common, are widely used to assess the development of symptoms.[1-3] To assess actual physical changes, however, objective assessment methods, which for CRS are based on computed tomographic (CT) or cone-beam CT (CBCT) scans, are needed.[4,5] In CT and CBCT imaging, the results are estimated from the changes in the thickness of the mucous membrane in the nasal sinuses.

The most prevalent scaling system of mucous membrane thickness in the maxillary sinuses, and thus the degree of CRS severity, is the Lund-Mackay (LM) staging system.[6] The LM staging system serves as a fairly quick and repeatable tool for estimating the severity of CRS, but the staging is also imprecise and unspecific. As a result, small changes are difficult to detect with LM staging. Modified staging systems such as Zinreich's modified LM staging have been suggested for better accuracy.[7] In a study by Okushi et al,[8] LM staging was shown to be more consistent than Zinreich's modified LM staging but was less accurate.

Another drawback with these staging systems is that they rely heavily on the subjective estimation of a clinician. Both staging systems are evaluated from 2-dimensional images, and 3-dimensinoal (3D) information from the radiologic examination is not used. The thickness of the mucous membrane and its portion of the whole volume of the maxillary sinus are approximated from the scans. In adult patients, the volume of a maxillary sinus varies from approximately 4.5 to 35.2 cm^3, with a mean volume of 14.7 cm^3.[9] With such a large variation, reliable estimation of the actual volume is very difficult and requires an objective measuring tool that also decreases the effect of subjective

[1]Department of Ear and Oral Diseases, Tampere University Hospital and Department of Otorhinolaryngology, University of Tampere, Tampere, Finland

Corresponding Author:
Olli Valtonen, MD, Tampere University Hospital, Department of Ear and Oral Diseases, PO Box 2000, Tampere, FIN-33521, Finland.
Email: olli.valtonen@pshp.fi

estimation. Measuring the actual volume of the maxillary sinuses on the basis of a 3D reconstruction of CT or CBCT scans could provide more accurate information about the results of medical procedures.

The feasibility of 3D volumetric measurements in evaluating maxillary sinuses in CRS was shown in a study by Deeb et al.[10] In previous studies, 3D volumetric assessment has been used to evaluate the effect of intramuscular corticosteroid treatment in patients with CRS.[4,5] Change in 3D volumetric measures has better correlated to several subjective symptoms than LM or Zinreich's modified LM staging. The 3D volumetric measurement method has not, however, been studied as a potential assessment method of the outcome of surgical methods in the operative treatment of the nose and paranasal sinuses.

The aim of this study was to ascertain whether the 3D volumetric measurement method could be used for the evaluation of operative treatment results in patients with CRS. The 3D volumetric measurement method was also compared with the LM and Zinreich's modified LM staging systems. Possible correlations with SNOT-22 results were also examined.

Methods

A total of 72 adult patients with CRS were included in the study. Patients were operated either with uncinectomy (n = 37) or ostial balloon dilation (n = 35). CBCT images of the paranasal sinuses were examined before treatment and at 12 months postoperatively. All patients had their main radiologic findings in the maxillary sinuses. By the end of the study, 10 patients had opted out and 1 patient was excluded because of extensive artifacts on CBCT scans. For the purposes of this study, a total of 61 patients (42 women and 19 men) and 122 maxillary sinuses were analysed. The study population comprised 30 patients from the uncinectomy group and 31 patients from the ostial balloon dilation group. The age range of the patients was 20 to 63 years, with a mean age of 38.4 ± 11.3 years.

The pneumatized volume of the maxillary sinuses was measured from pre- and postoperative CBCT scans using volumetric software (OnDemand3D). We first manually provided the software with desired starting points in the region of interest, and from these points it began coloring all the pixels with the correct light density value. Because there are no universal Hounsfield unit values for CBCT imaging, these had to be defined using the software's own scaling function. After defining light density values in Hounsfield units (−1,000 to −430 Hounsfield units) to areas containing air in the maxillary sinuses, the software was able to create 3D models of them. From the produced voxels of these 3D models, the pneumatized volume inside the maxillary sinuses was calculated by the software by multiplying the number of selected voxels with the volume of a voxel.

When defining the region of interest, the software in some cases included structures from the nasal cavities that had to be manually excluded from the 3D models. These excluded structures consisted of parts from the osteomeatal unit and ethmoid sinuses. The focus of the study was on the volumetric measurements of the maxillary sinuses. The walls of the maxillary sinuses were usually well identified by the software and rarely caused any problems in the process.

Measuring mucous membrane thickness with the software in our use proved to be challenging. In some cases, very thin layers of the mucous membrane could not be measured properly. Because of its simpler and more reliable processing, we chose to measure the volume of the pneumatized space rather than the mucous membrane itself. The same images were used to evaluate the thickness of the mucous membrane using the LM and Zinreich staging systems. Volumetric results were calculated in cubic millimeters. LM stages were evaluated for maxillary sinuses and osteomeatal complexes. Zinreich stages were evaluated only for the maxillary sinuses, because this scale does not note osteomeatal complexes. Because the extent of inflammation was limited mainly to the maxillary sinuses in our study, a more extensive staging evaluation of the nose and paranasal sinuses was excluded.

The results in pneumatized volume and LM and Zinreich scores are presented mainly in total results, in which both sinuses are taken into account. The scale for LM score in total results, including maxillary sinuses and osteomeatal complexes from both sides, ranges from 0 to 8. For Zinreich's staging system, the scale for total results ranges from 0 to 10, which includes the maxillary sinuses from both sides. Only when it comes to the smallest detected change, the results from individual maxillary sinuses are presented.

The SNOT-22 questionnaire, first validated in 2009,[11] was also filled out by all patients preoperatively and 12 months postoperatively. The correlation between the total SNOT-22 changes and the changes in both staging systems and the volumetric method was studied. In a study by Hopkins et al,[11] the minimally important difference was found to be approximately 9 points on the SNOT-22, which was also taken into account.

For statistical analysis, we used SPSS version 22. The mean and median results of the volumetric measurements were analyzed using the Wilcoxon 1-sample test. The correlations of the 3D volumetric measures, LM staging, Zinreich's modified LM staging, and SNOT-22 were analysed using the Spearman correlation test.

This study was approved by the ethics committee of Pirkanmaa Hospital District (Tampere University Hospital, Tampere, Finland), and written consent was obtained from all participants.

Table 1. Numbers of Patients Detected Using the Volumetric Method in Different Volume Change Scales (Both Negative and Positive).[a]

	Volumetric Change					
	<5%	⩾5%	⩾10%	⩾15%	⩾20%	⩾25%
Volumetric Method	18/61 (30%)	43/61 (70%)	28/61 (46%)	21/61 (34%)	17/61 (29%)	11/61 (18%)
Lund-Mackay	14/18 (78%)	18/43 (42%)	8/28 (29%)	4/21 (19%)	3/17 (18%)	2/11 (18%)
Zinreich's modified Lund-Mackay staging	14/18 (78%)	18/43 (42%)	10/28 (36%)	5/21 (24%)	2/17 (12%)	0/11 (0%)

[a]Number and percentage of cases that were not detected by Lund-Mackay staging or Zinreich's modified Lund-Mackay staging.

Results

The mean volume of the total pneumatized volume in the maxillary sinuses per patient was 28.1 ± 10.6 cm^3 preoperatively and 30.1 ± 10.8 cm^3 postoperatively. The mean change of the total pneumatized volume in the maxillary sinuses after operative treatment per patient was 2.0 ± 7.5 cm^3 ($P = .146$). The median for volumetric changes was 0.97 cm^3, and the interquartile range was 4.7 cm^3.

The mean score for LM staging was 1.5 ± 1.6 preoperatively and 1.1 ± 1.2 postoperatively. Corresponding scores for the Zinreich staging system were 2.1 ± 1.8 and 1.7 ± 1.4. The mean SNOT-22 score was 43.9 ± 18.2 preoperatively and 28.7 ± 16.2 postoperatively.

In our study, changes in pneumatized volume were detected in every maxillary sinus using the volumetric method. The smallest observed change in pneumatized volume per individual maxillary sinus in our research material using the volumetric method was 0.0017 cm^3. The smallest observed pneumatized volume change per individual maxillary sinus using LM staging was 0.49 cm^3. A similar change of 0.53 cm^3 was observed using Zinreich's staging system. These results were obtained by gathering all the maxillary sinuses that had a change in the staging system scores in question, and the smallest volume change in these sinuses was then observed.

With a minimum change in total volumetric measurements of 5%, both the LM and Zinreich staging systems failed to detect changes in 18 of 43 patients (42%) (Table 1). For 10% volumetric change, LM staging failed to detect changes in 8 of 28 patients (29%) and Zinreich's staging system in 10 of 28 patients (36%). With a 20% change in volume, the LM system showed no change in 3 of 17 patients (18%), and Zinreich's staging system failed to detect changes in 2 of 17 patients (12%). With respect to all of the patients in our study, both the LM and Zinreich modified LM staging systems showed no change in 32 of 61 patients (53%).

The alterations in the maxillary sinuses of patients measured using the 3D volumetric method correlated well with changes in Zinreich's modified LM staging (−0.77, $P \leqslant .01$) (Figure 1) and to some extent with changes in LM staging (−0.59, $P \leqslant .01$) (Table 2). There was a weak correlation of the volumetric change to the SNOT-22 change (0.38, $P \leqslant .01$) (Figures 2 and 3) and a negative correlation between the SNOT-22 score and Zinreich's modified LM staging (−0.42, $P \leqslant .01$) and LM staging (−0.21, $P = .10$) (Table 2).

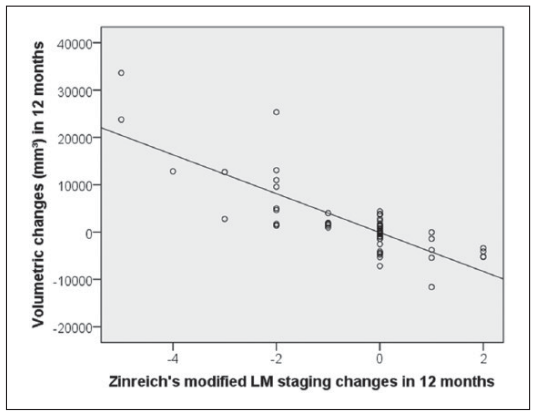

Figure 1. Correlation between 3-dimensional volumetric changes and Zinreich's modified Lund-Mackay (LM) staging change (Spearman's $\rho = -0.77$, $P \leqslant .01$). Volumetric changes are presented in cubic millimeters.

We also divided and studied the results by performed operation (Table 3). There were no statistically significant differences (Mann-Whitney U test, $P > .05$) in volumetric change, LM change, or Zinreich's modified LM staging change between the 2 surgical approaches.

Discussion

The results of our study indicate an observable correlation between the 3D volumetric method and Zinreich's LM staging (Figure 1). The improvement of score based on Zinreich's staging corresponds to the improvement of the pneumatized volume in the maxillary sinuses based on the 3D volumetric measurements. LM staging, however, shows a weaker correlation to the 3D volumetric method. The uncinectomy group did

Table 2. Correlations of Volumetric Method With Staging Systems and SNOT-22 (Spearman's ρ).

	LM Staging	Zinreich's Modified LM Staging	Volumetric Method	SNOT-22
LM staging	1.00 (—)	0.48* (≤0.01)	−0.59* (≤0.01)	−0.21 (0.10)
Zinreich's modified LM staging	0.48* (≤0.01)	1.00 (—)	−0.77 (≤0.01)	−0.42* (≤0.01)
Volumetric method	−0.59* (≤0.01)	−0.77* (≤0.01)	1.00 (—)	0.38* (≤0.01)
SNOT-22	−0.21 (0.10)	−0.42* (≤0.01)	0.38* (≤0.01)	1.00 (—)

Abbreviations: LM, Lund-Mackay; SNOT-22, Sino-Nasal Outcome Test.
*Correlation is significant at the P ≤ .01 level (2-tailed).

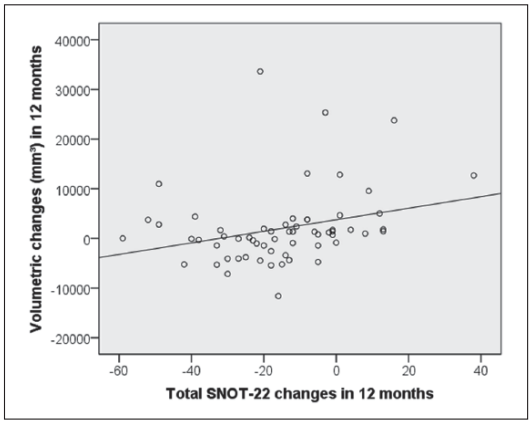

Figure 2. Correlation between 3-dimensional volumetric changes and Sino-Nasal Outcome Test (SNOT-22) changes (Spearman's ρ = 0.38, *P* ≤ .01). Volumetric changes are presented in cubic millimeters.

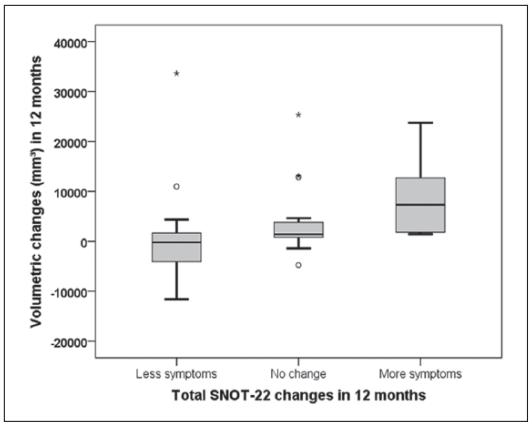

Figure 3. Correlation between the 3-dimensional volumetric changes and the Sino-Nasal Outcome Test changes (Spearman's ρ = 0.47, *P* ≤ .01). Volumetric changes are presented in cubic millimeters. Sino-Nasal Outcome Test (SNOT-22) results are shown in the following way: fewer symptoms = improvement by 9 or more points, no change = change in points less than 9, more symptoms = deterioration by 9 or more points.

not differ from the ostial balloon dilation group in pre- and postoperative change in the 3D volumetric method, LM method, or Zinreich's modified LM staging (Table 3).

In a study by Likness et al,[4] the 3D volumetric method was shown to be the most comprehensive and sensitive of these methods in 1-month follow-up after treatment of patients with CRS with a single dose of intramuscular triamcinolone. Furthermore, the correlation between 3D volumetric method and 2-dimensional single-slice coronal CT imaging was 0.82. Zinreich's modified LM staging had a good correlation with the 3D volumetric method (0.77) and was better than LM staging (0.54). In their study, the volumetric measurements were assessed in mucous membrane volume percentages of the total sinus volume rather than using actual volumes. Therefore, the results cannot be compared with our results.

In our study, neither the staging systems nor the 3D volumetric method had a clear correlation with SNOT-22 results. There was a weak correlation between the change in SNOT-22 score and the change in the 3D volumetric method, the LM staging and Zinreich's modified LM staging, but the correlations were irrational. The pneumatized volumes of the maxillary sinuses are shown to decrease, while the results are improved in total SNOT-22 score (Figures 2 and 3). Also, the change in LM staging and Zinreich's modified LM staging correlated negatively with the SNOT-22 change, which was also irrational. A similar result was reported previously by Hopkins et al.[12] They could not find a clear correlation between LM and SNOT-22 scores, although some correlation was found between higher preoperative LM staging and changes in SNOT-22.

Volumetric measurement has previously been used to evaluate maxillary sinus volumes in pediatric patients with CRS. Kim et al[13] found that the volume of the maxillary sinuses decreased and the bony thickness of the paranasal sinuses increased with long-standing pediatric CRS. However, different phenotypes of CRS can give different

Table 3. Results Shown by the Performed Surgical Method.[a]

	Patients	Gender (F/M)	Age, y	Volumetric Method (cm^3)	SNOT-22	LM Staging	Zinreich's Modified LM Staging
Uncinectomy	30	20/10	21-63				
Preoperative				27.0 ± 11.4	44.7 ± 15.1	1.3 ± 1.3	2.4 ± 2.0
Postoperative				29.9 ± 12.1	28.9 ± 12.1	1.1 ± 1.0	1.7 ± 1.4
Change				+2.9 ± 8.9*	−15.8 ± 16.0*	−0.2 ± 1.2*	−0.6 ± 1.5*
Ostial balloon dilation	31	22/9	20-59				
Preoperative				29.1 ± 9.8	43.2 ± 21.1	1.8 ± 1.9	2.0 ± 1.4
Postoperative				30.2 ± 9.5	28.6 ± 19.6	1.3 ± 1.4	1.6 ± 1.4
Change				+1.1 ± 6.0*	−14.7 ± 20.6*	−0.5 ± 1.2*	−0.4 ± 1.4*

Abbreviations: LM, Lund-Mackay; SNOT-22, Sino-Nasal Outcome Test.
[a]Mean total volumetric results are presented in cubic centimeters. SNOT-22, LM, and Zinreich's modified LM staging results are presented as mean scores. LM staging is based on a range of 0 to 8 and Zinreich's scale of 0 to 10.
*$P > .05$ (Mann-Whitney *U* test).

results, as reported in a study by Gregurić et al.[14] That study showed that CT scores with LM in CRS with nasal polyps resembled the severity of nasal symptoms better than CRS without nasal polyps.

In a study by Pallanch et al,[5] a total of 48 patients with CRS were treated with a single dose of triamcinolone without any operative treatment, and CT images were taken before and 1 month after the treatment. They found that the 3D volumetric method correlated better with patient symptoms than LM staging. For example, in polyp examination, total examination score, olfactory symptoms, and 3 nasal symptoms assessed together (olfactory symptoms, nasal discharge, and blockage) the additional information gained with the volumetric method was found to be statistically significant when compared with LM staging.

The observable correlation between the volumetric method and the development of symptoms in other studies is most likely due to the intramuscular cortisone used to reduce the inflammation in the mucous membrane, resulting in reductions in symptoms and mucous membrane thickness. However, in operative treatments of the maxillary sinus ostium in patients with CRS, the mucous membrane itself is affected only in the region of operation. The main long-term objectives are to increase ventilation and mucociliary function in the maxillary sinuses, to decrease mucosal inflammation, and to increase the pneumatized volume in the maxillary sinuses. No intramuscular or topical cortisone was included in our study, which most likely affected the results.

More than half of our patients had no change in LM or Zinreich's score postoperatively. In these cases, the changes in pneumatized volume and mucous membrane thickness were too small to be detected using these staging systems. This indicates that both the LM and Zinreich's staging systems are not sensitive enough to detect minor mucosal changes in patients with CRS.

In our study, the findings of CRS were mainly in the maxillary sinuses, and the ethmoid sinuses were not assessed, although the ethmoid sinuses play an important role in CRS. Volumetric measurements of the ethmoid sinuses would have been difficult to assess because of many small sinuses, and it would have been a place for error. Still, this could be seen as a weakness of the study. The findings in ethmoid sinuses, however, were minuscule in our study. The number of patients and the deviation of the results are also possible weaknesses. On the other hand, a clear timeline, 2 distinct approaches, and the different evaluation methods can be seen as strengths of this study.

Of the 3 methods, the LM and Zinreich methods are less sensitive than the 3D volumetric method. However, these 2 methods have the advantage of quick estimation of the mucous membrane thickness and mostly good repeatability, which make them applicable in clinical practice. At present, the 3D volumetric method is more time consuming, but it has potential for research purposes because of its better accuracy in detecting small alterations. The results of our study indicate that the outcome of maxillary sinus operations should not be assessed solely by radiologic findings and mucous membrane thickness in the maxillary sinuses.

Conclusions

The 3D volumetric method is more sensitive in detecting small alterations in pneumatized volumes of the maxillary sinuses than LM staging and Zinreich's modified LM staging. The 3D volumetric method correlates better with Zinreich's modified LM staging than with LM staging. For research purposes, the 3D volumetric method could provide an applicable tool. Radiologic findings seem to have relatively poor correlation with clinical symptoms measured with symptom questionnaires. This study proved CBCT imaging unnecessary as

a postoperative control method, thus indicating that it should not be used in clinical practice for this purpose.

Declaration of Conflicting Interests

The author(s) declared no potential conflicts of interest with respect to the research, authorship, and/or publication of this article.

Funding

The author(s) received no financial support for the research, authorship, and/or publication of this article.

ORCID iD

Olli Valtonen https://orcid.org/0000-0001-9423-0269

References

1. Fokkens WJ, Lund VJ, Mullol J, et al. EPOS 2012: European position paper on rhinosinusitis and nasal polyps 2012. A summary for otorhinolaryngologists. *Rhinology*. 2012;50(1):1-12.
2. Alakärppä AI, Koskenkorva TJ, Koivunen PT, Alho OP. Quality of life before and after sinonasal surgery: a population-based matched cohort study. *Eur Arch Otorhinolaryngol*. 2017;274:795-802.
3. Bizaki AJ, Taulu R, Numminen J, Rautiainen M. Quality of life after endoscopic sinus surgery or balloon sinuplasty: a randomized clinical study. *Rhinology*. 2014;52(4):300-305.
4. Likness MM, Pallanch JF, Sherris DA, Kita H, Mashtare TL, Ponikau JU. Computed tomography scans as an objective measure of disease severity in chronic rhinosinusitis. *Otolaryngol Head Neck Surg*. 2014;150(2):305-311.
5. Pallanch JF, Yu L, Delone D, et al. Three-dimensional volumetric computed tomographic scoring as an objective outcome measure for chronic rhinosinusitis: clinical correlations and comparison to Lund-Mackay scoring. *Int Forum Allergy Rhinol*. 2013;3(12):963-972.
6. Lund VJ, Mackay IS. Staging in rhinosinusitus. *Rhinology*. 1993;31(4):183-184.
7. Zinreich SJ. Imaging for staging of rhinosinusitis. *Ann Otol Rhinol Laryngol Suppl*. 2004;193:19-23.
8. Okushi T, Nakayama T, Morimoto S, et al. A modified Lund-Mackay system for radiological evaluation of chronic rhinosinusitis. *Auris Nasus Larynx*. 2013;40(6):548-553.
9. Ariji Y, Kuroki T, Moriguchi S, Ariji E, Kanda S. Age changes in the volume of the human maxillary sinus: a study using computed tomography. *Dentomaxillofac Radiol*. 1994;23(3):163-168.
10. Deeb R, Malani PN, Gill B, et al. Three-dimensional volumetric measurements and analysis of the maxillary sinus. *Am J Rhinol Allergy*. 2011;25(3):152-156.
11. Hopkins C, Gillett S, Slack R, Lund VJ, Browne JP. Psychometric validity of the 22-item Sinonasal Outcome Test. *Clin Otolaryngol*. 2009;34(5):447-454.
12. Hopkins C, Browne JP, Slack R, Lund V, Brown P. The Lund-Mackay staging system for chronic rhinosinusitis: how is it used and what does it predict? *Otolaryngol Head Neck Surg*. 2007;137(4):555-561.
13. Kim HY, Kim MB, Dhong HJ, et al. Changes of maxillary sinus volume and bony thickness of the paranasal sinuses in longstanding pediatric chronic rhinosinusitis. *Int J Pediatr Otorhinolaryngol*. 2008;72(1):103-108.
14. Gregurić T, Trkulja V, Baudoin T, Grgić MV, Šmigovec I, Kalogjera L. Association between computed tomography findings and clinical symptoms in chronic rhinosinusitis with and without nasal polyps. *Eur Arch Otorhinolaryngol*. 2017;274(5):2165-2173.

PUBLICATION II

Three-Dimensional Printing of the Nasal Cavities for Clinical Experiments

Valtonen O, Ormiskangas J, Kivekäs I, Rantanen V, Dean M, Poe D, Järnstedt J, Lekkala J, Saarenrinne P, Rautiainen M

Scientific Reports. 10(1):502, 2020
doi: 10.1038/s41598-020-57537-2

SCIENTIFIC REPORTS
nature research

OPEN

Three-Dimensional Printing of the Nasal Cavities for Clinical Experiments

Olli Valtonen[1,2*], Jaakko Ormiskangas[2], Ilkka Kivekäs[1,2], Ville Rantanen[2], Marc Dean[3,4], Dennis Poe[5], Jorma Järnstedt[6], Jukka Lekkala[2], Pentti Saarenrinne[7] & Markus Rautiainen[1,2]

3D printing has produced many beneficial applications for surgery. The technique´s applicability in replicating nasal cavity anatomy for clinical use has not been studied. Our aim was to determine whether 3D printing could realistically replicate the nasal cavities and the airflow passing through them from a clinical point of view. We included Cone Beam Computed Tomography (CBCT) scans of five patients with symptoms of chronic nasal congestion. These CBCT scans were used to print plastic 3D prints of the nasal cavities, which were also CBCT scanned and the measurements were compared. The results *in vivo* were higher than the results *in vitro* in maxillary sinus volumes with a ratio of 1.05 ± 0.01 (mean ± SD) and in the nasal cavities with a ratio of 1.20 ± 0.1 (mean ± SD). Linear measurements *in vitro* were very close to those *in vivo*. Rhinomanometric results showed some differences, but rhinomanometric graphs *in vitro* were close to the graphs *in vivo*. 3D printing proved to be a suitable and fast method for replicating nasal cavity structures and for the experimental testing of nasal function. It can be used as a complementary examination tool for rhinomanometry.

Recently, 3D modelling and printing technology have been used in a variety of medical applications, such as surgical planning, design of implants and tissue for individual patients, research and as an educational and training tool[1]. 3D modelling and printing technology have also been used for the planning of implants and operations for craniofacial and skull base pathologies[2]. In addition, the technology has been used in the planning of head and neck tumour surgery[3]. The technology also offers vast possibilities in the field of reconstructive surgery[4].

To date, however, not all the possibilities offered by 3D printing technology have been utilised in clinical practice. For example, due to the complicated anatomy of the nose, 3D printing technology has not yet been used for modelling of the anatomy of the nasal cavities for clinical purposes or as a tool for the planning of nasal surgical procedures.

Previously, individual models of the anatomy of the nose and nasal cavities were 3D modelled in silicone[5–8]. The production of these models was, however, slow and labourious. These models were used to study airflow in the nasal cavities using liquid and small particles as substances, but the results were not compared with measurements from actual patients. The methods used were particle image velocimetry (PIV) and computational fluid dynamics (CFD), both of which are labourious and time-consuming methods.

In the present study, our main objective was to assess whether 3D printing could be used to realistically replicate the nasal cavities and the airflow passing through them from a clinical viewpoint. We investigate the applicability of plastic 3D prints of the nasal cavities and paranasal sinuses printed from cone beam computed tomography (CBCT) acquired images. A secondary objective was to determine how well the plastic 3D prints corresponded to the nasal function *in vivo*.

[1]Department of Otorhinolaryngology – Head and Neck Surgery, Tampere University Hospital, Tampere, Finland. [2]Faculty of Medicine and Health Technology, Tampere University, Tampere, Finland. [3]Texas Tech University Health Sciences Center, Lubbock, Texas, USA. [4]Ear & Sinus Institute, Fort Worth, Texas, USA. [5]Boston Children's Hospital, Department of Otolaryngology, Boston, Massachusetts, USA. [6]Medical Imaging Centre, Department of Radiology, Tampere University Hospital, Tampere, Finland. [7]Faculty of Engineering and Natural Sciences, Tampere University, Tampere, Finland. *email: olli.valtonen@pshp.fi

Materials and Methods

CBCT scans of five adult patients with symptoms of chronic nasal congestion were included in this study. In total, ten individual nasal cavities and maxillary sinuses were studied. Exclusion criteria were chronic rhinosinusitis, nasal cavity polyps and tumours. CBCT was used for patient imaging and data acquisition due to its generalised use for this patient group in our hospital. CBCT exposes patients to a relatively low dose of radiation, less than conventional high resolution CT[9]. For CBCT imaging, we used the Scanora™ 3Dx (Soredex, Inc., Tuusula, Finland). The following imaging parameters were used: 0.2 mm CT slice thickness, voxel size 0.2 mm, 90 kVp, 8 mA and 4 s radiation time.

The plastic 3D prints were printed from CBCT scans acquired from the patients. After imaging, the CBCT data were saved in Digital Imaging and Communications in Medicine (DICOM) format. Matlab® software (MathWorks, Inc., Natick, Massachusetts, United States) was then used to process the DICOM images. The CBCT scans were then combined by stacking the 2D image slices, resulting in a 3D model with a voxel size of 0.2 mm in x, y and z directions. Each image slice in the x-y plane was pre-processed by removing noise with a square-shaped average filter and emphasizing the edges in the image using unsharp masking. Then, the tissue types were classified based on voxel light density values. The areas with the density values greater than the values of the areas of the pneumatised volumes were considered solid, and thus the greyscale 3D model was converted to a binary model. The model was corrected by removing small disconnected regions by performing a morphological opening of the 2D image slices along each axis. Finally, the data were saved in Standard Tessellation Language (STL) format for the 3D printing. Before printing, the STL models were processed with Blender software (The Blender Foundation) by using the Remesh operation to fix any possible errors in the models and to make them compatible with the Slic3r software (open source 3D slicing engine) that was used to generate the toolpaths for the printer.

The plastic 3D prints were produced on a Lulzbot® Taz 4 3D printer (Aleph Objects, Inc., Loveland, Colorado, United States) using the Fused Deposition Modeling (FDM) printing technique with a nozzle size of 0.4 mm and a layer thickness of 0.25 mm. In the FDM printing technique, the raw material is deposited through a print head[10]. The extruded string of fused thermoplastic material is immediately bound to the layer below[1]. Polylactic acid (PLA), a commonly used corn-based thermoplastic material for 3D printing, was used as the raw material[10].

The plastic 3D prints were printed from the level of the nasopharynx to the level of the frontal sinus in 1:1 size. Since it would have been challenging to remove supporting structures afterwards, no supporting structures were generated for the 3D prints. The printing of one plastic 3D print took approximately 48 hours. No additional clean-up of the printed objects was required. However, some printing artefacts were left in the cavities after printing due to the lack of supporting structures for the overhanging parts. When all five 3D prints had been printed, CBCT images were taken of each print for further analysis and to confirm that the prints corresponded with the data of the real patients.

The volumetric measurements of the pneumatised volumes in the patients' nasal cavities and maxillary sinuses were measured from the patients's CBCT scans by using pixel light density values from −1000 to −430 Hounsfield units (HU). The same values were also used for measuring pneumatised volumes in CBCT scans in our previous study[11]. The volumetric measurements were made using OnDemand3D™ (version 1.0, CyberMed, Inc., Yuseong-gu, Daejeon, South Korea). For volumetric measurements of the 3D prints, the equivalent pixel light density values for the CBCT scans were defined with the measuring software's scaling function to be from −1000 to −800 HU due to the printing material used. Similar nasal cavity and maxillary sinus volumetric measurements were evaluated from all CBCT scans. The volumetric software (OnDemand3D™) used in our study often included excess structures in the areas of the volumetric measurements despite the defined values. However, these structures were manually excluded.

Linear measurements in the nasal cavities were made using the same software in all three dimensions in the following way: septum length from the tip of the nose to the closest endpoint of the nasal septum, nasal cavity height at the same endpoint of the nasal septum and the width of the nasal cavity at the same location (Fig. 1). These benchmarks were chosen due to the lower risk of artefacts.

Rhinomanometric resistance measurements of the patients and the 3D prints were also compared. The measurements were done by using anterior rhinomanometry with an NR6 Rhinomanometer (GM Instruments Ltd, Kilwinning, Scotland, United Kingdom) and Nasal Acoustic Rhinomanometer Information System (NARIS) version 3.2 software (GM Instruments Ltd, Kilwinning, Scotland, United Kingdom). The results were measured from the airflow rates by using the Broms method. Rhinomanometry from the 3D prints was done by using the same instrument as used with real patients. In rhinomanometry, the airflow was produced by one of the investigators breathing through a plastic tube connected to the nasopharynx of the 3D prints.

In rhinomanometry, one of the patients and the corresponding 3D print were excluded from this analysis because the patient's rhinomanometry failed technically. This was noticed after the patient had undergone a nasal operation that resulted in the circumstances in the nose being altered from the original situation, and therefore another rhinomanometry could not be done reliably. As a result, a total of eight individual nasal cavities and maxillary sinuses were studied with rhinomanometry.

Due to the printing induced volume and linear measurement differences observed between the patient and the 3D print measurements, we used a scaling formula to make the rhinomanometric results *in vitro* comparable with the results *in vivo*. Furthermore, we assumed the airflow in the nose being laminar rather than turbulent in the scaling due to the mild flow rates stemmed from the use of Broms method. Thus, the scaling was based on an analogy from laminar tube flow Hagen-Poiseuille equation by taking into account nasal cavity volumes and septum lengths. The scaling for the unilateral rhinomanometric results *in vitro* was calculated by using the following formula derived from Hagen-Poiseuille equation: results *in vitro* multiplied by nasal septum length ratio (*in vivo*/*in vitro*) to the power of three divided by nasal cavity volume ratio (*in vivo*/*in vitro*) squared.

In addition, due to the relatively small number of cases and the deviation of the rhinomanometric results, the use of geometric mean instead of arithmetic mean was found to be more illustrative in presenting the

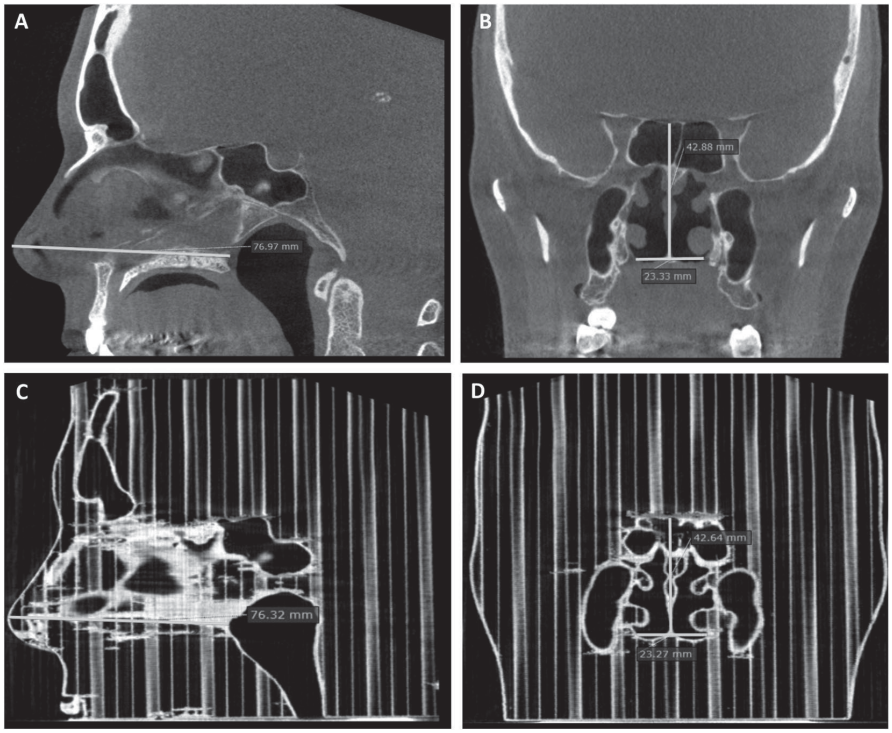

Figure 1. Linear measurements of the nose. Above: Septum length (**A**) and at the first endpoint of the nasal septum both nasal cavity height and width (**B**) in patient CBCT scans. Below: Similar measurements in the corresponding 3D print scans (**C,D**).

rhinomanometric results. The geometric standard deviation (GSD) was calculated using the following formula: $GSD(X) = e^{SD(\ln X)}$, in which e is Euler number, SD is arithmetic standard deviation, ln is natural logarithm and X is measurements.

Institutional review board approval for the study was obtained from Tampere University Hospital, Tampere, Finland. This study was carried out in accordance with the Declaration of Helsinki. Prior to collection of patient data, informed consent was obtained from all participants. All patient data were acquired from the medical records database of Tampere University Hospital.

Results

We were able to perform reliable measurements both with the patient and 3D print CBCT scans (Table 1). In the volumes of the maxillary sinuses, the results *in vivo* were higher with a ratio of 1.05 ± 0.01 (mean $\pm$ SD) compared with the volumetric results *in vitro* (Table 2). In the nasal cavities, the volumetric measurements were higher *in vivo* with a ratio of 1.20 ± 0.1 (mean $\pm$ SD) when compared with the results *in vitro*. In every linear measurement, the results were higher in the measurements *in vivo*: 1.03 ± 0.02 (mean $\pm$ SD) in nasal septum length, 1.04 ± 0.03 (mean $\pm$ SD) in the height of the nasal cavity and 1.06 ± 0.1 (mean $\pm$ SD) in the width of the nasal cavity.

In rhinomanometric results, the resistance *in vivo* was less in inspiration with a geometric mean ratio of 0.77 and in expiration with a ratio of 0.71 (Table 3). Standard deviation factors were 2.78 and 2.32, respectively. When the results *in vitro* were scaled based on nasal cavity volume and septum length differences, the similar ratios were 1.03 and 0.95 with standard deviation factors of 2.86 and 2.39, respectively. The total rhinomanometric resistance results were analogous to the unilateral measurement results. The graphs *in vitro* generated by the rhinomanometric software were close to the conditions *in vivo* (Fig. 2). The rhinomanometric graphs are provided more comprehensively in the Supplemetary Information (Suppl. Inf.).

Discussion

In the present study, we demonstrate the printing of the nasal cavities and maxillary sinuses in 3D prints from CBCT scans acquired from real patients for the first time. Moreover, the quality of the 3D prints were, for the first time, verified by imaging the 3D prints with CBCT and comparing the acquired scans with the patient data. The correspondence between the 3D prints and the original patients in the volumetric and linear measurements was high. Furthermore, we compared the rhinomanometric resistance measurements of the 3D prints to the clinical circumstances. For the first time, in order to better model clinical circumstances, we used a real person's breathing

	Septum length (mm)	Septum height (mm)	Nasal cavity width (mm)		Maxillary sinus volume (cm^3)	Nasal cavity volume (cm^3)	Rhinomanometry, inspiration (Pa/[cm^3/s])	Rhinomanometry, expiration (Pa/[cm^3/s])
Patient 1	81.0	43.2	17.3	Left Right	18.0 17.6	13.2 14.6	0.312 2.199	0.376 2.590
Patient 2	84.8	48.9	10.6	Left Right	16.3 14.4	15.6 12.6	0.212 0.913	0.133 0.884
Patient 3	90.5	45.6	22.9	Left Right	20.7 19.6	19.9 18.5	0.247 0.848	0.331 0.863
Patient 4	80.0	45.2	19.2	Left Right	12.9 12.4	13.2 10.0	0.377 1.297	0.458 1.326
Patient 5	77.0	42.9	23.3	Left Right	24.3 22.6	21.4 19.8	—	—
3D print 1	79.2	40.8	16.6	Left Right	17.1 16.7	10.4 12.1	0.726 0.498	0.708 0.610
3D print 2	82.6	46.5	10.3	Left Right	15.3 13.5	13.0 8.9	0.064 1.617	0.089 1.718
3D print 3	88.8	45.3	23.2	Left Right	20.1 19.0	18.3 16.4	0.527 2.215	0.733 2.202
3D print 4	75.8	42.1	15.5	Left Right	12.3 11.9	11.3 7.8	1.265 2.078	1.222 2.420
3D print 5	76.3	42.6	23.3	Left Right	23.3 21.6	19.4 16.9	—	—

Table 1. Measurements from every patient and corresponding 3D prints. Rhinomanometric results from patient 5 and corresponding 3D print were excluded due to a technical fail.

	Maxillary sinuses (cm^3)	Nasal cavities (cm^3)	Nasal septum length (mm)	Nasal cavity height (mm)	Nasal cavity width (mm)
In vivo	17.9 ± 4.0	15.9 ± 3.8	82.6 ± 5.2	45.1 ± 2.4	18.7 ± 5.2
In vitro	17.1 ± 3.9	13.4 ± 4.1	80.5 ± 5.3	43.5 ± 2.3	17.8 ± 5.5
Comparison	1.05 ± 0.01	1.20 ± 0.1	1.03 ± 0.02	1.04 ± 0.03	1.06 ± 0.1

Table 2. Mean volumetric (cm^3) and linear (mm) results (mean ± SD). Five patients (10 maxillary sinuses and nasal cavities, 5 nasal septums) and the corresponding 3D prints are included. In comparison, the mean ratio of the measurements is calculated by comparing the measurements *in vivo* and *in vitro*. Standard deviation of the comparison is shown as percentage points.

	Inspiration GM (GSD)	Expiration GM (GSD)	Total inspiration GM (GSD)	Total expiration GM (GSD)
In vivo	0.58 (2.34)	0.61 (2.52)	0.23 (1.30)	0.24 (1.65)
In vitro	0.76 (3.19)	0.87 (2.89)	0.28 (2.96)	0.33 (2.68)
Comparison	0.77 (2.78)	0.71 (2.32)	0.81 (2.49)	0.71 (1.81)
In vitro (scaled)	0.57 (3.15)	0.64 (2.87)	0.22 (3.11)	0.26 (2.84)
Comparison with *in vivo* and scaled results *in vitro*	1.03 (2.86)	0.95 (2.39)	1.04 (2.66)	0.91 (1.97)

Table 3. Geometric mean rhinomanometric resistance measurements (Pa/[cm^3/s]). Geometric standard deviation factors are presented in brackets. Inspiratory and expiratory results include eight different nasal cavities from four patients and corresponding 3D prints. The total results from the four patients and 3D prints take both left and right nasal cavities into account. In comparison, the geometric mean ratio of the measurements is calculated by comparing the measurements *in vivo* and *in vitro*. The scaled results *in vitro* and corresponding comparison are also presented. GM = Geometric Mean, GSD = Geometric standard deviation factor.

to provide the airflow of the 3D prints. According to our findings, the accuracy of the 3D prints of the nasal cavities both structurally and functionally are so close to the original circumstances that the 3D prints can be used for the modelling of the nasal cavities *in vitro*.

In the volumetric measurements of the maxillary sinuses and linear measurements, the 3D prints proved to be slightly smaller than the actual patients, although, the differences were small (Table 2). When it comes to measuring the relatively well-bordered anatomical structures using the volumetric method in 3D prints, the results are very close to the conditions *in vivo*. The maxillary sinuses can be accurately isolated for measuring, thus, the volumetric measurements in maxillary sinuses are reliable and can be used in size comparison. In the nasal cavities, artefacts produced in printing the delicate structures of the nasal cavities were the reason for high result in this comparison. Linear measurements also proved to be very close to the original measurements due to the absence

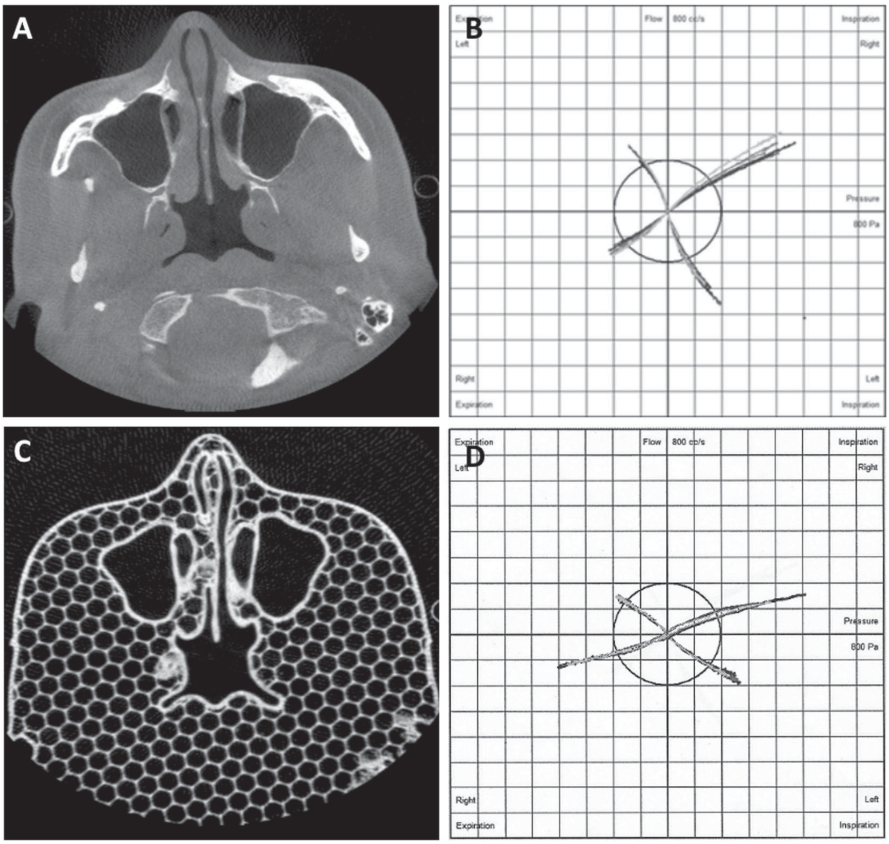

Figure 2. Corresponding results *in vivo* and *in vitro*. Above: Axial CBCT image (**A**) from a patient and rhinomanometry (**B**) from the same patient. Below: Corresponding CBCT image (**C**) and rhinomanometry (**D**) from the 3D print.

of major artefacts in the measuring points of the 3D prints. Moreover, during printing, the size of the 3D prints can be scaled according to the desired size, which gives added versatility to this printing method.

Caution is always required in replicating small and detailed structures as artefacts may be introduced into the 3D print, but despite this the printed result was satisfactory. In our study, the most challenging part of replicating the nasal cavities was to replicate the upper part of the nasal cavity together with the ethmoidal cells. These anatomical structures were vulnerable to any kind of image artefact in the original CBCT scans. In addition, the lack of supporting structures during the printing phase also caused our 3D prints to be exposed to printing artefacts, for example, print surface roughness and narrower structures. Furthermore, we noticed that printing these delicate structures starting from the bottom of the nasal cavity meant that some of the structures were left without any support, and thus, there was the risk of collapse. In most of the models, the upper nasal cavities were narrowed and the inferior nasal conchae had bent under weight. This caused the actual pneumatised area to diminish, which can also be seen in our nasal cavity volume results. These printing technique induced artefacts could most likely be avoided, for example, by beginning printing from above and, if it is practically possible, using soluble supporting structures during the printing process.

Similar observations regarding artefacts with fine anatomical structures were also made in a study where producing 3D prints caused an overall dimensional error of 2.67% for a 3D model of a dry skull[12]. However, the thin bones, small foramina and acute bone projections were not printed as accurately as the rest of the structures.

In the modelling of sinonasal structures, 3D printing would be a reliable tool for research purposes and also an option for PIV experiments and CFD modelling. The 3D printing method is faster, easier and more affordable than PIV and CFD with silicone models, which can take from days to weeks to perform[5–8]. However, PIV experiments do have a future in the exact assessment of airflow in the nasal cavities, which is not possible with the presented method. In our study, the plastic 3D prints were produced in two days. The printing time can be reduced by changing the scale of the 3D prints. The nozzle of the printer and layer thickness can also be changed, thereby affecting the printing time. However, these changes will also have an effect on the surface precision of the 3D prints. In addition, the 3D printing process can be automated, and the procedure can be performed around the clock.

We were able to perform rhinomanometric measurements using the 3D prints. The resistance to airflow proved to be higher *in vitro* compared to the results *in vivo* (Table 3). When the results *in vitro* were scaled based on nasal cavity volumes for a more realistic comparison, the results *in vivo* and *in vitro* were closer to each other. This indicates that rhinomanometric results from various sizes *in vitro* could be scaled with reasonable accuracy to make cases comparable to rhinomanometry *in vivo*.

Rhinomanometric results in our study were likely affected by the properties of the rigid plastic material used as it, in terms of its qualities, was not directly proportional to the actual mucus membrane. In future studies acrylonitrile butadiene styrene (ABS) could be considered an alternative rigid material to PLA. Another option, for example, could be thermoplastic polyurethane (TPU) which is more elastic than PLA. Furthermore, many of the delicate structures in the nasal cavities were troublesome to replicate in printing, with the result of narrowing of some structures that could affect the results. The 3D prints, although printed in 1:1 size, proved to be slightly smaller than the actual patients, which necessitated our use of a scaling formula in our evaluation of the rhinomanometric results.

Our rhinomanometric measurements were conducted with normal breathing. However, temporal information of breathing flow rates was not given by our rhinomanometry device. To be precise, breathing flow rates should be temporally identical between *in vivo* and *in vitro* to be completely certain of a correct comparison. Therefore, the time dependency of the rhinomanometric results should be investigated in future. In a similar way, completely stationary flow resistances should be compared to the present rhinomanometric results. Such studies could reveal important information of how unsteady flow may affect rhinomanometric results. In addition, it has been previously reported that rhinomanometric results *in vivo* could be considerably higher than those obtained by time independent CFD[13,14]. The time dependence of the rhinomanometric results could be an important factor in explaining such differences.

Our 3D modelling method makes all additionally mentioned flow resistance measurements possible. We could expect temporally identical rhinomanometric measurements to reduce the standard deviations in mean ratios between *in vivo* and *in vitro* compared with the present results. Already in the current study, comparison ratios with nasal cavity scaling produced results with reasonable agreement.

Conclusions

3D printing technology proved to be a suitable and fast method for replicating nasal cavity structures and for the experimental testing of nasal function. The technology enables the detailed study of rhinomanometric measurements, and thus can be used as a complementary examination tool for rhinomanometry for clinical and research purposes. More study to optimise the printing techniques, print materials and modelling processes is warranted to refine this promising model.

Data availability

All data are available on request.

Received: 10 September 2019; Accepted: 2 January 2020;
Published online: 16 January 2020

References

1. Rengier, F. *et al*. 3D printing based on imaging data: review of medical applications. *Int. J. Comput. Assist. Radiol. Surg.* **5**, 335–341, https://doi.org/10.1007/s11548-010-0476-x (2010).
2. Crafts, T. D. *et al*. Three-Dimensional Printing and Its Applications in Otorhinolaryngology-Head and Neck Surgery. *Otolaryngol. Head. Neck Surg.* **156**, 999–1010, https://doi.org/10.1177/0194599816678372 (2017).
3. Ganry, L. *et al*. Three-dimensional surgical modelling with an open-source software protocol: study of precision and reproducibility in mandibular reconstruction with the fibula free flap. *Int. J. Oral. Maxillofac. Surg.* **46**, 946–957, https://doi.org/10.1016/j.ijom.2017.02.1276 (2017).
4. Bauermeister, A. J., Zuriarrain, A. & Newman, M. I. Three-Dimensional Printing in Plastic and Reconstructive Surgery: A Systematic Review. *Ann. Plast. Surg.* https://doi.org/10.1097/SAP.0000000000000671 (2015).
5. Cozzi, F., Felisati, G. & Quadrio, M. In *Journal of Physics: Conference Series* Vol. 882 (IOP Publishing Ltd., 2017).
6. Spence, C. J. T., Buchmann, N. A., Jermy, M. C. & Moore, S. M. Stereoscopic PIV measurements of flow in the nasal cavity with high flow therapy. *Exp. Fluids* **50**, 1005–1017, https://doi.org/10.1007/s00348-010-0984-z (2011).
7. Im, S. *et al*. Tomographic PIV measurements of flow patterns in a nasal cavity with geometry acquisition. *Experiments in Fluids* **55**, https://doi.org/10.1007/s00348-013-1644-x (2014).
8. Hopkins, L. M., Kelly, J. T., Wexler, A. S. & Prasad, A. K. Particle image velocimetry measurements in complex geometries. *Exp. Fluids* **29**, 91–95, https://doi.org/10.1007/s003480050430 (2000).
9. Al Abduwani, J., ZilinSkiene, L., Colley, S. & Ahmed, S. Cone beam CT paranasal sinuses versus standard multidetector and low dose multidetector CT studies. *Am. J. Otolaryngol.* **37**, 59–64, https://doi.org/10.1016/j.amjoto.2015.08.002 (2016).
10. Lipson, H., Kurman, M., John, W. & Sons. *Fabricated: the new world of 3D printing* (John Wiley & Sons Inc., 2013).
11. Valtonen, O., Bizaki, A., Kivekäs, I. & Rautiainen, M. Three-Dimensional Volumetric Evaluation of the Maxillary Sinuses in Chronic Rhinosinusitis Surgery. *Ann. Otol. Rhinol. Laryngol.* **127**, 931–936, https://doi.org/10.1177/0003489418801386 (2018).
12. Silva, D. N. *et al*. Dimensional error in selective laser sintering and 3D-printing of models for craniomaxillary anatomy reconstruction. *J. Craniomaxillofac Surg.* **36**, 443–449, https://doi.org/10.1016/j.jcms.2008.04.003 (2008).
13. Osman, J. *et al*. In *Current Directions in Biomedical Engineering* Vol. 2 617 (2016).
14. Hemtiwakorn, K., Mahasitthiwat, V., Tungjitkusolmun, S., Hamamoto, K. & Pintavirooj, C. Patient-specific aided surgery approach of deviated nasal septum using computational fluid dynamics. *IEEJ Trans. Electr. Electron. Eng.* **10**, 274–286, https://doi.org/10.1002/tee.22084 (2015).

Acknowledgements

The author(s) received financial support from the Finnish ORL-HNS Foundation, Tampere Tuberculosis Foundation, and Väinö and Laina Kivi Foundation for the research, authorship, and/or publication of this article.

Author contributions

All authors took part in designing the study. O.V., J.O., V.R., I.K. and J.J. performed the experiments and measurements. O.V. and J.O. processed all the data. O.V. produced all the tables and figures. O.V. and J.O. wrote the manuscript and I.K., P.S. and M.R. provided comments. All authors took part in finalising the manuscript and approved it.

Competing interests

The authors declare no competing interests.

Additional information

Supplementary information is available for this paper at https://doi.org/10.1038/s41598-020-57537-2.

Correspondence and requests for materials should be addressed to O.V.

Reprints and permissions information is available at www.nature.com/reprints.

Publisher's note Springer Nature remains neutral with regard to jurisdictional claims in published maps and institutional affiliations.

PUBLICATION III

Assessment of PIV Performance in Validating CFD Models from Nasal Cavity CBCT Scans

Ormiskangas J, Valtonen O, Kivekäs I, Dean M, Poe D, Järnstedt J, Lekkala J, Harju T, Saarenrinne P, Rautiainen M

Respiratory Physiology and Neurobiology. 282:103508, 2020
doi: 10.1016/j.resp.2020.103508

Respiratory Physiology & Neurobiology 282 (2020) 103508

Contents lists available at ScienceDirect

Respiratory Physiology & Neurobiology

journal homepage: www.elsevier.com/locate/resphysiol

Assessment of PIV performance in validating CFD models from nasal cavity CBCT scans

Jaakko Ormiskangas [a,b,*], Olli Valtonen [a,c], Ilkka Kivekäs [a,c], Marc Dean [d,e], Dennis Poe [f], Jorma Järnstedt [g], Jukka Lekkala [a], Teemu Harju [a,c], Pentti Saarenrinne [b], Markus Rautiainen [a,c]

[a] Faculty of Medicine and Health Technology, Tampere University, Tampere, Finland
[b] Faculty of Engineering and Natural Sciences, Automation Technology and Mechanical Engineering Unit, Tampere University, Tampere, Finland
[c] Department of Otorhinolaryngology – Head and Neck Surgery, Tampere University Hospital, Tampere, Finland
[d] Texas Tech University Health Sciences Center, Lubbock, Texas, USA
[e] Ear & Sinus Institute, Fort Worth, Texas, USA
[f] Boston Children's Hospital, Department of Otolaryngology, Boston, Massachusetts, USA
[g] Medical Imaging Centre, Department of Radiology, Tampere University Hospital, Tampere, Finland

ARTICLE INFO

Keywords:
CFD
PIV
nasal airflow
CBCT
3D silicone modelling

ABSTRACT

Objective: The aim of our study was to investigate how well Particle Image Velocimetry (PIV) measurements could serve Computational Fluid Dynamics (CFD) model validation for nasal airflow.
Material and methods: : For the PIV measurements, a silicone model of the nose based on cone beam computed tomography (CBCT) scans of a patient was made. Corresponding CFD calculations were conducted with laminar and two turbulent models (k-ω and k-ω SST).
Results: CFD and PIV results corresponded well in our study. Especially, the correspondence of CFD calculations between the laminar and turbulent models was found to be even stronger. When comparing CFD with PIV, we found that the results were most convergent in the wider parts of the nasal cavities.
Conclusion: PIV measurements in realistically modelled nasal cavities succeed acceptably and CFD calculations produce corresponding results with PIV measurements. Greater model scaling is, however, necessary for better validations with PIV and comparisons of competing CFD models.

1. Introduction

Currently, clinicians have rudimentary analysis tools at their disposal with which to assess the nasal cavities. The most commonly used rhinometric measurements for the assessment of the nasal cavities are rhinomanometry and acoustic rhinometry. Vogt et al. have previously published an excellent review on the subject of rhinomanometry (Vogt, Jalowayski et al., 2010). Unfortunately, a patient's subjective assessment does not always correlate with objective clinical measurement methods (André et al., 2009; Nip et al., 2018).

Clinicians, therefore, have to rely on their experience, intuition and subjective assessment of nasal function upon which to base their treatment or operative management. Due to the three dimensional complexity of the nasal cavities, it is impossible for the surgeon to evaluate the fluid mechanical consequences of surgical manoeuvres. Such information requires a solution to the Navier-Stokes equations that govern airflow in the nasal cavities. Fortunately, computed tomography (CT) and cone-beam computed tomography (CBCT) scans of the patient can be used to create a computational mesh for Computational Fluid Dynamics (CFD) simulations that can solve these equations.

CFD modelling of the nasal cavities is not, however, straightforward. The fundamental question in nasal airflow is whether it remains laminar or is partly turbulent. In addition, airflow also varies as a function of time and location in the nasal cavities. Due to these and other challenges, researchers have conducted CFD studies using various approaches. Quadrio et al. (2014) have carried out an excellent review of CFD studies. Similar reviews have also been published in which the challenges of the clinical use of CFD have been discussed (Zubair et al., 2012; Kim et al., 2013).

Turbulence modelling is usually based on the widely used Reynolds-

* Corresponding author at: Faculty of Medicine and Health Technology, Faculty of Engineering and Natural Sciences, Automation Technology and Mechanical Engineering Unit, Tampere University, FIN-33520 Tampere, Finland.
E-mail address: jaakko.ormiskangas@tuni.fi (J. Ormiskangas).

https://doi.org/10.1016/j.resp.2020.103508
Received 14 April 2020; Received in revised form 8 July 2020; Accepted 26 July 2020
Available online 30 July 2020

averaged Navier-Stokes (RANS) models, which rely on Reynolds averaging of turbulent fluctuations. The most common approach to the problem is to use two-equation RANS models that introduce the Boussinesq linear eddy viscosity assumption, where turbulent viscosity is assumed to be isotropic and is a property of the flow. These two-equation models, such as k-ε, k-ω and k-ω SST, are reasonably good for most cases. Further from the scope of RANS turbulence modelling, Large Eddy Simulation (LES) and Direct Numerical Simulation (DNS) are more detailed but computationally often too expensive, which make them inconvenient for practical use.

The various CFD models need validation of the results. These results are often very case specific because no universally optimal RANS model has been found. Particle Image velocimetry (PIV)-based measurements with transparent silicone models can be applied for these CFD validations. Nasal cavity airflow *in vitro* has been studied with Stereoscopic Particle Image Velocimetry (SPIV) (Spence et al., 2011; Spence et al., 2012). There have also been studies where PIV and CFD have been used for the study of nasal cavity airflow (Doorly et al., 2008; Chung and Kim, 2008; Na et al., 2012; Zubair et al., 2015; Lintermann and Schröder, 2017). Cozzi et al. (2017) conducted SPIV and LES calculations, where the maxillary sinuses were also included in the silicone model.

The clinical treatment of the nose would benefit from a planning tool that uses CT imaging, analyses the patient's problems and provides suggestions for the diagnosis and proper surgical or medical treatment. Such a diagnostics and surgical planning tool could be based on results obtained from CFD. In order to select the optimal CFD model, we would need a comparison to PIV measurements. Unfortunately, previous PIV studies have lacked overall comparisons between PIV and various CFD models. Therefore, this study aims to investigate how well PIV measurements can serve CFD model validation in studies of the nose. For this purpose, laminar and two turbulent CFD models (k-ω and k-ω SST) are compared with PIV measurements in a silicone model of the nasal cavities.

2. Material and Methods

Institutional review board approval for the study was obtained from Tampere University Hospital, Tampere, Finland. All patient data were acquired from the medical records database of Tampere University Hospital.

A nasal airflow corresponding to the constant inspiratory flow rate of calm breathing of 10 l/min *in vivo* was studied. In addition to the flow experiments and calculations of 10 l/min, we also assessed how different CFD models would behave when calculations were performed with a doubled Reynolds number corresponding to human nasal breathing of 20 l/min. The inspiratory phase can be regarded as being more important than the expiratory phase because patients with nasal obstruction usually feel that inspiratory breathing is more difficult. All PIV measurements and CFD calculations were made using the silicone model.

We have provided the comprehensive setup of the study in Supplementary Information (**Suppl. Inf**.)

2.1. NASAL CAVITY GEOMETRY AND SILICONE MODEL PRODUCTION

The procedure for producing the silicone model of the nasal cavities used in the PIV measurements closely followed the approach previously presented by Hopkins et al. (2000). Pre-operative nasal CBCT scans, with a slice resolution of 0.2 mm, of one adult patient with chronic nasal obstruction and inferior turbinate enlargement without chronic sinusitis, nasal polyps or other pathology were used in our study.

OnDemand3D™ software was used in the processing of the patient CBCT scans with Hounsfield Unit (HU) values from -1000 to -430, as previously described (Valtonen et al., 2018; Valtonen et al., 2020). A Standard Tessellation Language (STL) file, scaled by a factor of 1.85, formed from patient CBCT scans was used to produce a water soluble polyvinyl alcohol (PVA) print. This was then used to create a silicone model (Fig. 1).

CBCT scans of the silicone model, with a slice resolution of 0.3 mm, were also taken to create an STL file for CFD calculations. Confirmed from the OnDemand3D™ software's own scaling function, the same HU values that were used with the patient CBCT scans were applied.

2.2. PIV EXPERIMENTS

The silicone model and laser measurement planes for the PIV measurements are presented in Fig. 2. In addition, comprehensive parameters and setup are presented in the Supplementary Information (Suppl. Inf.). From the fluid dynamic point of view, dimensional similarity between *in vivo* and *in vitro* was obtained by matching Reynolds numbers. This resulted in the following flow rate *in vitro*:

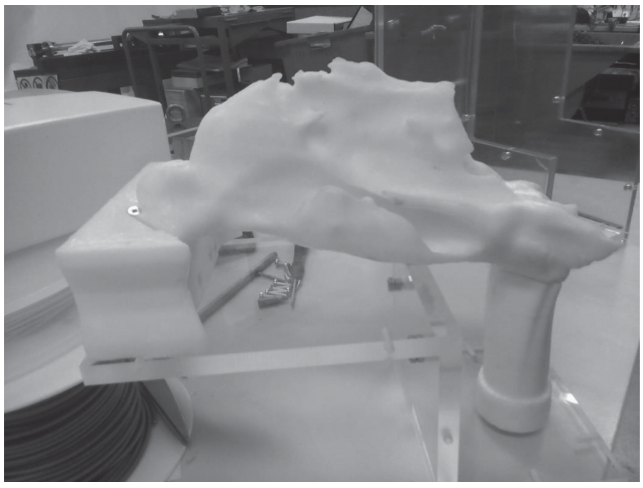

Fig. 1. The printed negative of the nasal cavities. The anterior parts of the nasal cavities are on the left side. Negatives of the nasal flow passages were printed in separate parts because printer dimensions were limited.

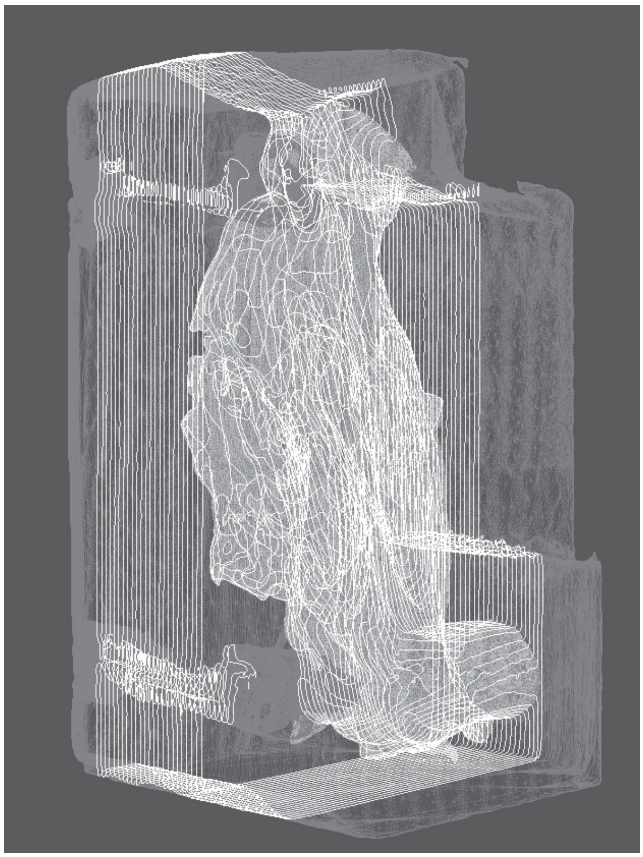

Fig. 2. Silicone model and laser measurement planes for the PIV measurements. The model is presented in actual study position in which the model is set at a 10 degree angle from the vertical position. The anterior part of the nasal cavity is on top. Laser light sheet positions are visualised in vertical planes. The planes enter in and out of the model at the vertical lines.

$$Q_{in-vitro} = Q_{in-vivo}\frac{D_{in-vitro}}{D_{in-vivo}}\frac{\nu_{in-vitro}}{\nu_{in-vivo}} = \frac{10*1.85*11.7}{16} l/min = 13.53 l/min = 0.225\ l\Big/s$$

in which Q is volume flow rate, D is model scaling compared to conditions *in vivo* and ν is kinematic viscosity. All measurements were gathered with this steady state inspiratory volume flow rate of 0.225 l/s. The silicone model was held in a liquid tank in which constant pressure was achieved by liquid overflowing from the tank.

2.3. CFD CALCULATIONS

CFD calculations were conducted with open source OpenFoam 5.0 software. The flow was assumed to be incompressible. In addition, the same geometry was used as in the PIV experiments. The studied CFD models comprised a laminar model and two turbulent models (k-ω and k-ω SST). For the inlet, uniform total pressure boundary condition was used. For the outlet, the boundary condition was the PIV experiments' flow rate of 0.225 l/s. In turbulent cases, a turbulent inlet intensity of 10 % was investigated to study the maximal differences between the laminar and turbulent models.

In addition to calculating and measuring with the flow rate of 10 l/min *in vivo*, CFD calculations with the doubled Reynolds number corresponding to human breathing of 20 l/min were studied. This was conducted by changing the dynamic viscosity without adjusting the other flow properties. The dynamic viscosity was changed instead of volume flow rate to avoid any detectable inlet velocity profile variations stemming from the use of total pressure boundary condition. One calculation took roughly one week to complete in 24 processors.

2.4. DATA ANALYSIS

For the analysis, four coronal cross-sections were chosen: the anterior tip of the inferior turbinate, the anterior tip of the middle turbinate, the posterior part of the inferior turbinate and the nasopharynx (Fig. 3). The Reynolds numbers in these analysed four cross-sections were 308, 212, 155 and 485, respectively. The first three coronal cross-sections of the nasal cavities were divided into three vertical parts and further divided in to left and right sides in order to better illustrate the route of the flow (Fig. 3). The fourth cross-section was only divided into left and right sides.

Time averaged axial mean flow velocity and axial volume flow rate ratios were measured from PIV and calculated from CFD in these cross-sections. These represent the velocity and the distribution of the flow in the nasal cavities. Axial volume flow rate ratios were calculated by dividing local flow rates over summarised total flow rates.

To assess the stress caused by the flow to the boundary of the flow

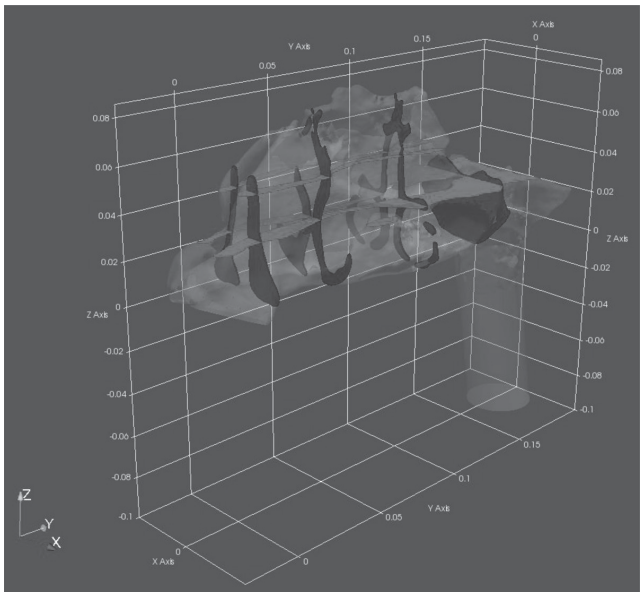

Fig. 3. Study geometry for both CFD and PIV. The coronal planes in blue represent analysis cross-sections. The horizontal planes in red vertically divide the study geometry into three parts.

and the nasal cavity surface, median wall shear stresses (WSS) were calculated in the same cross-sections from CFD. In the analyses, the origo was located at the nasolabial angle. The numerical post-processing was made with open-source visualisation and data analysis software ParaView 5.0.1.

3. Results

Axial mean flow velocities calculated from laminar CFD showed the highest results in the left nasal cavity's lower third in the first cross-section (0.33 m/s) and in the middle third in the second cross-section (0.43 m/s) (Table 1) (Fig. 4.**a**). Corresponding measurements with PIV were 0.34 m/s and 0.39 m/s (Fig. 4.**b**). In the right nasal cavity, the calculated axial mean flow velocities in laminar CFD were highest in the lower third of the first cross-section (0.45 m/s) and in the lower third of the third cross-section (0.29 m/s). Corresponding measurements with PIV were 0.42 m/s and 0.18 m/s. In the fourth cross-section, the axial mean velocities were equal between laminar CFD and PIV in both the left (0.10 m/s) and right sides (0.15 m/s). The differences in axial mean velocities between the laminar and turbulent (k-ω and k-ω SST) CFD

Table 1
Area averaged mean axial velocities (m/s) in the nose for flow rate of 13.53 l/min *in vitro* corresponding to human breathing of 10 l/min. The coronal cross-sections (1-4) and division to vertical thirds (lower, middle, upper) are visually presented in Fig. 3. Left and right nasal cavities are analysed separately. The first three cross-sections are analysed in **Table 1a.** The fourth coronal cross-section was analysed as a whole due to the location behind the nasal septum in **Table 1b**. In the fourth cross-section, the division is done by using the centre line of the nasal septum as a landmark

Table 1a.

	1st			2nd			3rd		
	CFD (laminar)	CFD (turbulent)	PIV	CFD (laminar)	CFD (turbulent)	PIV	CFD (laminar)	CFD (turbulent)	PIV
Lower third									
Left	0.33	0.33	0.34	0.23	0.23	0.19	0.25	0.25	0.24
Right	0.45	0.45	0.42	0.25	0.25	0.19	0.29	0.29	0.18
Middle third									
Left	0.15	0.15	0.19	0.43	0.42	0.39	0.28	0.28	0.16
Right	0.05	0.05	0.03	0.25	0.24	0.27	0.21	0.21	0.07
Upper third									
Left	−0.03	−0.03	−0.03	0.14	0.14	0.03	0.14	0.14	0.06
Right	0.00	0.00	0.00	0.02	0.02	0.00	0.18	0.18	0.10

Table 1b.

	4th		
	CFD (laminar)	CFD (turbulent)	PIV
Left	0.10	0.10	0.10
Right	0.15	0.15	0.15

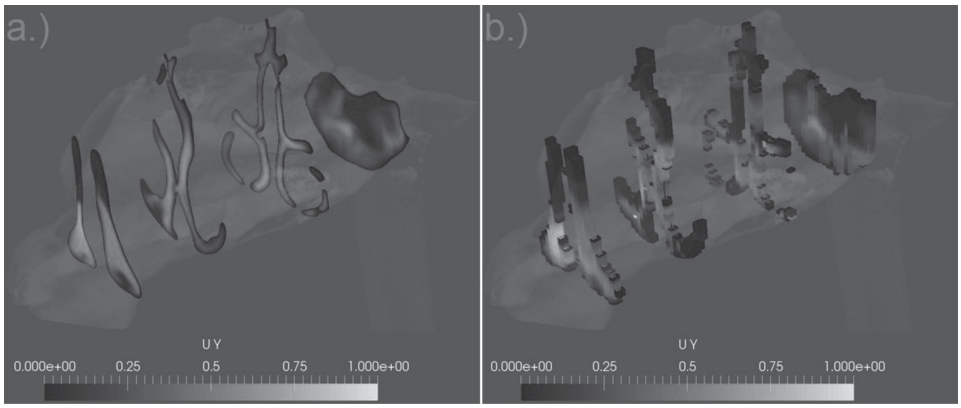

Fig. 4. The velocities in the four analysed coronal cross-sections. The smallest values are presented in violet and the highest in yellow. **a.**) Axial mean flow velocities (m/s) from laminar CFD results. **b.)** Axial mean flow velocities (m/s) from PIV measurements.

models were small.

The main volume of the flow calculated from CFD in the left nasal cavity's first cross-section was in the lower third with a ratio of 0.47 (Table 2). The PIV measurement in the same location was 0.48. In the right nasal cavity, the main volume of the flow calculated from laminar CFD was in the lower third of the nasal cavity in all three most anterior cross-sections with ratios ranging from 0.35 to 0.42. Corresponding PIV measurements were from 0.35 to 0.41. In the fourth cross-section, the volume of the flow was equal between laminar CFD and PIV for the left (0.42) and right sides (0.58). The differences in axial volume flow rate ratios between the laminar and turbulent (k-ω and k-ω SST) CFD models were small.

Median wall shear stress was highest in the lower third of the first cross-section at 7.76 Pa (Table 3, Fig. 5). In the second cross-section, median WSS varied from 2.07 to 6.55 Pa and in the third cross-section from 4.02 to 5.97 Pa. In the whole fourth cross-section, median WSS was 2.92 Pa.

CFD calculations with the calculated flow corresponding to the flow of 20 l/min *in vivo* did not show any considerable differences between the CFD models (Tables 4–5,).

Table 3
Median wall shear stresses (Pa) in the nose for flow rate of 13.53 l/min *in vitro* calculated from CFD corresponding to human breathing of 10 l/min. The coronal cross-sections (1-4) and division to vertical thirds (lower, middle, upper) are visually presented in Fig. 3. The fourth coronal cross-section was analysed as a whole due to the location behind the nasal septum. The median WSS result for the fourth coronal cross-section was 2.92 Pa.

	1st	2nd	3rd
Lower third	7.76	3.13	5.91
Middle third	0.42	6.55	5.97
Upper third	0.09	2.07	4.02

4. Discussion

In this study, we have presented numerical comparisons between a mathematical model of nasal airflow (CFD) and the measured flow (PIV) in a realistic nasal cavity acquired from CBCT scans for the first time. CFD and PIV results corresponded well in our study. Moreover, the

Table 2
Area averaged volume flow rate ratios in the nose for flow rate of 13.53 l/min *in vitro* corresponding to human breathing of 10 l/min. Results are presented as a ratio of flow rates per total volume flow. The coronal cross-sections (1-4) and division to vertical thirds (lower, middle, upper) are visually presented in Fig. 3. Left and right nasal cavities are analysed separately. The first three cross-sections are analysed in **Table 2a.** The fourth coronal cross-section was analysed as a whole due to the location behind the nasal septum in **Table 2b**. In the fourth cross-section the division is done by using the centre line of the nasal septum as a landmark.

Table 2a.

	1st			2nd			3rd		
	CFD (laminar)	CFD (turbulent)	PIV	CFD (laminar)	CFD (turbulent)	PIV	CFD (laminar)	CFD (turbulent)	PIV
Lower third									
Left	0.47	0.47	0.48	0.22	0.22	0.23	0.27	0.27	0.37
Right	0.42	0.42	0.41	0.36	0.36	0.35	0.35	0.35	0.35
Middle third									
Left	0.10	0.09	0.11	0.22	0.22	0.24	0.13	0.13	0.13
Right	0.02	0.02	0.01	0.12	0.11	0.15	0.12	0.11	0.06
Upper third									
Left	0.00	0.00	0.00	0.08	0.08	0.03	0.09	0.09	0.05
Right	0.00	0.00	0.00	0.00	0.00	0.00	0.05	0.05	0.04

Table 2b.

	4th		
	CFD (laminar)	CFD (turbulent)	PIV
Left	0.42	0.42	0.42
Right	0.58	0.58	0.58

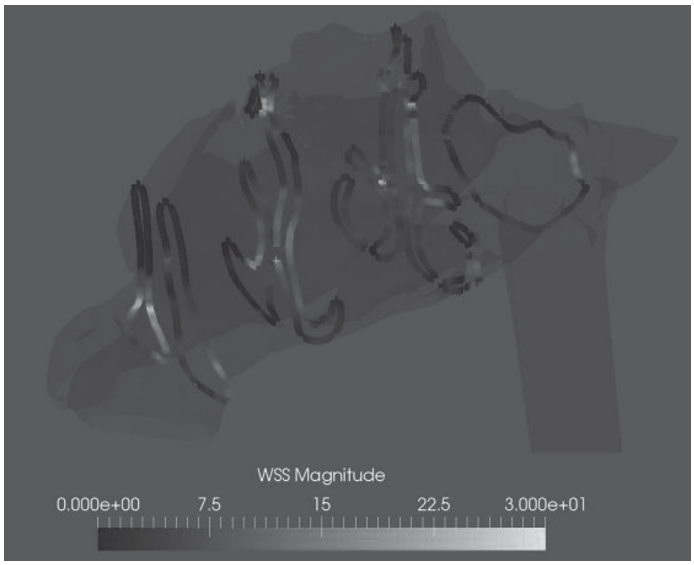

Fig. 5. Mean wall shear stresses (Pa) in the four analysed coronal cross-sections. The smallest values are presented in violet and the highest in yellow.

Table 4
Area averaged mean axial velocities (m/s) in the nose for flow rate of 13.53 l/min *in vitro* corresponding to human breathing of 20 l/min. The coronal cross-sections (1-4) and division to vertical thirds (lower, middle, upper) are visually presented in Fig. 3. Left and right nasal cavities are analysed separately. The first three cross-sections are analysed in **Table 4a.** The fourth coronal cross-section was analysed as a whole due to the location behind nasal septum in **Table 4b**. In the fourth cross-section, the division is done by using the centre line of the nasal septum as a landmark.

Table 4a.

	1st		2nd		3rd	
	CFD (laminar)	CFD (turbulent)	CFD (laminar)	CFD (turbulent)	CFD (laminar)	CFD (turbulent)
Lower third						
Left	0.34	0.33	0.23	0.23	0.26	0.26
Right	0.44	0.44	0.24	0.24	0.28	0.28
Middle third						
Left	0.17	0.17	0.44	0.44	0.29	0.29
Right	0.05	0.05	0.26	0.26	0.24	0.24
Upper third						
Left	−0.04	−0.04	0.15	0.15	0.13	0.13
Right	0.00	−0.01	0.02	0.02	0.19	0.20

Table 4b.

	4th	
	CFD (laminar)	CFD (turbulent)
Left	0.10	0.10
Right	0.15	0.15

correspondence of CFD calculations between laminar and turbulent (k-ω and k-ω SST) models was found to be even stronger. When comparing CFD with PIV, we found that the results were most convergent in the wider parts of the nasal cavities. In addition, the distribution of the flow volume proved to be convergent between CFD and PIV despite the smaller flow velocities in PIV in some locations. The most notable differences were observed in the narrowest passages of the nasal cavities. The results from both CFD and PIV showed the main flow streaming mainly in the lower and middle thirds of the nasal cavities.

At first, the flow through the nasal cavities was found to be the strongest in the anterior part of the inferior nasal turbinates, after which the flow spread to a vertically wider area (Table 1, Table 2**)**. However, the main flow stayed mainly at the level of the inferior and middle nasal turbinates. The results were convergent between the flow velocity and the distribution of the flow volume. The strongest axial flow could be visually observed mainly in the narrow mid-parts of the nasal cavities (Fig. 4 a,b).

The shear stresses in various areas may have significance on the subjective feeling of nasal patency. In our study, median wall shear stresses, calculated from CFD, were the highest on the surface of the lower and middle thirds of the nasal cavities (Table 3). These areas contain the inferior and middle nasal turbinates which are also the

Table 5
Area averaged volume flow rate ratios in the nose for flow rate of 13.53 l/min *in vitro* corresponding to human breathing of 20 l/min. Results are presented as a ratio of flow rates per total volume flow. The coronal cross-sections (1-4) and division to vertical thirds (lower, middle, upper) are visually presented in Fig. 3. Left and right nasal cavities are analysed separately. The first three cross-sections are analysed in **Table 5a.** The fourth coronal cross-section was analysed as a whole due to the location behind the nasal septum in **Table 5b**. In the fourth cross-section, the division is done by using the centre line of the nasal septum as a landmark.

Table 5a.

	1st		2nd		3rd	
	CFD (laminar)	CFD (turbulent)	CFD (laminar)	CFD (turbulent)	CFD (laminar)	CFD (turbulent)
Lower third						
Left	0.48	0.48	0.22	0.22	0.27	0.27
Right	0.41	0.41	0.34	0.34	0.33	0.33
Middle third						
Left	0.10	0.10	0.23	0.23	0.13	0.14
Right	0.02	0.02	0.12	0.12	0.13	0.13
Upper third						
Left	0.00	0.00	0.08	0.08	0.08	0.08
Right	0.00	0.00	0.00	0.00	0.05	0.05

Table 5b.

	4th	
	CFD (laminar)	CFD (turbulent)
Left	0.41	0.41
Right	0.59	0.59

structures that are most often the reason for the symptoms of nasal blockage caused by swelling (Willatt, 2009). In the posterior parts of the nasal cavities, the median wall shear stresses are more evenly divided. However, a few sudden local structural changes increased wall shear stresses locally as can be seen, for example, in the upper part of the second cross-sections (Fig. 5).

Our CFD and PIV results are somewhat in agreement with the results of previous studies (Doorly et al., 2008; Chung and Kim, 2008; Na et al., 2012; Zubair et al., 2015; Lintermann and Schröder, 2017; Cozzi et al., 2017). The studies from Lintermann et al., Chung et al. and Na et al. all presented similar findings of the flow passing mainly through the lower and middle thirds of the nasal cavities (Chung and Kim, 2008; Na et al., 2012; Lintermann and Schröder, 2017). In the studies by Cozzi et al. and Zubair et al., the results between CFD and PIV had a fair agreement, which is in line with our results (Cozzi et al., 2017; Zubair et al., 2015). A precise comparison between studies is, however, challenging because previous studies have not reported overall numerical comparisons between various CFD models and PIV in the nasal cavities. In addition, the Reynolds numbers, study setups, CFD models and the extent and accuracy of the anatomical structures used in previous studies have varied. Therefore, it remains difficult to assess which CFD model performs optimally in the nasal cavities based on PIV measurements.

CFD succeeded well in our study in all locations with both laminar and turbulent models. The differences between these three models were small, and it is therefore difficult to assess which model obtains the most correct results. In addition, as was previously studied with static pressure measurements in high turbulent conditions (100 l/min *in vivo*) using stereolithography resin material by Mylavarapu et al. (2009), finding the most convenient turbulent CFD model is also challenging with their approach. Their study showed the k-ω turbulence model achieved the best experimental agreement with an average error of about 20% over all pressure ports along the nasal cavity. The reason for the investigated high flow rate in their study was the insensitivity of the static pressure probes to small values. Therefore, realistic human breathing flow rates are not technically easy to study with pressure measurements along a nasal cavity.

In addition to PIV measurements, Li et al. studied hot-wire anemometer velocity results against CFD results in a nasal cavity model scaled by a factor of 20 (Li et al., 2017). The K-ω CFD model obtained the best RANS model results for flow rates of 33.6 l/min and 66 l/min *in vivo*. LES and DNS results remained better than any RANS model. However, for human breathing of 10.8 l/min, the laminar model obtained the best results among the RANS models and did not differ much from the LES or DNS models.

In principle, PIV measurements can be made anywhere in the nasal cavity, but the most reliable results are obtained in the middle of the cavities where velocity gradients are usually the smallest. Conversely, pressure measurements, which were out of the scope of our study, are easier to perform at the walls. The differences are also clear in model scaling between these two approaches. PIV measurements should be made with a large scaling to increase measurement resolution, whereas the opposite is better for pressure measurement ranges.

For PIV measurements, the present study geometry of the nasal cavities is one of the most realistic used. In this setup, PVA was found to be challenging to dissolve in water and took more time than expected. Two silicone model processing artefacts left a nasal septum perforation to the level of the second and third cross-section (Fig. 3). These perforations were the result of the challenges faced in the modelling and processing of very narrow structures. However, these perforations did not cause any unexpected disturbances to the CFD calculations. Thus, we interpreted the effect of the perforations as being relatively small from the viewpoint of CFD model validation.

Overall, the PIV results are shown to be reasonably good in the anterior parts of the nasal cavity as well as in the end of the nasal cavities. More distinguishable results are observed, especially in the middle parts of the nasal cavities where the narrowest passages are present. Detailed and obstructed passages of the nasal cavities are generally harder to measure but are ideal from a CFD validation perspective, possessing more details from a clinical perspective. Hence, there exists a trade-off between CFD model validation precision and the accuracy of the studied nasal cavity geometries. Based on the findings of the current study, our view is that when using PIV measurements, simplifications are needed, and wider passages with greater model scaling should be preferred from the study geometry or other similar realistic geometries.

When it comes to PIV measurements, more erroneous laser sheet positioning and a wider range of velocities across the laser sheet thickness emerge as nasal cavity widths decrease. Conversely, infinitely small laser sheet thickness is not an optimal solution either because particles with the slightest off-plane velocities escape the laser sheet between double-frame images. Hence, an optimal value for laser sheet thickness

depends on laser sheet positioning precision and a ratio between in-plane and out-of-plane velocities.

All the aforementioned problems with PIV could, however, be reduced by greater silicone model scaling. Our scaling of 1.85 is in the typical range of the other conducted PIV studies (Doorly et al., 2008; Chung and Kim 2008; Na et al., 2012; Zubair et al., 2015; Lintermann and Schröder 2017; Cozzi et al., 2017). In addition to greater scaling, PIV measurements could be conducted in a two-fold way to identify and possibly reduce measurement errors and to solve turbulent quantities. At first, experiments should be carried out in purely laminar conditions. In the second part of the measurements, the viscosity of the experiments should be lowered to make the Reynolds number higher corresponding to the actual investigated conditions. Comparisons between the first and second parts of the measurements could solve turbulence quantities more reliably than conventional one-part measurements.

We conducted experiments and calculations with incompressible fluid with constant flow rates. It has been found elsewhere that steady flow assumption is sufficient for most times of the respiratory cycle in PIV measurements of the nasal cavities (Spence et al., 2012). Lee et al. found similar results with unsteady CFD simulations by using LES (Lee et al., 2010). In our study with a steady flow rate, the results remained mostly stationary. However, mean flow unsteadiness was mostly present at the beginning of the end part of the nasal cavities. This phenomenon was more dominant in the left part of the nasal cavities, which was narrower, especially in the upper parts of the cavity.

The quasi-steady flow assumption is usually made with CFD studies. Furthermore, current clinical rhinomanometry results are usually reported without a reference to temporal information. A flow compressibility study in a simplified 2-dimensional geometry claimed unsteadiness of the rhinomanometric results emerging primarily from flow storage effect, which cannot be modelled in the incompressible PIV experiments (Groß and Peters, 2011). To the best of our knowledge, no detailed CFD nasal airflow study with unsteadiness and flow compressibility has been conducted, where the results are simultaneously compared to more simple assumptions. Unfortunately, such studies can only be easily validated with global assessment of the flow without information on the local details. Therefore, compared to PIV experiments, flow compressibility studies are only partly suitable for comparing different CFD models.

Silicone models could be used for experimental compressible studies with global assessment of the flow. The problem is often that silicone models for the PIV experiments are scaled to be larger than conditions *in vivo*. As a result the measurement area of the rhinomanometric devices used in clinics may not be sufficient. In addition, excessive scaling of the model might affect the interpretation of the rhinomanometric results of the 3D model compared to clinical circumstances.

Fortunately, 3D printing in plastic has been studied as a convenient alternative to silicone models in the global assessment of the flow (Valtonen et al., 2020). The benefit of plastic is cheaper and faster production, although certain technical problems still exist. Large series of 3D printed plastic models *in vitro* could provide an alternative to PIV experiments in CFD model validation.

CFD could be useful in obtaining a wider understanding of a patient's subjective feeling of nasal blockage. For example, it might be possible that calculated WSS and pressure losses across the upper respiratory system could be connected to the patient's subjective feelings on nasal obstruction, although this needs further study. Other affecting variables that must be taken into account in future studies are probably heat and mass transfer from the mucus membrane, which were out of the scope of the current study.

According to the findings of our study, PIV measurements in realistically modelled nasal cavities succeeded acceptably and CFD calculations produced corresponding results with PIV mean flow measurements. Therefore, CFD could be considered as an option in assessing nasal airflow. Currently, CFD calculations are too time-consuming and complex for clinical practice. These calculations should therefore be made faster by orders of magnitude and more automated pre-processing of patient data is also needed.

5. Conclusions

In our study, we found that PIV measurements in realistically modelled nasal cavities succeeded acceptably and CFD calculations produced corresponding results with PIV measurements. The differences between laminar and turbulent CFD model results were found to be small in most parts of the nasal cavities. This finding supports the suitability of the laminar flow approximation in studying natural human breathing in the nasal cavities. However, greater model scaling is necessary for better validations with PIV and comparisons of competing CFD models. CFD of nasal CBCT scans could be considered an additional option for rhinomanometry in assessing and analysing nasal airflow and the effect of pathologies on it. Currently, CFD has its limitations and it needs to be modified in order to be more straightforward for clinical use.

Data Availability

All data are available on request.

Declaration of Competing Interest

The authors declare that there is no conflict of interest.

Acknowledgements

The author(s) received financial support from the Finnish ORL-HNS Foundation, Orion Research Foundation sr, Tampere Tuberculosis Foundation, and the Väinö and Laina Kivi Foundation for the research, authorship, and/or publication of this article.

Appendix A. Supplementary data

Supplementary material related to this article can be found, in the online version, at doi:https://doi.org/10.1016/j.resp.2020.103508.

References

André, R.F., Vuyk, H.D., Ahmed, A., Graamans, K., Nolst Trenité, G.J., 2009. Correlation between subjective and objective evaluation of the nasal airway. A systematic review of the highest level of evidence. Clinical Otolaryngology 34 (6), 518–525. https://doi.org/10.1111/j.1749-4486.2009.02042.x.

Chung, S.K., Kim, S.K., 2008. Digital particle image velocimetry studies of nasal airflow. Respiratory Physiology and Neurobiology 163 (1-3), 111–120. https://doi.org/10.1016/j.resp.2008.07.023.

Cozzi, F., Felisati, G., Quadrio, M., 2017. Velocity measurements in nasal cavities by means of Stereoscopic PIV - Preliminary tests. Journal of Physics: Conference Series 882 (1). https://doi.org/10.1088/1742-6596/882/1/012010.

Doorly, D.J., Taylor, D.J., Schroter, R.C., 2008. Mechanics of airflow in the human nasal airways. Respiratory Physiology and Neurobiology 163 (1), 100–110. https://doi.org/10.1016/j.resp.2008.07.027.

Groß, T.F., Peters, F., 2011. A fluid mechanical interpretation of hysteresis in rhinomanometry. ISRN otolaryngology 126520. https://doi.org/10.5402/2011/126520.

Hopkins, L.M., Kelly, J.T., Wexler, A.S., Prasad, A.K., 2000. Particle image velocimetry measurements in complex geometries. Experiments in Fluids 29 (1), 91–95. https://doi.org/10.1007/s003480050430.

Kim, S.K., Na, Y., Kim, J., Chung, S., 2013. Patient specific CFD models of nasal airflow: Overview of methods and challenges. Journal of Biomechanics 46 (2), 299–306. https://doi.org/10.1016/j.jbiomech.2012.11.022.

Lee, J., Na, Y., Kim, S., Chung, S., 2010. Unsteady flow characteristics through a human nasal airway. Respiratory Physiology and Neurobiology 172 (3), 136–146. https://doi.org/10.1016/j.resp.2010.05.010.

Li, C., Jiang, J., Dong, H., Zhao, K., 2017. Computational modeling and validation of human nasal airflow under various breathing conditions. Journal of Biomechanics 64, 59–68, 10.1016./j.jbiomech.2017.08.031.

Lintermann, A., Schröder, W., 2017. A Hierarchical Numerical Journey Through the Nasal Cavity: from Nose-Like Models to Real Anatomies. Flow Turbulence and Combustion 102, 89–116. https://doi.org/10.1007/s10494-017-9876-0.

Mylavarapu, G., Murugappan, S., Mihaescu, M., Kalra, M., Khosla, S., Gutmark, E., 2009. Validation of computational fluid dynamics methodology used for human upper

airway flow simulations. Journal of Biomechanics 42 (10), 1553–1559. https://doi.org/10.1016/j.jbiomech.2009.03.035.
Na, Y., Chung, K.S., Chung, S., Kim, S.K., 2012. Effects of single-sided inferior turbinectomy on nasal function and airflow characteristics. Respiratory Physiology and Neurobiology 180 (2), 289–297. https://doi.org/10.1016/j.resp.2011.12.005.
Nip, L., Tan, M., Whitcroft, K.L., Gupta, R., Leung, T.S., Andrews, P., 2018. Patient experience of nasal obstruction and its clinical assessment. The Journal of Laryngology and Otology 132 (4), 318–322. https://doi.org/10.1017/S0022215117002146.
Quadrio, M., Pipolo, C., Corti, S., Lenzi, R., Messina, F., Pesci, C., Felisati, G., 2014. Review of computational fluid dynamics in the assessment of nasal air flow and analysis of its limitations. European Archives of Oto-Rhino-Laryngology 271 (9), 2349–2354. https://doi.org/10.1007/s00405-013-2742-3.
Spence, C.J.T., Buchmann, N.A., Jermy, M.C., 2012. Unsteady flow in the nasal cavity with high flow therapy measured by stereoscopic PIV. Experiments in Fluids 52 (3), 569–579. https://doi.org/10.1007/s00348-011-1044-z.
Spence, C.J.T., Buchmann, N.A., Jermy, M.C., Moore, S.M., 2011. Stereoscopic PIV measurements of flow in the nasal cavity with high flow therapy. Experiments in Fluids 50 (4), 1005–1017. https://doi.org/10.1007/s00348-010-0984-z.
Valtonen, O., Bizaki, A., Kivekäs, I., Rautiainen, M., 2018. Three-Dimensional Volumetric Evaluation of the Maxillary Sinuses in Chronic Rhinosinusitis Surgery. Annals of Otology, Rhinology and Laryngology 127 (12), 931–936. https://doi.org/10.1177/0003489418801386.
Valtonen, O., Ormiskangas, J., Kivekäs, I., Rantanen, V., Dean, M., Poe, D., Järnstedt, J., Lekkala, J., Saarenrinne, P., Rautiainen, M., 2020. Three-Dimensional Printing of the Nasal Cavities for Clinical Experiments. Scientific Reports 10 (1), 502. https://doi.org/10.1038/s41598-020-57537-2.
Vogt, K., Jalowayski, A.A., Althaus, W., Cao, C., Han, D., Hasse, W., Hoffrichter, H., Mösges, R., Pallanch, J., Shah-Hosseini, K., Peksis, K., Wernecke, K.D., Zhang, L., Zaporoshenko, P., 2010. 4-Phase-Rhinomanometry (4PR)–basics and practice 2010. Rhinology.Supplement 21, 1–50.
Willatt, D., 2009. The evidence for reducing inferior turbinates. Rhinology 47 (3), 227–236. https://doi.org/10.4193/Rhin09.017.
Zubair, M., Abdullah, M.Z., Ismail, R., Shuaib, I.L., Hamid, S.A., Ahmad, K.A., 2012. Review: A critical overview of limitations of cfd modeling in nasal airflow. Journal of Medical and Biological Engineering 32 (2), 77–84. https://doi.org/10.5405/jmbe.948.
Zubair, M., Ahmad, K.A., Abdullah, M.Z., Sufian, S.F., 2015. Characteristic airflow patterns during inspiration and expiration: Experimental and numerical investigation. Journal of Medical and Biological Engineering 35 (3), 387–394. https://doi.org/10.1007/s40846-015-0037-4.

PUBLICATION IV

Three-Dimensional Measurements in Assessing the Results of Inferior Turbinate Surgery

Valtonen O, Ormiskangas J, Harju T, Rautiainen M, Kivekäs I

Annals of Otology, Rhinology & Laryngology. 2021 Jul 1;34894211028516 (Online ahead of print)
doi:10.1177/00034894211028516

Original Article

Three-Dimensional Measurements in Assessing the Results of Inferior Turbinate Surgery

Annals of Otology, Rhinology & Laryngology
1–8

DOI: 10.1177/00034894211028516
journals.sagepub.com/home/aor


Olli Valtonen, MD[1,2*], Jaakko Ormiskangas, MSc (Tech.)[2,3*], Teemu Harju, MD, PhD[1,2], Markus Rautiainen, MD, PhD[1,2], and Ilkka Kivekäs, MD, PhD[1,2]

Abstract

Objectives: Acoustic rhinometry is widely used in evaluating patients with nasal congestion, but it only has a partial correlation with patient symptoms. The use and focus of cone beam computed tomography (CBCT) scans are mainly on the paranasal sinuses and less on the nasal cavities. Therefore, information acquired from CBCT scans is not used to its full extent. In our present study, we have studied patients with enlarged inferior turbinates. Our aim was to investigate and compare the use of 3D volumetric measurements and cross-sectional area measurements taken from CBCT scans to results obtained from acoustic rhinometry.

Material and methods: In total, 25 patients with enlarged inferior turbinates were studied. CBCT scans were obtained preoperatively and at twelve months postoperatively. 3D volumetric and cross-sectional area measurements were compared to results from acoustic rhinometry, the visual analogue scale (VAS) and Glasgow Health Status Inventory (GHSI) questionnaires.

Results: A statistically significant change in 3D volume and cross-sectional area was measured in the anterior part of the inferior turbinate and surrounding air space after inferior turbinate surgery. VAS and GHSI results had mild correlations with the 3D volume and cross-sectional area measurements of the anterior part of the inferior turbinate. Acoustic rhinometry correlated with the air space 3D volume measurements in the anterior part.

Conclusions: Fully utilized CBCT scans provide more comprehensive and accurate information. Furthermore, 3D analysis of the inferior turbinates provides valuable information and more precise measurements compared to acoustic rhinometry.

Keywords

3D, volumetry, nasal cavity, turbinate, RFTA

Introduction

Today, the 2 most common objective methods for assessing nasal congestion are acoustic rhinometry and rhinomanometry.[1,2] Both methods have proven to be fast and mostly reliable in measuring dimensions and breathing resistance in the nose. The use of these methods has, however, been problematic, especially when the patient's subjective sensations of nasal blockage or patency are taken into account. Moreover, the Visual Analogue Scale (VAS) and other symptom questionnaires have failed to show a consensus of correlation with acoustic rhinometry or rhinomanometry.[3]

In previous studies, the assessment of the volume of the nasal cavities has been mostly done using information gained from acoustic rhinometry. However, acoustic rhinometry, especially in the posterior regions, is known to overestimate the dimensions of the nasal cavity.[4-7] Indeed, in a study by Cankurtaran et al, acoustic rhinometry was found to have overestimated the volume of the nasal cavity airway

[1]Department of Otorhinolaryngology – Head and Neck Surgery, Tampere University Hospital, Tampere, Finland
[2]Faculty of Medicine and Health Technology, Tampere University, Tampere, Finland
[3]Faculty of Engineering and Natural Sciences, Automation Technology and Mechanical Engineering Unit, Tampere University, Tampere, Finland

*Main authors

Corresponding Author:
Olli Valtonen, MD, Department of Otorhinolaryngology – Head and Neck Surgery, Tampere University Hospital, P.O. Box 2000, FIN-33521 Tampere, Finland.
Email: olli.valtonen@pshp.fi

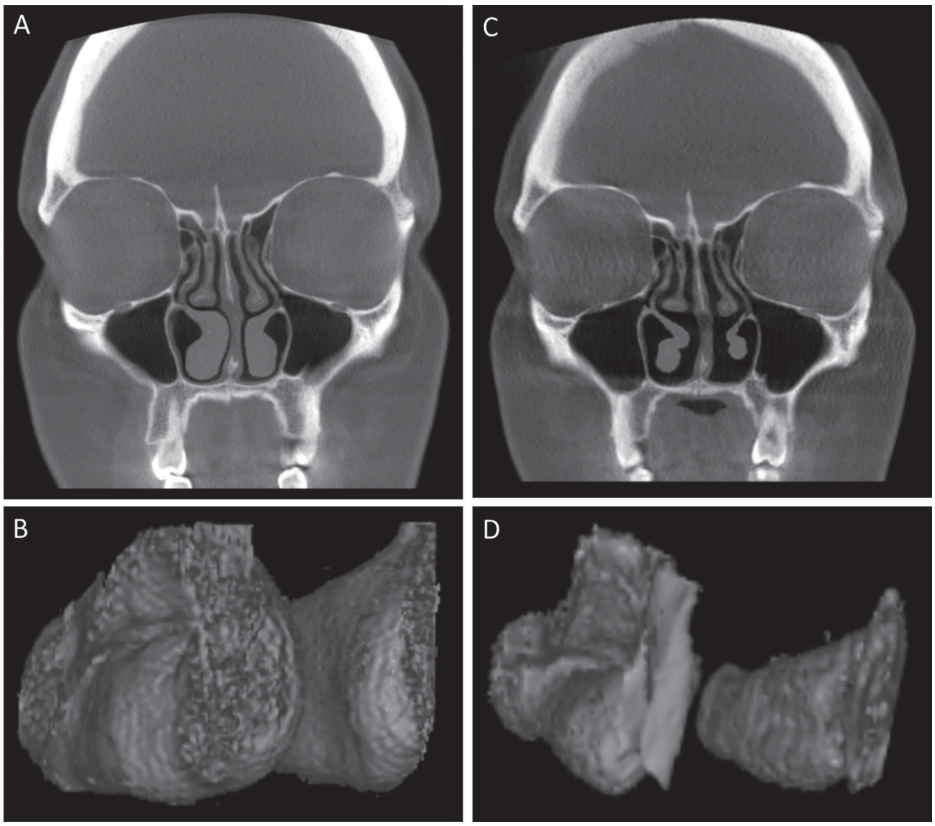

Figure 1. An example of the preoperative patient CBCT scans (A) with marked inferior turbinates (red) used as a basis for the production of the inferior turbinate 3D models (B) which were used in the 3D volumetric measurements. Corresponding examples of the postoperative patient CBCT scans (C) and the produced inferior turbinate 3D models (D) are also presented.

by more than 20%. To date, however, the actual 3D volumetric measurements from pre- and postoperative CT or magnetic resonance imaging (MRI) scans and any possible benefits compared to acoustic rhinometry in patients with operated nasal cavities have not been extensively studied.

Inferior turbinate surgery with different methods is one of the main surgical procedures for treating nasal congestion. Usually, acoustic rhinometry and different subjective assessment methods are chosen to evaluate the effects of these operations on the circumstances in the nasal cavity. In previous studies, the postoperative follow-up times have been fairly short, and the most commonly used time span between pre- and postoperative data gathering has varied from a few weeks to a few months.[8] The long-term effects of these operations on volumetric dimensions, acoustic rhinometry results, patient symptoms and their correlations from 1 or more years of follow-up have not as yet been studied sufficiently.

In the present study, the aim was to study and compare the use of 3D volumetric measurements accompanied with cross-sectional area measurements to those results obtained from acoustic rhinometry. Moreover, the potential of 3D volumetric and cross-sectional area measurements in reflecting the patients' subjective sensations was also studied using VAS and quality of life (QOL) scores.

Materials and Methods

In the present study, 26 patients with chronic nasal obstruction were included. These patients had enlarged inferior

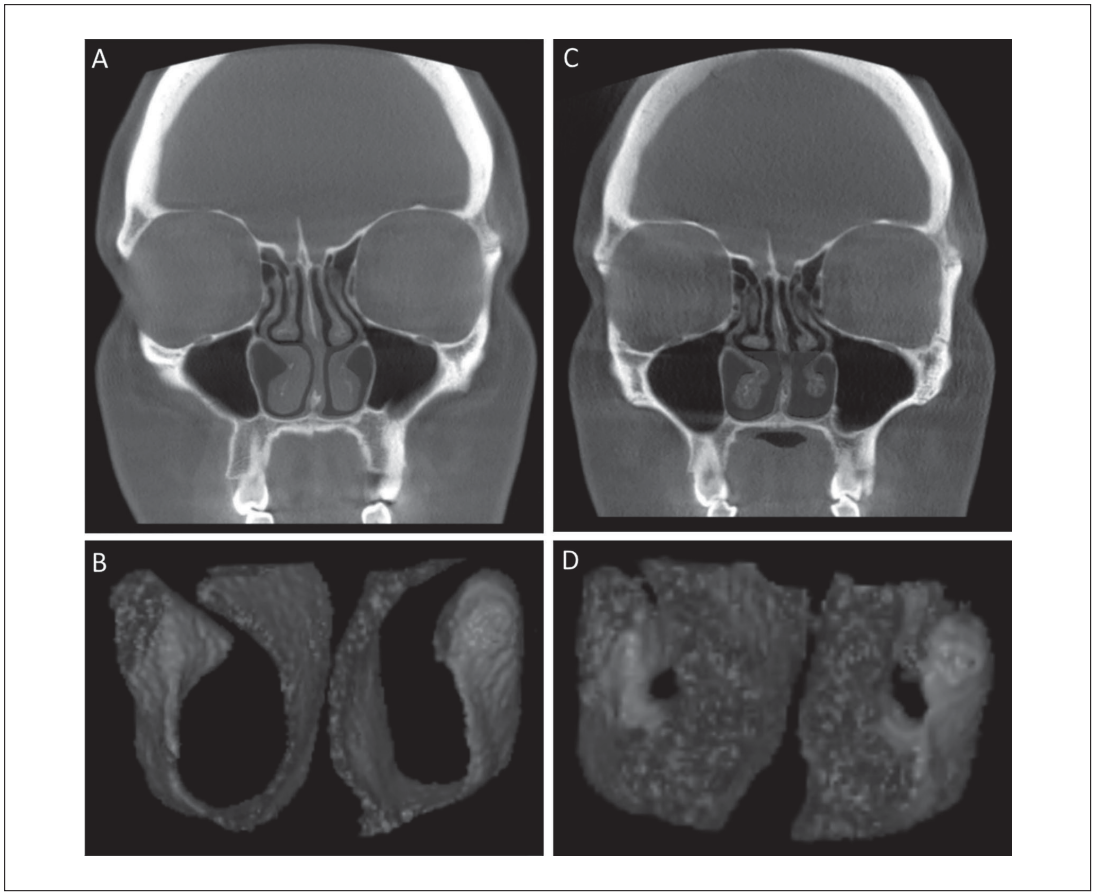

Figure 2. An example of the preoperative patient CBCT scans (A) with marked air spaces (blue) surrounding the operated anterior parts of the inferior turbinates used as a basis for the production of the air space 3D models (B) which were used in the 3D volumetric measurements. Corresponding examples of the postoperative patient CBCT scans (C) and the produced air space 3D models (D) are also presented.

turbinates and underwent radiofrequency thermal ablation (RFTA) treatment (Sutter RF generator BM-780 II, Freiburg, Germany) to the inferior turbinates on both sides. The patients were scanned preoperatively and at twelve months postoperatively with cone beam computed tomography (CBCT) (Planmeca Max, Planmeca, Helsinki, Finland).

CBCT data were saved to a file in Digital Imaging and Communications in Medicine (DICOM) format and downloaded to OnDemand3D™ software (version 1.0, CyberMed, Inc., Yuseong-gu, Daejeon, South Korea). OnDemand3D™ software was used to perform the 3D volumetric and cross-sectional area measurements.

On both sides, the volume of the whole inferior turbinate was 3D modeled and measured from the pre- and postoperative CBCT scans (Figure 1). The same measurements were performed on the operated anterior part of the inferior turbinate and the air space surrounding the turbinate (Figure 2). The anterior part consisted of an area from 5 to 20 mm posterior from the anterior peak of the inferior turbinate. Hounsfield Unit (HU) values from −429 to 400 were used to measure the inferior turbinate. These values were obtained using the measuring software's own scaling function. HU values from −1000 to −430 were used for the measurement of the pneumatized area according to previous studies.[9-11] Some 3D modeling artefacts, included to the 3D measurements by the software, were manually excluded from the structures of interest.

We also used CBCT scans to measure the coronal cross-sectional areas from both the inferior turbinates and the air spaces surrounding the inferior turbinates. The measurement

Table 1. Median volumetric pre- and postoperative results. Turbinate volume represents the inferior turbinate as a whole and the anterior part measurements are presented in the 5 to 20 mm results (n = 25). The results are shown from both sides separately and the total results represent the combined results from both the left and right sides. The lower quartile (Q_{25}) and upper quartile (Q_{75}) are shown with the median. The statistical significance of the change between pre- and postoperative results, analysed with Wilcoxon signed-rank test, is also disclosed.

	Median volume (cm^3)						
	Left (pre)	Right (pre)	Total (pre)	Left (post)	Right (post)	Total (post)	Total (change)
Turbinate	4.9 Q_{25} = 3.8 Q_{75} = 6.8	5.6 Q_{25} = 4.6 Q_{75} = 7.2	11.7 Q_{25} = 9.0 Q_{75} = 13.1	4.8 Q_{25} = 3.9 Q_{75} = 6.3	4.5 Q_{25} = 3.5 Q_{75} = 5.7	9.3 Q_{25} = 8.0 Q_{75} = 11.2	−1.7 Q_{25} = −3.3 Q_{75} = 0.0 $P < .01$
Turbinate (5-20 mm)	2.1 Q_{25} = 1.4 Q_{75} = 2.6	2.2 Q_{25} = 1.6 Q_{75} = 2.6	4.2 Q_{25} = 3.3 Q_{75} = 4.9	1.6 Q_{25} = 1.3 Q_{75} = 2.0	1.4 Q_{25} = 1.3 Q_{75} = 1.6	3.0 Q_{25} = 2.7 Q_{75} = 3.3	−1.2 Q_{25} = −2.0 Q_{75} = −0.4 $P < .001$
Air (5-20 mm)	1.4 Q_{25} = 0.9 Q_{75} = 1.8	1.2 Q_{25} = 0.7 Q_{75} = 1.6	2.3 Q_{25} = 2.0 Q_{75} = 3.4	1.6 Q_{25} = 1.2 Q_{75} = 2.2	1.9 Q_{25} = 1.5 Q_{75} = 2.3	3.4 Q_{25} = 2.7 Q_{75} = 4.4	0.8 Q_{25} = 0.2 Q_{75} = 1.9 $P < .001$

of the cross-sectional areas started 5 mm and ended 50 mm posterior from the anterior peak of the inferior turbinate. The distance between each measuring point was 5 mm. For these measurements, we used the Smart Pen function of OnDemand3D™ with some manual corrections.

For both the volumetric and cross-sectional area measurements, the uppermost limit of the region of interest (ROI) was set at the lowest level of the middle turbinates. The nasal cavity floor was used as the lowest level of the ROI. Using the OnDemand3D™ software, the volumetric and cross-sectional area measurements of the pre- and postoperative CBCT scans took approximately 7 to 10 hours per patient.

The patients were asked to fill in the VAS questionnaire preoperatively and at 12 postoperatively in order to assess the severity of nasal obstruction. To assess the effects of a health problem on quality of life, the patients were asked to fill in the Glasgow Health Status Inventory (GHSI) questionnaire. Acoustic rhinometry (Acoustic rhinometer A1, GM instruments Ltd, Kilwinning, UK) was also performed pre- and postoperatively. An encompassing analysis of the acoustic rhinometry and subjective questionnaire results has been presented in a previous study.[12] The acoustic rhinometry tests without adrenaline and the results from both MCA2 and V2-5 were used in this study.

Before the final data analysis, 1 patient was excluded from the study due to extensive artefacts in the CBCT scans caused by dental fillings which prevented 3D measurements. Thus, 25 patients were included in the present study's data analysis. In addition, with regard to only the correlation analysis, 1 patient had to be excluded due to missing acoustic rhinometry measurements. This resulted in a total of 24 patients being included in this analysis.

All the data were analyzed using SPSS (version 26, IBM, Armonk, NY, USA) software. The Wilcoxon signed-rank test was used to analyze the statistical significance of the measurement results. The Spearman correlation test was used for correlation analysis.

Institutional Review Board approval for the study (R13144) was obtained from the Ethics Committee of Tampere University Hospital, Tampere, Finland.

Results

The preoperative median total volume from the combined left and right inferior turbinates was 11.7 cm^3. The median total volume postoperatively was 9.3 cm^3. In the anterior 5 to 20 mm of the inferior turbinate, the preoperative inferior turbinate total volume of 4.2 cm^3 decreased postoperatively to 3.0 cm^3. Corresponding volumetric results for the pneumatized area in the anterior part increased from 2.3 to 3.4 cm^3. The changes between preoperative and postoperative volumes were statistically significant in all the measured areas (Table 1).

When the preoperative and postoperative measurements were analyzed together, comprising 48 cases in total, the volumetric measurements of the pneumatized nasal cavity in the anterior part of the measured region correlated with V2-5 results from acoustic rhinometry (0.523, $P < .001$) and with VAS scores (−0.279, $P < .05$) (Figure 3). Turbinate volume correlated with VAS (0.390, $P < .001$) and QOL (−0.433, $P < .001$) scores in the anterior part of its volume. However, the measurements of the whole length of the inferior turbinate or the changes in it did not correlate with the other parameters. Moreover, the volume changes in the anterior part of the inferior turbinate or the air space

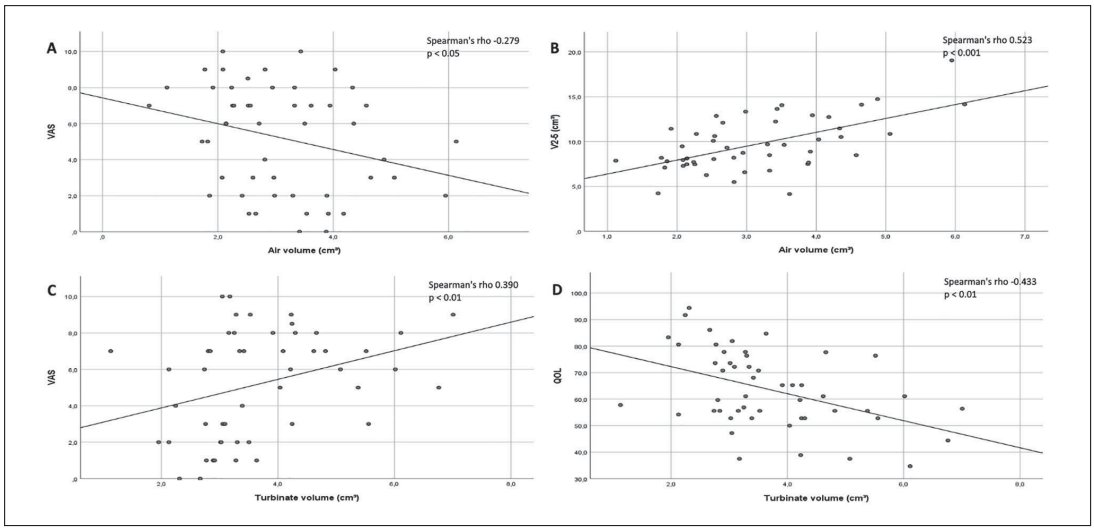

Figure 3. Correlation graphs for the 3D volumetric measurements of the individual anterior parts of the inferior turbinates (n = 48). The air volume (cm^3) correlations between VAS score and V2-5 (cm^3) are presented in graphs (A) and (B). The turbinate volume (cm^3) correlations between VAS and QOL scores are presented in graphs (C) and (D). Spearman's rho number and R^2 correlation line are included in the graphs.

surrounding it did not correlate with changes in the other parameters.

The main cross-sectional area changes from pre- to postoperative values were found in the region of the operated anterior part of the inferior turbinate and the pneumatized area surrounding it (Figure 4). These changes were also statistically significant. Some smaller cross-sectional area changes with a statistical significance were also found in the posterior regions of the inferior turbinate. When the pre- and postoperative measurements were analyzed together, the cross-sectional area measurements correlated with VAS and QOL scores in the most anterior measurement points but did not correlate with the other parameters (Table 2). The cross-sectional area changes did not correlate with changes in the other parameters.

Discussion

At present, CBCT scans are widely used as part of the examination of patients with symptoms of nasal congestion. The information gained from these scans, however, is not used to its full extent. In our present study, we demonstrate the use of 3D volumetric measurements combined with cross-sectional area measurements to assess the results of operative treatment in the inferior turbinates from CBCT scans. These methods proved to be accurate in measuring the inferior turbinate and the surrounding air space and in assessing the changes in them. Moreover, the measurements produced both objective and descriptive results on the effects of the RFTA treatment.

In the whole length of the inferior turbinate, the change from pre- to postoperative volume was −15%. A corresponding volume change for the anterior part of the inferior turbinate was −28% and +41% for the surrounding air space. These findings reflect well the given treatment's effect on the operated turbinates, where the anterior part of the inferior turbinates is treated.

Some changes in the inferior turbinate and the surrounding air cross-sectional area measurements were also found in the middle and posterior measuring points (Figure 4). In the middle regions, for example, both the cross-sectional area of the turbinates and the air had decreased. In addition, even though the most posterior regions of the inferior turbinate were not operated, the effect of the operation seemed to be parallel, though statistically significant at a mild level, to the anterior part of the inferior turbinate. It is possible therefore that these changes could be due to a neural or vascular process in the inferior turbinate and possibly even in the whole nasal cavity. These findings suggest that other compensatory changes might occur in the other parts of the nasal cavity after inferior turbinate surgery that could subsequently have an effect on the patients' sensation of nasal obstruction or patency. However, our study focused only on the inferior turbinates and their surroundings, and therefore further studies are required to assess this possible phenomenon.

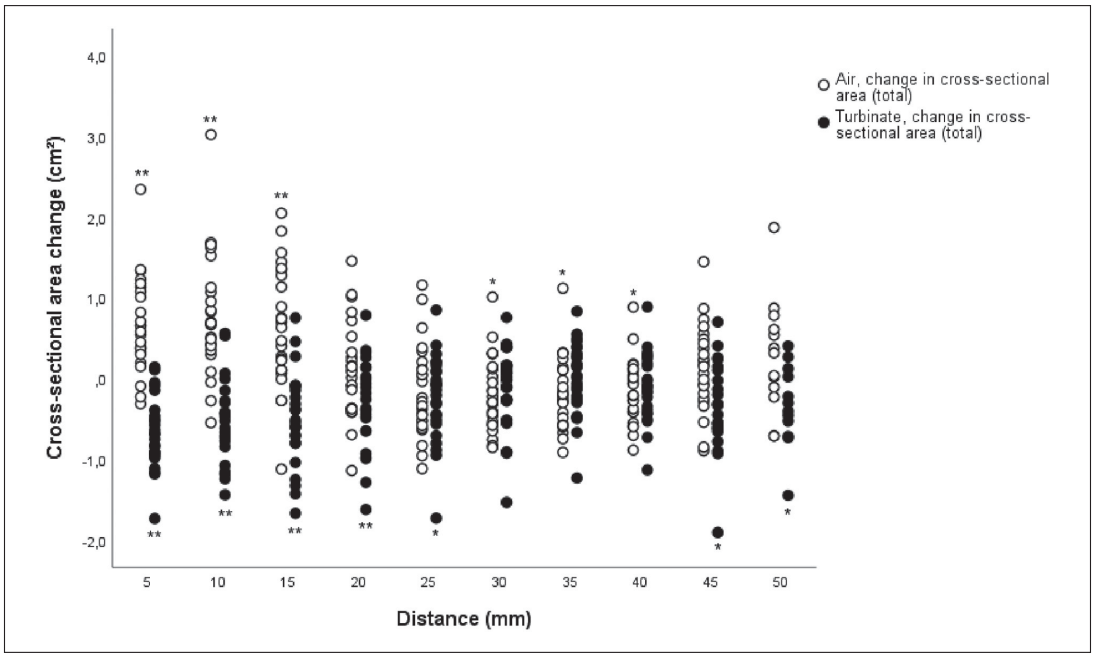

Figure 4. Cross-sectional area changes in both inferior turbinate and surrounding air in every measuring point (n = 25). The total results represent the combined left and right nasal cavity results. The distance represents the measuring point distance from the anterior peak of the inferior turbinate. Statistically significant inferior turbinate or air space changes per every measuring point, analysed with Wilcoxon signed-rank test, are marked with an asterisk.
*$P < .05$. **$P < .01$.

Table 2. Cross-sectional area correlation with VAS and QOL scores in the area of the anterior part of the inferior turbinate for both pre- and postoperative results (n = 48). The correlation coefficient with VAS and QOL is shown for every cross-sectional area measuring point from the anterior part (5-20 mm) of the inferior turbinate. The statistically significant results, analysed with Spearman's rho test, are presented with an asterisk.

Cross-sectional area correlation with VAS and QOL								
	Air				Turbinate			
	5 mm	10 mm	15 mm	20 mm	5 mm	10 mm	15 mm	20 mm
VAS	−0.408**	−0.411**	−0.261	0.006	0.539**	0.439**	0.379**	0.242
QOL	0.280*	0.323*	0.242	−0.031	−0.400**	−0.377**	−0.411**	−0.251

*$P < .05$. **$P < .01$.

We found correlations between the volume of the pneumatized area around the anterior part of the inferior turbinates and both the V2-5 results from acoustic rhinometry and VAS scores, although these correlations were mild (Figure 3). Both subjective assessment methods had a mild correlation with the anterior turbinate volume measurements. These findings are in line with the observations of previous studies, where the subjective measurement methods did not produce strong correlating results with objective clinical assessment methods.[3,13-16] In these previous studies, VAS scale results correlated with results that varied from no correlation to fairly good correlation when compared to acoustic rhinometry or rhinomanometry.

We are aware of only a few studies in which the volumetric measurements of the nasal cavity structures taken from CT or MRI scans have been used alongside results from acoustic rhinometry to assess operated nasal cavity volumes. Kilavuz et al[17] studied electrocautery and

radiofrequency tissue reduction in the treatment of inferior turbinate hypertrophy and found the effects of both operative methods on inferior turbinate volumes to be close to each other when measured from MRI scans. However, the correlation of the MRI scan measurements with the results from acoustic rhinometry were not compared. A study by Numminen et al[18] compared nasal cavity volume measurements from high-resolution computed tomography (HRCT) scans with acoustic rhinometry. They came to the conclusion that acoustic rhinometry produces good results in the anterior and middle parts of the nasal cavity but weaker results in the posterior parts. However, the study used patients undergoing uncinectomy without any turbinate operations. One study measuring actual nasal cavity 3D volumes from CT scans concentrated mainly on evaluating the results of septorhinoplasty without assessing the correspondence of the volumetric measurements with other used methods, such as VAS, acoustic rhinometry or rhinomanometry.[19] The study showed that septorhinoplasty caused a significant increase in nasal cavity volume, which was demonstrated with 3D measurements.

The results of inferior turbinate surgery have previously been studied by measuring the whole inferior turbinate volume and concentrating on the acquired change in it.[17,20] These studies have used either CT or MRI scans to measure and compare inferior turbinate volumes pre- and postoperatively. In a study by Bozan et al, inferior turbinate volumes were calculated from linear measurements. In the study by Kilavuz et al, however, the technique used for inferior turbinate volume measurements was not clearly described. The only method used to assess the parameters of the nasal cavity air space was acoustic rhinometry. Unfortunately, these studies did not assess how well these 2 different methods correlated with each other or how accurate they were. Thus, the results are not fully comparable with our 3D measurements.

Although measuring nasal cavity air space dimensions with acoustic rhinometry is relatively reliable and fast to perform, the method has its limitations and uncertainties. In previous studies by Cankurtaran et al,[4] Hilberg et al[5] and Terheyden et al,[6] the acoustic rhinometry results considerably overestimated the cross-sectional areas in, and especially after the mid parts of the nasal cavity when compared to the actual CT measurements. This has been interpreted to be caused by the sound loss through the ostia to the paranasal sinuses or by the interaction of the nasal cavity and the paranasal sinuses. Therefore, the possible changes in the middle and posterior parts of the nasal cavity cannot be reliably assessed with acoustic rhinometry, which means that possible significant changes in the nasal cavities remain unobserved. Our finding that V2-5 results had a mild correlation with only the volumetric measurements of the anterior region support this finding (Figure 3).

The limitation of the methods we used in our study is that they are still time consuming. However, combined information from the 3D volumetric method and cross-sectional area measurements provide an objective method for assessing the results of inferior turbinate surgery and other operations of the nasal cavity. As previously mentioned, the assessment results are more precise than those provided by acoustic rhinometry, especially in the mid and posterior parts of the nasal cavity.

Today, the 3D volumetric method combined with cross-sectional area measurements are only applicable for study purposes, and more studies are needed to adjust and speed up the process. The comprehensive assessment of nasal cavity anatomy, changes to it and the effect they have on nasal cavity airflows and patient symptoms will most likely require studies that are carried out using 3D modeling software that can 3D model the airflow conditions and the effect on the mucous membrane.

Conclusions

A significant 3D volume and cross-sectional area decrease was measured in the anterior part of the inferior turbinate after RFTA treatment, whereas the surrounding air increased significantly. The treatment led to some possible compensatory changes, especially in the middle and posterior parts of the inferior turbinates. Overall, 3D volumetric and cross-sectional area measurements had mild to moderate correlation with other parameters. In evaluating the effects of inferior turbinate surgery, 3D volumetric and cross-sectional area measurements proved to be accurate. CBCT scans can be used more comprehensively as a diagnostics tool and for further analytics.

Declaration of Conflicting Interests

The author(s) declared no potential conflicts of interest with respect to the research, authorship, and/or publication of this article.

Funding

The author(s) disclosed receipt of the following financial support for the research, authorship, and/or publication of this article: The author(s) received financial support from the Finnish ORL-HNS Foundation, the Orion Research Foundation sr, Tampere Tuberculosis Foundation and the Väinö and Laina Kivi Foundation for the research, authorship and/or publication of this article.

ORCID iD

Olli Valtonen https://orcid.org/0000-0001-9423-0269

Data availability

All data are available on request.

References

1. Valero A, Navarro AM, Del Cuvillo A, et al. Position paper on nasal obstruction: evaluation and treatment. *J Investig Allergol Clin Immunol*. 2018;28:67-90.
2. Vogt K, Bachmann-Harildstad G, Lintermann A, Nechyporenko A, Peters F, Wernecke KD. The new agreement of the international RIGA consensus conference on nasal airway function tests. *Rhinology*. 2018;56:133-143.
3. André RF, Vuyk HD, Ahmed A, Graamans K, Nolst Trenité GJ. Correlation between subjective and objective evaluation of the nasal airway. A systematic review of the highest level of evidence. *Clin Otolaryngol*. 2009;34:518-525.
4. Cankurtaran M, Celik H, Coşkun M, Hizal E, Cakmak O. Acoustic rhinometry in healthy humans: accuracy of area estimates and ability to quantify certain anatomic structures in the nasal cavity. *Ann Otol Rhinol Laryngol*. 2007;116:906-916.
5. Hilberg O, Lyholm B, Michelsen A, Pedersen OF, Jacobsen O. Acoustic reflections during rhinometry: spatial resolution and sound loss. *J Appl Physiol (1985)*. 1998;84:1030-1039.
6. Terheyden H, Maune S, Mertens J, Hilberg O. Acoustic rhinometry: validation by three-dimensionally reconstructed computer tomographic scans. *J Appl Physiol (1985)*. 2000;89:1013-1021.
7. Muñoz-Cano R, Salvador R, Valero A, et al. Accuracy of acoustic rhinometry versus computed tomography in the evaluation of nasal cavity in patients with nasal polyposis. *Rhinology*. 2010;48:224-227.
8. Hytönen ML, Bäck LJ, Malmivaara AV, Roine RP. Radiofrequency thermal ablation for patients with nasal symptoms: a systematic review of effectiveness and complications. *Eur Arch Otorhinolaryngol*. 2009;266:1257-1266.
9. Valtonen O, Bizaki A, Kivekäs I, Rautiainen M. Three-dimensional volumetric evaluation of the maxillary sinuses in chronic rhinosinusitis surgery. *Ann Otol Rhinol Laryngol*. 2018;127:931-936.
10. Valtonen O, Ormiskangas J, Kivekas I, et al. Three-dimensional printing of the nasal cavities for clinical experiments. *Sci Rep*. 2020;10:502.
11. Ormiskangas J, Valtonen O, Kivekäs I, et al. Assessment of PIV performance in validating CFD models from nasal cavity CBCT scans. *Respir Physiol Neurobiol*. 2020;282:103508.
12. Harju T, Numminen J. The effect of inferior turbinate surgery on nasal symptoms and inferior turbinate contractility. *Am J Otolaryngol*. 2020;42:102778.
13. Reber M, Rahm F, Monnier P. The role of acoustic rhinometry in the pre- and postoperative evaluation of surgery for nasal obstruction. *Rhinology*. 1998;36:184-187.
14. Gungor A, Moinuddin R, Nelson RH, Corey JP. Detection of the nasal cycle with acoustic rhinometry: techniques and applications. *Otolaryngol Head Neck Surg*. 1999;120:238-247.
15. Suzina AH, Hamzah M, Samsudin AR. Objective assessment of nasal resistance in patients with nasal disease. *J Laryngol Otol*. 2003;117:609-613.
16. Sipilä J, Suonpää J, Silvoniemi P, Laippala P. Correlations between subjective sensation of nasal patency and rhinomanometry in both unilateral and total nasal assessment. *ORL J Otorhinolaryngol Relat Spec*. 1995;57:260-263.
17. Kilavuz AE, Songu M, Ozkul Y, Ozturkcan S, Katilmis H. Radiofrequency versus electrocautery for inferior turbinate hypertrophy. *J Craniofac Surg*. 2014;25:1998-2001.
18. Numminen J, Dastidar P, Heinonen T, Karhuketo T, Rautiainen M. Reliability of acoustic rhinometry. *Respir Med*. 2003;97:421-427.
19. Tugrul S, Dogan R, Hassouna H, Sharifov R, Ozturan O, Eren SB. Three-dimensional computed tomography volume and physiology of nasal cavity after septhorhinoplasty. *J Craniofac Surg*. 2019;30:2445-2448.
20. Bozan A, Eriş HN, Dizdar D, Göde S, Taşdelen B, Alpay HC. Effects of turbinoplasty versus outfracture and bipolar cautery on the compensatory inferior turbinate hypertrophy in septoplasty patients. *Braz J Otorhinolaryngol*. 2019;85:565-570.